Physical structure of wheat bran and its comprised layers

by

Andrew Lawrence Mense

B.S., Kansas State University, 2010
M.S., Kansas State University, 2012

AN ABSTRACT OF A DISSERTATION

submitted in partial fulfillment of the requirements for the degree

DOCTOR OF PHILOSOPHY

Department of Grain Science and Industry
College of Agriculture

KANSAS STATE UNIVERSITY
Manhattan, Kansas

2018

Abstract

Wheat bran is a by-product of the wheat flour milling industry. The number of food products containing wheat bran is on the rise because it is a well-recognized good source of dietary fiber. Currently, bran is a low-value commodity used mostly in animal feed, but it has the potential for more extensive applications. To understand the functional and nutritional properties of wheat bran and better use wheat bran in food, it is critical to understand the physical structure of wheat bran.

For the first time, solid-state ^{13}C cross-polarization magic-angle spinning nuclear magnetic resonance (^{13}C CP/MAS NMR), X-ray diffraction (XRD), and small angle X-ray scattering (SAXS) were used to study the physical structure of wheat bran and its dissected layers. The XRD and Solid-State ^{13}C CP/MAS NMR both confirmed the presence of crystalline cellulose in untreated bran, enzymatically treated bran, and dissected bran layers.

Destarched and deproteinized wheat bran (DSDPB) was treated with a mixture of either 7 or 9% sodium hydroxide and 12% urea solvent and structure of the extracted polymers was investigated. Three and 6 cycle dissolution schemes, were examined involving the repeated cooling of the solvent bran mixture to -12.6 °C and then agitating it at 25 °C. When 7% NaOH/12% urea (6 cycle) was applied to DSDPB, 84.1% of the material was solubilized including 89.8% of the arabinoxylans (AX). This procedure recovered more wheat bran AX for characterization than any previous study using alkaline dissolution.

Wheat bran was enzymatically and hydrothermally treated to maximize the soluble fraction. Unlike previous research, the starch and protein were kept and not removed before endoxylanase treatment. The retained protein and glucose polymers (starch, β-glucan, cellulose) could provide functional benefits in addition to the arabinoxylan and could make the process

more economical. Wheat bran hydrolyzed with thermostable α-amylase, protease, and xylanase was the recommended treatment. The combined solubles had a viscosity of 23 cP (10% w/w solids) and ranged in estimated molecular weight from ~600 to 20,000. The percentage of untreated wheat bran AX that was solubilized was 50% and the percentage of AX in the solubles was 23%.

Physical structure of wheat bran and its comprised layers

by

Andrew Lawrence Mense

B.S., Kansas State University, 2010
M.S., Kansas State University, 2012

A DISSERTATION

submitted in partial fulfillment of the requirements for the degree

DOCTOR OF PHILOSOPHY

Department of Grain Science and Industry
College of Agriculture

KANSAS STATE UNIVERSITY
Manhattan, Kansas

2018

Approved by:

Major Professor
Yong-Cheng Shi

Copyright

Abstract

Wheat bran is a by-product of the wheat flour milling industry. The number of food products containing wheat bran is on the rise because it is a well-recognized good source of dietary fiber. Currently, bran is a low-value commodity used mostly in animal feed, but it has the potential for more extensive applications. To understand the functional and nutritional properties of wheat bran and better use wheat bran in food, it is critical to understand the physical structure of wheat bran.

For the first time, solid-state ^{13}C cross-polarization magic-angle spinning nuclear magnetic resonance (^{13}C CP/MAS NMR), X-ray diffraction (XRD), and small angle X-ray scattering (SAXS) were used to study the physical structure of wheat bran and its dissected layers. The XRD and Solid-State ^{13}C CP/MAS NMR both confirmed the presence of crystalline cellulose in untreated bran, enzymatically treated bran, and dissected bran layers.

Destarched and deproteinized wheat bran (DSDPB) was treated with a mixture of either 7 or 9% sodium hydroxide and 12% urea solvent and structure of the extracted polymers was investigated. Three and 6 cycle dissolution schemes, were examined involving the repeated cooling of the solvent bran mixture to -12.6 °C and then agitating it at 25 °C. When 7% NaOH/12% urea (6 cycle) was applied to DSDPB, 84.1% of the material was solubilized including 89.8% of the arabinoxylans (AX). This procedure recovered more wheat bran AX for characterization than any previous study using alkaline dissolution.

Wheat bran was enzymatically and hydrothermally treated to maximize the soluble fraction. Unlike previous research, the starch and protein were kept and not removed before endoxylanase treatment. The retained protein and glucose polymers (starch, β-glucan, cellulose) could provide functional benefits in addition to the arabinoxylan and could make the process

more economical. Wheat bran hydrolyzed with thermostable α-amylase, protease, and xylanase was the recommended treatment. The combined solubles had a viscosity of 23 cP (10% w/w solids) and ranged in estimated molecular weight from ~600 to 20,000. The percentage of untreated wheat bran AX that was solubilized was 50% and the percentage of AX in the solubles was 23%.

Table of Contents

List of Figures

List of Tables

Acknowledgements

I would like to thank Dr. Yong-Cheng Shi for his help and guidance throughout my research. He pushed me to become a better scientist by challenging me and allowing me to learn from mistakes. I also appreciate the funding he provided to support my research. I would also like to thank my committee, including Dr. Jon Faubion, Dr. Hulya Dogan, and Dr. Gerald Reeck for their kind words and support. I would also like to thank my outside chair, Dr. Jayendra Amamcharla, for his time and efforts.

I owe a debt of gratitude to my lab mates of the Carbohydrate Polymers laboratory for their support and for keeping the lab a light-hearted place to work. They were always open to hearing new ideas and solutions to research problems. I would also like to thank my former lab mates Dr. Sherrill Cropper and Reona Oshikiri for their continued support and encouragement throughout my doctorate. I am grateful to the Grain Science support staff for guiding me through all the necessary paperwork and logistics necessary for completing my degree.

I am fortunate to have the incredible support of my wife Bekah, my parents Leland and Christy, siblings, family, friends, and my dog Annie that gave me continual encouragement to complete my doctorate.

Dedication

This thesis is in dedication to my wife Bekah, my parents, and all my family and friends.

Preface

All chapters were written for a specified journal. Therefore, the required journal format was followed for each manuscript, with references following the conclusions.

Chapter 1 - Review of the physical structure and location of chemical components in wheat bran

Abstract

Wheat bran is a by-product of the wheat flour milling industry. The number of food products containing wheat bran is on the rise because it is a well-recognized good source of dietary fiber. Currently, bran is a low-value commodity used mostly in animal feed, but it has the potential for more extensive applications. A variety of microscopic and spectroscopic techniques have been used to study the structural elements of bran, their components, and their organization. This review focuses on the micro- and ultra-structure of wheat bran and addresses the location and organization of chemical components within those structures. A better knowledge of structural factors that limit enzymatic, acid hydrolysis, and dissolution of wheat bran could broaden its use and increase its value.

Introduction

Wheat bran is a layered composite material. The outer to the inner layers of bran are: epidermis, hypodermis, cross cells, tube cells, testa, nucellar epidermis, and aleurone (Bradbury et al., 1956; Antoine et al., 2003). Wheat bran layers can be condensed down to three layers, i.e. the outer pericarp (epidermis and hypodermis), intermediate layer (cross cells, tube cells, testa, and nucellar epidermis), and the aleurone (Antoine et al., 2003). Approximately 90 million tons of wheat bran are produced by the wheat flour milling industry each year (Arte et al., 2016). Wheat bran is a source of protein (13-19.5%) (Arte et al., 2016) and arabinoxylan (AX), the

latter accounting for 40% of destarched wheat bran (Beaugrand et al., 2004a). Currently, wheat bran is a valuable source of dietary fiber. The cell wall components are both physically and covalently associated (Beaugrand et al., 2004b), thus limiting their water-solubility and digestibility. To understand its health benefits, it is essential to understand the physical structure of wheat bran and the factors that limit extractability of its cell wall polymers. Bran components can be further processed by hydrothermal treatment, acid hydrolysis, alkaline treatment, or they can be fermented or transformed enzymatically. The knowledge of grain (e.g. bran) structure and composition influence processing (Jääskeläinen et al., 2013), which can lead to the production of a number of nutritious ingredients (Rosa-Sibakov et al., 2015). The answer to the question, how the wheat bran is assembled can also help answer how can we take wheat bran apart. These answers can lead to the production of value-added products from wheat bran such as arabinoxylooligosaccharides as described in Swennen et al. (2006).

Wheat bran has been the subject of a variety of reviews related to chemical composition, structure, health benefits, and processing (Kiszonas et al., 2013; Apprich et al., 2014; Prückler et al., 2014; Balandrán-Quintana et al., 2015; Onipe et al., 2015; Rosa-Sibakov et al., 2015). This review focuses on the micro- and ultra-structure of wheat bran and addresses the location and organization of chemical components within those structures, which has not been previously reviewed.

Wheat bran has been examined by a number of microscopic and spectral techniques, and key findings are summarized in **Tables 1.1-1.4**. The microscopic techniques include; bright field (**Table 1.1**), fluorescence (**Table 1.2**), confocal laser scanning microscopy (CSLM) (**Table 1.2**), environmental scanning electron microscopy (ESEM) (**Table 1.3**), scanning electron microscopy (SEM) (**Table 1.3**), and transmission electron microscopy (TEM) (**Table 1.4**). The spectroscopic

techniques include laser-induced breakdown spectroscopy (LIBS), solid-state ^{13}C cross-polarization magic-angle spinning nuclear magnetic resonance (^{13}C CP/MAS NMR) (**Table 1.5**), attenuated total reflectance-Fourier transform infrared spectroscopy (ATR-FTIR), Raman, synchrotron infrared microspectroscopy, and confocal laser microspectrofluorometry. The LIBS technique consists of a laser (e.g. Argon Fluoride) that is used to ablate (remove) tissue such as the layers that constitute wheat bran and can be used to indirectly detect tissue cohesiveness (Martelli et al., 2009). Quantitative microscopic analysis can be used to determine ablation flux, which can be related to tissue cohesiveness (Martelli et al., 2009).

Wheat Bran

The mature wheat kernel caryopsis is surrounded by the pericarp, seed coat, and nucellar epidermis, which protects the endosperm and embryo. The outer pericarp and intermediate layer comprise the anatomical wheat bran. The nucellar epidermis is tightly associated with the aleurone layer of the endosperm. From a botanical stand point, aleurone is the outer layer of the endosperm, but during the dry milling process, the aleurone separates with the wheat bran so it is commonly referred to as one of the bran layers (Delcour and Hoseney, 2010). The aleurone will be discussed as a wheat bran layer in this review. The factors affecting solubilization of wheat bran and its individual layers can be better understood by determining the location and physical structure of chemical components in the bran layers, and how the cell wall structure is affected by various treatments. This knowledge would allow for the selection of the appropriate processing method to produce value-added products.

Aleurone and components

The general composition of the aleurone layer is described as a one layer of thick-walled (6-8 µm) polygonal-shaped cells that are non-lignified (Antoine et al., 2003; Harris et al., 2005; Barron and Rouau, 2008; Jääskeläinen et al., 2013). The aleurone cells occur between the starchy endosperm and nucellar epidermis. Aleurone cells are the only metabolically active cells that carry over into commercial wheat bran (Beaugrand et al., 2004a). Aleurone cell walls consist primarily of AX with small amounts of mixed-linkage β-glucan (Barron and Rouau, 2008; Jääskeläinen et al., 2013). Cellulose in only a minor component of the aleurone layer (~1.5%) (Antoine et al., 2003), so the aleurone layer is probably mostly amorphous. Granular inclusions or globoids are present in aleurone cells (Antoine et al., 2003; Jääskeläinen et al., 2013). Lipids (Hell et al., 2005; Barron and Rouau, 2008), proteins (Bacic and Stone, 1981b; Jääskeläinen et al., 2013; Arte et al., 2016), niacin deposits (Fulcher and Wood, 1982), and hollow globoids composed of phytin (Jääskeläinen et al., 2013) are found inside aleurone cells. Protein was reported to be present mainly inside the cell (Bacic and Stone, 1981b), not in the cell wall, as confirmed by using Raman microscopy (Jääskeläinen et al., 2013).

The aleurone layer in bran is comprised of anticlinal and periclinal cell walls (Saadi et al., 1998). When looking at a cross section of wheat bran, the anticlinal cell walls are those that are positioned perpendicular to the pericarp and endosperm (Saadi et al., 1998). The periclinal walls of aleurone are those that abut the nucellar epidermis and that abut the endosperm (Saadi et al., 1998). Aleurone cell walls are also bilayered with an inner and outer wall layer (Beaugrand et al., 2004b) enclosing a middle lamella (**Table 1.4**) (Bacic and Stone, 1981a).

The location of chemical components (AX, phenolic compounds, β-glucan, and protein) in the aleurone cell wall has been examined by FTIR, Raman microspectroscopy, fluorescence microscopy, CSLM, and TEM, and will help lay the basis for understanding aleurone structure and how it can be taken apart. Higher AX concentrations were found in the aleurone layer junction zones (the 90° turn of the wall) where the anticlinal and periclinal walls intersect using synchrotron infrared microspectroscopy (Jamme et al., 2008). Immunolabeling revealed high amounts of AX in the junction zone near the nucellar epidermis (Guillon et al., 2004; Jamme et al., 2008; Dornez et al., 2011b). Immunolabeling of feruloylated AX confirmed that an arabinoxylan polymer formed esters with ferulic acid at the O-5 of the arabinose unit, and the junction zone near the nucellar epidermis had the highest level of the labeled polymer (Philippe et al., 2007). The periclinal and anticlinal walls were generally rich in feruloylated AX (Philippe et al., 2007). Dornez et al. (2011a) reported that a fluorescent xylanase probe stained the anticlinal and periclinal walls equally indicating homogeneity in the distribution of AX in the two types of walls. This was also confirmed by TEM as discussed in **Table 1.4** (Phillipe et al., 2007). Raman spectroscopy (Jääskeläinen et al., 2013) and immunolabelling imaged with both TEM and CSLM (Guillon et al., 2004) showed that AX was concentrated in the middle lamella compared to the inner wall layer. However, AX was also reported to be mostly nonexistent in the middle lamella with the immunolabelling technique (Jamme et al., 2008).

To determine the location and distribution of phenolic material in the aleurone layer, Saadi et al. (1998) used a confocal laser microspectrofluorometer and reported that the UV-induced autofluorescence indicated the presence of phenolic material and therefore feruloylated AX, from lowest to highest intensity in periclinal walls near endosperm < periclinal walls near nucellar epidermis < anticlinal walls < junction zones of the anticlinal and periclinal walls.

Confocal Raman microspectroscopy showed anticlinal cell walls contained twice as much ferulic acid as the periclinal walls (Piot et al., 2000), and ATR-FTIR spectroscopy showed that esterified phenolic acids were more concentrated in the periclinal walls that abut the nucellar epidermis (Barron and Rouau, 2008). Raman spectroscopy found that ferulic acid was more concentrated in the middle lamella compared to the inner wall layer (Jääskeläinen et al., 2013), which matches the location of the AX in the aleurone cell wall. This was expected because the ferulic acid and AX are ester linked.

The location of β-glucan and protein in the microstructure and ultrastructure of the aleurone layer has been examined by FITR, Raman spectroscopy, TEM, CSLM, and immunolabeling (Morrison et al., 1975; Guillon et al., 2004; Barron and Rouau 2008; Jamme et al., 2008; Dornez et al., 2011b; Jääskeläinen et al., 2013). ATR-FTIR measurements (Barron and Rouau 2008) provided evidence of a higher concentration of β-glucans in walls close to the starchy endosperm as opposed to other regions of the aleurone, in agreement with synchrotron infrared microspectroscopy data showing a higher concentration of β-glucans in the periclinal wall near the endosperm (Jamme et al., 2008). Immunolabeling (Guillon et al., 2004; Jamme et al., 2008; Dornez et al., 2011b) showed that β-glucan was absent from the junction zone near the nucellar epidermis. Raman spectroscopy showed the levels of protein and β-glucan were greater in the inner layer (close to the lumen) of the aleurone cell wall (Jääskeläinen et al., 2013). Guillon et al. (2004) reported the same findings for β-glucan using both TEM and CSLM. The aleurone inner wall layer (near the lumen) stained only faintly for protein with amido black (Morrison et al., 1975), again in agreement with Jääskeläinen et al. (2013).

Xylanase treatment of the aleurone layer and corresponding observation using microscopy have been used to understand the structure of the aleurone and how to take apart the

aleurone layer. Beaugrand et al. (2005) treated isolated aleurone with xylanase and found that the periclinal walls abuting both the endosperm and nucellar epidermis were digested leaving a portion of the anticlinal wall as imaged using UV fluorescence. However, the absence of UV-autofluorescence did not indicate the complete loss of cell wall structure, only the loss of AX ester linked to ferulic acid (Van Craeyveld et al., 2010). The treatment of wheat bran with xylanase did not result in the loss of aleurone cell wall structure even though most of the AX was hydrolyzed from the layer as described in **Table 1.2** (Van Craeyveld et al., 2010; Arte et al., 2016). Presumably, the presence of β-glucan (Guillon et al. 2004; Jamme et al., 2008; Dornez et al., 2011b; Jääskeläinen et al., 2013) and protein (Morrison et al., 1975; Jääskeläinen et al., 2013) in the aleurone cell wall was still providing it with structure. Interestingly, a TEM image of the junction zones near the endosperm and nucellar epidermis initially resisted change by xylanase hydrolysis (Beaugrand et al., 2004b), which were reported to be concentrated with AX (Jamme et al., 2008). However, even though the distribution of phenolic acid and AX was not uniform between the periclinal walls, anticlinal walls, and junction zones, xylanase was able to hydrolyze almost all aleurone AX (**Table 1.1**, Beaugrand et al., 2004b; and Van Craeyveld et al., 2010; Arte et al., 2016). This agrees with Beaugrand et al. (2004a), which concluded that ferulic acid monomer ester linkages did not hinder xylanase hydrolysis of AX (**Table 1.1**). However, the presence of ferulic dimers in the aleurone layer, which cross-link AX polymers together, could affect AX resistance to xylanase hydrolysis and consequently aleurone layer structure loss (Beaugrand et al., 2004a). The localization of ferulic dimers in the aleurone layer could help understand why regions of the aleurone layer resist hydrolysis more than others.

In addition to the hydrolysis of the microstructure, the loss of the ultrastructure throughout xylanase treatment of the aleurone cell wall gives additional insight into how the

aleurone layer is assembled and how it can be deconstructed. The PATAg stained cell walls, imaged with TEM, showed that the inner wall layer structure initially resisted change by xylanase hydrolysis while the outer wall layer succumbed to changes (Beaugrand et al., 2004b). Similarly, the inner wall layer is left intact after germination whereas the outer layer is destroyed (**Tables 1.1 and 1.2**) (Fulcher et al., 1972). The inner layer is believed to have a structure different from the outer layer (Beaugrand et al., 2004b; Guillon et al., 2004; Jääskeläinen et al., 2013). Studies (Rhodes et al., 2002; Rhodes and Stone, 2002) using florescence microscopy suggest that not all phenolic compounds in aleurone are linked by ester groups to a polysaccharide but could be covalently linked to protein (**Table 1.2**). In the aleurone cell wall, the low level of protein is localized near the lumen in the inner cell wall region as indicated by Raman spectroscopy and staining (amido black). It seems possible that covalent linkages may be present between protein and ferulic acid on AX (Rhodes et al., 2002; Rhodes and Stone, 2002).

The kinetics of xylanase hydrolysis of AX in the aleurone layer of destarched wheat bran has been evaluated (Beaugrand et al., 2004b). Initially, xylanase action on intact bran resulted in the loss of UV-induced autofluorescence in the periclinal wall near the endosperm (Beaugrand et al., 2004b). As hydrolysis of the anticlinal wall progressed towards the nucellar epidermis, the anticlinal wall collapsed, probably because AX constitutes much of its cell wall (Antoine et al., 2003). This corresponded to the loss of UV-induced autofluorescence throughout the cell which, in turn, coincided with both the loss of immunofluorescence of poorly substituted AX and the presence of immunogold labeling of xylanase throughout the aleurone layer (Beaugrand et al., 2004b). Finally, after 24 h of xylanase hydrolysis, the aleurone layer was completely destroyed as shown by toluidine blue staining (Beaugrand et al., 2004b). The aleurone layer is essentially

completely amorphous, which could help explain the loss of cell wall structure due to xylanase hydrolysis.

The resistance and susceptibility of the aleurone cell wall structure to thermal, protease, and alkaline treatments and corresponding observation using microscopy also have been used to understand the structure of the aleurone. Water extraction (24 h, 60 °C) did not alter the inner and outer wall layers of the aleurone cell wall stained with periodic acid-thiocarbohydrazide silver proteinate reagent (PATAg) (**Table 1.4**) (Beaugrand et al., 2004b). Aleurone cell wall structure was intact even after hydrothermal treatments at 180 °C and 200 °C (**Table 1.1**) (Merali et al., 2015). The aleurone cell wall resisted outward structural change due to hydrothermal treatment.

Carbohydrate and protein hydrolyzing enzymes alone are also not likely able to destroy aleurone cell walls as confirmed with fluorescence microscopy (**Table 1.2**) (Van Craeyveld et al., 2010; Santala et al., 2013; Arte et al., 2016). A heating step prior to endoxylanase treatment to inhibit native endoxylanase inhibitors (Beaugrand et al., 2004c) and possibly alter aleurone physical structure is seemingly necessary for the hydrolysis and loss of aleurone cell structure. Xylanase inhibitor protein 1 was located in the nucellar epidermis near the aleurone layer as described in **Table 1.2** (Jerkovic et al., 2010). This heating step can be associated with starch hydrolysis and/or an enzyme denaturation step prior to endoxylanase treatment. The complete loss of aleurone cell structure could help release and solubilize both aleurone protein in the cell contents and AX in the cell wall, which both have functional benefits (Swennen et al., 2006; Balandrán-Quintana et al., 2015). The sequential extraction of aleurone with water, 8M urea, and 0.5M potassium hydroxide resulted in an intact bilayered cell wall structure (water treatment), partial disruption of cell wall organization (water + urea treatment), and a mass of microfibrils

(water + urea + potassium hydroxide treatment) (**Table 1.4**) (Bacic and Stone 1981b). Consequently, sodium hydroxide is a solvent commonly used to extract protein from wheat bran, particularly from the aleurone layer (Balandrán-Quintana et al., 2015).

Nucellar epidermis and components

The nucellar epidermis layer is located next to the outer face of the aleurone layer. The key components of the nucellar epidermis have been examined by ATR-FTIR, SEM, LIBS, and confocal Raman microspectrometry. Using ATR-FTIR, a cuticle layer of lipidic material was detected on the outer face of the nucellar epidermis (Barron and Rouau, 2008). This also was reported by Evers and Reed (1988) using SEM. The outer cuticle of the nucellar epidermis also has been referred to as the inner cuticle of the testa (Bradbury et al., 1956; Dornez et al., 2011b). The cells of the nucellar epidermis layer, as well as testa and pericarp, contain cytoplasm at 11 days anthesis, but they collapse during wheat kernel development and expansion (Beaugrand et al., 2004a). The nucellar lysate forms as the nucellar epidermis cells are crushed during maturation (Beaugrand et al., 2004a). The nucellar lysate is an amorphous layer connecting the aleurone layer to the nucellar epidermis (Evers and Reed, 1988; Beaugrand et al., 2005). When the nucellar epidermis, testa and pericarp cells matured, they lost both water and volume (Beaugrand et al., 2004a).

The location of chemical components in the nucellar epidermis layer has been examined by confocal Raman microspectrometry, immunolabelling, CSLM, and TEM. The outer- and inner-faces of the nucellar epidermis gave similar Raman spectra, and both were rich in AX but contained less AX esterified with phenolic acids compared to the aleurone layer (Barron and

Rouau, 2008). Immunolabeling also detected AX and to a lesser degree β-glucan in the nucellar epidermis as referenced in **Table 1.2** (Dornez et al., 2011b). CSLM and TEM shows that AX is also present between the nucellar epidermis and aleurone and may have a role in the adhesion of the two layers (Guillon et al., 2004). This agrees with the results of a study that used ESEM to image bran treated with LIBS (reference Martelli et al., (2009) in **Table 1.3**). The nucellar epidermis and the periclinal wall of the aleurone layer abuting the nucellar epidermis were removed together indicating their firm attachment.

Xylanase hydrolysis partially destroyed the nucellar epidermis as shown by faint staining with toluidine blue and the loss of the labeled poorly substituted AX (Beaugrand et al., 2004b). The nucellar lystate may be responsible for slowing xylanase penetration through the nucellar epidermis as the lysate was shown to be a point of accumulation (Beaugrand et al., 2004b; Beaugrand et al., 2005). The nucellar epidermis structure was also reported to be lost after xylanase treatment (Van Craeyveld et al., 2010).

Testa and components

The testa layer is located next to the outer face of the nucellar epidermis and is comprised of an outer cuticle layer, two cellular layers that contain pigment, and in inner cuticle (reference Bradbury et al., 1956 in **Table 1.1**). The structure of the testa have been studied by microscopic techniques. SEM shows that the outer cuticle is attached to both the cross and tube cells of the pericarp by an adcrusting substance (Evers and Reed, 1988). Imaging with Nile Blue (see Fulcher and Wood, 1982 in **Table 1.2**) showed the outer cuticle of the testa layer is thicker than its inner cuticle, which is also referred to as the outer cuticle of the nucellar epidermis. Using

SEM, Evers and Reed (1988) reported that the testa was composed of two cell layers positioned at an angle to each other. Light microscopy images stained with toluidine blue also showed the testa to be composed of two layers of cells with histological differences between the two (Beaugrand et al., 2004b).

The location of chemical components in the testa has been determined by FTIR and Raman spectroscopy. The outer- and inner-face of the testa layer had different ATR- FTIR spectra (Barron and Rouau, 2008). The inner side showed a strong absorption for carbohydrates while the outer face had strong absorbance corresponding to lipidic components as well as carbohydrates (Barron and Rouau, 2008). Raman microscopy confirmed that the inner side presented lipidic components, carbohydrate, and phenolic acids (Barron and Rouau, 2008). The testa layer, which included the thick outer cuticle, cellular layer, and inner cuticle, was shown to be tightly adhered to the nucellar epidermis using LIBS (reference Martelli et al., (2009) in **Table 1.3**). The testa was the only layer not to give UV-induced autofluorescence indicating a lack of phenolic compounds (Beaugrand et al., 2004b). The absence of phenolics in the testa could indicate a lack of linked arabinoxylan. There is a lack of knowledge about the structure and composition of the cell walls of the color layer in the testa.

Xylanase treatment did not alter the physical structure of the testa, and labeled xylanase was not absorbed by the testa layer (Beaugrand et al., 2004a; Beaugrand et al., 2005). In addition, the testa and pigment layer were shown to be resistant to sulphuric acid treatment (Bradbury et al., 1956). Cutin present in the testa has been stated to be resistant to enzymatic and chemical hydrolysis (Ha et al., 1997). However, treatment of destarched and deproteinized wheat bran with a NaOH/urea solvent dissolved the testa layer as referenced in **Table 1.1** (Mense and Shi, 2018).

Pericarp and components

The structure of the pericarp layer has been studied using bright field microscopy, florescence microscopy, and SEM. The pericarp layer consists of the outer pericarp; epidermis and hypodermis and the inner pericarp; cross cells and tube cells (Antoine et al., 2003). The outer pericarp cells are arranged with their long axes parallel to the length of the grain (Bradbury et al., 1956; Antoine et al., 2003). The outer pericarp is comprised of multiple layers (reference Antoine et al., (2003) and Jerkovic et al., (2010) in **Table 1.2 and 1.3** respectively). The inner pericarp contains cells with their long axes perpendicular (cross cells) to the length of the grain (Bradbury et al., 1956; Antoine et al., 2003). Fissures between pericarp cells have been imaged using SEM (**Table 1.3**) (Lee and Atkey, 1984). The pitted appearance of the outer pericarp cells, intermediate layer cells, cross cells, and tube cells may be due to thin areas or actual pits (Bradbury et al., 1956). Weakly bound water can accumulate in these spaces and hollow cells as discussed in **Table 1.1** (Jacobs et al., 2015). At 11 days anthesis the pericarp cells contained cytoplasm, but once maturity was reached the cells were crushed (Beaugrand et al., 2004a) and underwent autolysis (Xiong et al., 2013) and became empty (Hemery et al., 2010; Jääskeläinen et al., 2013). The chemical components detected would then be expected to be located in the cell walls and not within the cell.

The limitations in our knowledge of this layer make it difficult to understand how it can be taken apart. Using ATR-FTIR, a cuticle layer of lipidic material was detected on the outer face of the pericarp (Barron and Rouau, 2008). The outer- and inner-face of the pericarp showed similar ATR-FTIR spectra (Barron and Rouau, 2008). Due to laser-induced fluorescence which

overwhelmed the spectra no Raman scattering from the pericarp could be collected (Barron and Rouau, 2008; Jääskeläinen et al., 2013). This has limited Raman data on the polymers located in this layer. The difficultly in using microscopy to image AX in the pericarp has been discussed by Dornez et al. (2011b) and summarized in **Table 1.2**. Calcofluor and acid Fuchsin staining were not able to image AX and β-glucan in the pericarp. For these reasons, the location of chemical components in the pericarp are not as easily determined as other layers.

Solid-state ^{13}C cross-polarization magic-angle spinning nuclear magnetic resonance (^{13}C CP/MAS NMR) has been used to determine compositional details and in particular differentiate between crystalline and amorphous structure in wheat bran (Ha et al., 1997; Gauthier et al., 2002; Locci et al., 2008), starch (Flanagan et al., 2015), and cellulose (Park et al., 2010; Foston, 2014). The outer pericarp has the highest concentration of cellulose (~23%) compared to the intermediate (~12%) and aleurone (~1%) layers (Antoine et al., 2003). The pericarp layer is likely the source of the crystalline cellulose. A ^{13}C CP/MAS NMR spectrum of hard white winter wheat bran is shown in **Figure 1.1** and the resonance assignment for each peak is summarized in **Table 1.5**. The C-4 and C-6 crystalline resonances of wheat bran cellulose are identified at 88-89 ppm and 65 ppm, respectively (**Table 1.5, Figure 1.1**).

In addition to solid-state ^{13}C-NMR, X-ray diffraction (XRD) and small angle X-ray scattering (SAXS) could be used to study the crystalline structure (crystallinity percentage, crystallite size, microfibril dimensions, and the ratio of crystalline to amorphous cellulose) of biopolymers but have not been used to study wheat bran. Furthermore, X-ray diffraction, SAXS, and ^{13}C CP/MAS NMR have not been utilized to analyze each individual separated layer of wheat bran. X-ray diffraction can determine crystallinity and its long-range order (Warren et al., 2016) in biopolymers such as cellulose (Pingali et al., 2010; Murata et al., 2015) and analyze

structures with sub nanometer dimensions (Martínez-Sanz et al., 2015). In addition to XRD, SAXS is another scattering technique that can be used to study plant cell wall structure (analyze structures from 1 nm to hundreds of nm) with minimal sample preparation and alteration to the original structure (Martínez-Sanz et al., 2015). ^{13}C CP/MAS NMR, XRD, and SAXS coupled with microscopy provide an opportunity to increase our understanding of wheat bran structure. Processing techniques that increase solubility and bioavailability could be selected as a result of an increased understanding of their effect on cell wall structure.

Treatment of pericarp structure

Treatment of the pericarp and corresponding analysis of its crystalline cellulose structure using XRD and solid-state NMR and observation using microscopy could help to understand why this layer is so difficult to be completely dissolved. Crystallinity in cell walls is an important factor affecting enzymatic, acid, hydrothermal and alkaline treatment of biomass (Xu et al., 2013). Cellulose is considered the only cell wall polymer in plant biomass with a partially crystalline structure. No evidence has been gathered that other polymers in plant cell walls contributes to crystallinity (Xu et al., 2013). Cellulose crystallites within cellulose microfibrils aggregate with amorphous polysaccharides, and all are embedded in amorphous lignin (Martínez-Sanz et al., 2015). Cellulose crystallinity in wheat bran is not easily destroyed. When wheat bran was ground, boiled in a salt solution, then treated with pancreatic α-amylase and pullulanase and defatted with acetone it retained its crystallinity (Ha et al., 1997). Commercial wheat bran moistened and digested with *Pleurotus ostreatus* also maintained its cellulose crystallinity (Locci et al., 2008). Gauthier et al. (2002) treated wheat bran with 2M H_2SO_4 at 100

°C for 30 min, followed by 0.01 M NaOH for 4 days at room temperature, and finally with 0.04 M HNO_3. They reported that the residual product contained crystalline cellulose. When destarched and deproteinized bran was treated with a NaOH/urea solvent, 84% of the bran was dissolved, leaving the inner and outer pericarp cell walls intact (**Tables 1.1 and 1.3**) (Mense and Shi, 2018). X-ray diffraction showed that the insoluble bran fraction exhibited a crystalline cellulose structure (Mense and Shi, 2018). The crystalline nature of the cellulose in combination with physical entanglement and covalent linkages could have prevented complete solubilization (Mense and Shi, 2018). These results show that some cellulose present in the wheat bran has an ordered crystalline structure, and is resistant to heat, alkali, and acid.

Xylanase treatment did not alter the pericarp cell wall physical structure as observed with bright field microscopy (see Beaugrand et al., 2004b in **Table 1.1**). Labeled xylanase was not absorbed on the layer indicating that its physical structure is impervious to xylanase enzyme (see Beaugrand et al., 2004a in **Table 1.1**). Isolation of pericarp exposes its outer layer of epidermis and hypodermis cells. Even so, these layers were not immunolabelled with xylanase nor was their cell wall structure hydrolyzed. Xylanase did not alter the cross cells in the isolated intermediate layer pericarp (Beaugrand et al., 2005). Enzymatic hydrolysis has been ineffective at solubilizing the pericarp layer, which could be due in part to a crystalline cellulose cell wall structure. In addition, physical association of between cell wall polymers could exclude enzymes and other dissolution solvents. The pericarp layer is likely the most difficult layer in wheat bran to solubilize due to its resistance to heat, alkali, acid, and enzyme treatment.

Conclusions

There are many unknowns related to the physical structure of wheat bran. Hydrothermal and xylanase treatment of wheat bran did not destroy the cell wall structure of the aleurone layer but the aleurone layer arabinoxylan can be almost totally digested with xylanase. The nucellar lysate was described as a barrier that slowed xylanase hydrolysis of the nucellar epidermis. The testa layer lacked phenolics and thus linked arabinoxylans. Predictably, it was not labelled with or hydrolyzed by xylanase. The testa layer is a barrier to xylanase hydrolysis working from the inner to outer bran layers. It was reported to be resistant to sulphuric acid treatment but was shown to dissolve when treated with a NaOH/urea solvent. The pericarp contains cellulose which is partially crystalline. Cellulose is the only partially crystalline component in wheat bran. Crystalline cellulose has been detected in wheat bran using ^{13}C CP/MAS NMR and XRD. The pericarp resists dissolution by xylanase and alkaline treatment, with its cell wall structure remaining intact. The distribution and organization of polysaccharides within the pericarp are not well defined. Determining the location of polymers in the pericarp using fluorescent dyes and Raman spectroscopy have been challenging due the presence of autofluorescence and the limited access to the cell wall polymers. Analysis by XRD, SAXS, and ^{13}C CP/MAS NMR techniques coupled with microscopy could overcome these challenges, and increase our understanding of wheat bran cell wall physical structure, in particular its cellulose crystalline structure, and how various processing techniques affect it. The inability for enzymes and solvents to fully solubilize wheat bran, specifically the pericarp, could be due to covalent cross-links, physical entanglement, molecular weight, and physical inaccessibility. A clearer understanding of wheat

bran physical structure can aid in developing it as an ingredient or a source of ingredients that increase its use in the food industry.

Acknowledgements

We thank Drs. Jon Faubion and Paul Seib of Kansas State University for reviewing and editing the manuscript. This is contribution no. 18-190-J from the Kansas Agricultural Experiment Station.

References

Antoine, C., Peyron, S., Mabille, F., Lapierre, C., Bouchet, B., Abecassis, J., Rouau, X., 2003. Individual contribution of grain outer layers and their cell wall structure to the mechanical properties of wheat bran. J. Agric. Food Chem. 51, 2026-2033.

Apprich, S., Tirpanalan, Ö., Hell, J., Reisinger, M., Böhmdorfer, S., Siebenhandl-Ehn, S., Novalin, S., Kneifel, W., 2014. Wheat bran-based biorefinery 2: Valorization of products. LWT – Food Sci. Technol. 56, 222-231.

Arte, E., Katina, K., Holopainen-Mantila, U., Nordlund, E., 2016. Effect of hydrolyzing enzymes on wheat bran cell wall integrity and protein solubility. Cereal Chem. 93, 162-171.

Bacic, A., Stone, B.A., 1981a. Isolation and ultrastructure of aleurone cell walls from wheat and barley. Aust. J. Plant Physiol. 8, 453-474.

Bacic, A., Stone, B.A., 1981b. Chemistry and organization of aleurone cell wall components from wheat and barley. Aust. J. Plant Physiol. 8, 475-495.

Balandrán-Quintana, R.R., Mercado-Ruiz, J.N., Mendoza-Wilson, A.M., 2015. Wheat bran proteins: A review of their uses and potential. Food Rev. Int. 31, 279-293.

Barron, C., Rouau, X., 2008. FTIR and raman signatures of wheat grain peripheral tissues. Cereal Chem. 85, 619-625.

Beaugrand, J., Crônier, D., Thiebeau, P., Schreiber, L., Debeire, P., Chabbert, B., 2004a. Structure, chemical composition, and xylanase degradation of external layers isolated from developing wheat grain. J. Agric. Food Chem. 52, 7108-7117.

Beaugrand, J., Reis, D., Guillon, F., Debeire, P., Chabbert, B., 2004b. Xylanase-mediated hydrolysis of wheat bran: Evidence for subcellular heterogeneity of cell walls. Int. J. of Plant Sci. 165, 553-563.

Beaugrand, J., Crônier, D., Debeire, P., Chabbert, B., 2004c. Arabinoxylan and hydroxycinnamate content of wheat bran in relation to endoxylanase susceptibility. J. Cereal Sci. 40, 223-230.

Beaugrand, J., Paës, G., Reis, D., Takahashi, M., Debeire, P., O'Donohue, M., Chabbert, B., 2005. Probing the cell wall heterogeneity of micro-dissected wheat caryopsis using both active and inactive forms of a GH11 xylanase. Planta. 222, 246-257.

Bradbury, D., MacMasters, M.M., Cull, I.M., 1956. Structure of the mature wheat kernel II. Microscopic structure of pericarp, seed coat, and other coverings of the endosperm and germ of hard red winter wheat. Cereal Chem. 33, 342-360.

De Brier, N., Hemdane, S., Dornez, E., Gomand, S.V., Delcour, J.A., Courtin, C.M., 2015. Structural, chemical composition and enzymatic activities of pearlings, and bran obtained from pearled wheat (*Triticum aestivum* L.) by roller milling. J. Cereal. Sci. 62, 66-72.

Delcour, J. A., Hoseney, R. C., 2010. Principles of Cereal Science and Technology, third ed. St. Paul, MN AACC.

Dornez, E., Cuyvers, S., Holopainen, U., Nordlund, E., Poutanen, K., Delcour, J.A., Courtin, C.M., 2011a. Inactive fluorescently labeled xylanase as a novel probe for microscopic analysis of arabinoxylan containing cereal cell walls. J. Agric. Food Chem. 59, 6369-6375.

Dornez, E., Holopainen, U., Cuyvers, S., Poutanen, K., Delcour, J.A., Courtin, C.M., Nordlund, E., 2011b. Study of grain cell wall structures by microscopic analysis with four different staining techniques. J. Cereal Sci. 54, 363-373.

Escarnot, E., Dornez, E., Verspreet, J., Agneessens, R., Courtin, C.M., 2015. Quantification and visualization of dietary fibre components in spelt and wheat kernels. J. Cereal Sci. 62, 124-133.

Evers, A.D., Reed, M., 1988. Some novel observations by scanning electron microscopy on the seed coat and nucellus of the mature wheat grain. Cereal Chem. 65, 81-85.

Flanagan, B.M., Gidley, M.J., Warren, F.J., 2015. Rapid quantification of starch molecular order through multivariate modelling of ^{13}C CP/MAS NMR spectra. Chem. Commun. 51, 14856.

Foston, M., 2014. Advances in solid-state NMR of cellulose. Curr. Opin. Biotechnol. 27, 176-184.

Fulcher, R.G., O'Brien, T.P., Lee, J.W., 1972. Studies on the aleurone layer I. conventional and fluorescence microscopy of the cell wall with emphasis on phenol-carbohydrate complexes in wheat. Aust. J. Biol. Sci. 25, 23-34.

Fulcher, R.G., Wood, P.J., 1982. In book: New Frontiers in Food Microstructure 392 p, Chapter: Identification of cereal carbohydrates by fluorescence microscopy, Publisher: American Association of Cereal Chemists, Inc: St Paul, MN, USA illus, Editors: DB Bechtel, pp.111-147.

Gauthier, A., Derenne, S., Dupont, L., Guillon, E., Largeau, C., Dumonceau, J., Aplincourt, M., 2002. Characterization and comparison of two lingo-cellulosic substrates by 13C CP/MAS, XPS, conventional pyrolysis and thermochemolysis. Anal. Bioanal. Chem. 373, 830-838.

Guillon, F., Tranquet, O., Quillien, L., Utille, J.-P., Ortiz, J.J.O., Saulnier, L., 2004. Generation of polyclonal and monoclonal antibodies against arabinoxylans and their use for immunocytochemical location of arabinoxylans in cell walls of endosperm of wheat. J. Cereal Sci. 40, 167-182.

Ha, M-A., Jardine, W.G., Jarvis, M.C., 1997. Solid-State ^{13}C NMR of cell walls in wheat bran. J. Agric. Food Chem. 45, 117-119.

Harris, P.J., Chavan, R.R., Ferguson, L.R., 2005. Production and characterization of two wheat-bran fractions: an aleurone-rich and pericarp-rich fraction. Mol. Nutr. Food Res. 49, 536-545.

Hell, J., Donaldson, L., Michlmayr, H., Kraler, M., Kneifel, W., Potthast, A., Rosenau, T., Böhmdorfer, S., 2015. Effect of pretreatment on arabinoxylan distribution in wheat bran. Carbohydr. Polym. 121, 18-26.

Hemery, Y.M., Mabille, F., Martelli, M.R., Rouau, X., 2010. Influence of water content and negative temperatures on the mechanical properties and its constitutive layers. J. Food Eng. 98, 360-369.

Jääskeläinen, A.-S., Holopainen-Mantila, U., Tamminen, T., Vuorinen, T., 2013. Endosperm and aleurone cell structure in barley and wheat as studied by optical and raman microscopy. J. Cereal Sci. 57, 543-550.

Jacobs, P.J., Hemdane, S., Dornez, E., Delcour, J.A., Courtin, C.M., 2015. Study of hydration properties of wheat bran as a function of particle size. Food Chem. 179, 296-304.

Jamme, F., Robert, P., Bouchet, B., Saulnier, L., Dumas, P., Guillon, F., 2008. Aleurone cell walls of wheat grain: High spatial resolution investigation using synchrotron infrared microspectroscopy. Appl. Spectrosc. 62, 895-900.

Jerkovic, A., Kriegel, A.M., Bradner, J.R., Atwell, B.J., Roberts, T.H., Willows, R.D., 2010. Strategic distribution of protective proteins within bran layers of wheat protects the nutrient rich endosperm. Plant Physiol. 152, 1459-1470.

Kiszonas, A.M., Fuerst, P., Morris, C.F., 2013. Wheat arabinoxylans structure provides insight into function. Cereal Chem. 90, 387-395.

Lee, D.R., Atkey, P.T., 1983. Water loss from the developing caryopsis of wheat (*Triticum aestivum*). Can. J. Bot. 62, 1319-1326.

Locci, E., Laconi, S., Pompei, R., Scano, P., Lai, A., Marincola, F.C., 2008. Wheat bran biodegradation by Pleurotus ostreatus: A solid-state carbon-13 NMR study. Bioresour. Technol. 99, 4279-4284.

Martelli, M.R., Barron, C., Delaporte, P., Viennois, G., Rouau, X., Sadoudi, A., 2009. Pulsed laser ablation: A new approach to reveal wheat outer layer properties. J. Cereal Sci. 49, 354-362.

Martínez-Sanz, M.M., Gidley, M.J., Gilbert, E.P., 2015. Application of X-ray and neutron small angle scattering techniques to study the hierarchical structure of plant cell walls: A review. Carbohydr. Polym. 125, 120-134.

Mense, A.L. and Shi, Y.-C., 2018. Dissolution of wheat bran by NaOH/Urea solutions and structure of soluble materials. ACS Sustainable Chem. Eng. DOI: 10.1021/acssuschemeng.7b04707.

Merali, Z, Collins, S.R.A., Elliston, A., Wilson, D.R., Käsper, A., Waldron, K.W., 2015. Characterization of cell wall components of wheat bran following hydrothermal pretreatment and fractionation. Biotechnol. Biofuels. 8, 23.

Morrison, I.N., 1975. Ultrastructure of the cuticular membranes of the developing wheat grain. Can. J. Bot. 53, 2077-2087.

Morrison, I.N., Kuo, J., O'Brien, T.P., 1975. Histochemistry and fine structure of developing wheat aleurone cells. Planta. 123, 105-116.

Murata, Y., Kubo, S., Togawa, E., Ramle, S.F.B.M., Sulaiman, O., Hashim, R., Ibrahim, W.A., Kosugi, A., Hirooka, A., Abe, H., 2015. Detection of vascular bundles using cell wall birefringence on exposure to polarized light. Ind. Crops Prod. 65, 190-197.

Onipe, O.O., Jideani, A.I.O., Beswa, D., 2015. Composition and functionality of wheat bran and its application in some cereal food products. Int. J. Food Sci. Technol. 50, 2509-2518.

Park, S., Baker, J.O., Himmel, M.E., Parilla, P.A., Johnson, D. K., 2010. Cellulose crystallinity index: measurement techniques and their impact on interpreting cellulase performance. Biotechnol. Biofuels. 3, 10.

Philippe, S., Tranquet, O., Utille, J.-P., Saulnier, L., Guillon P., 2007. Investigation of ferulate deposition in endosperm cell walls of mature and developing wheat grains by using polyclonal antibody. Planta. 225, 1287-1299.

Pingali, S.V., Urban, V.S., Heller, W.T., McGaughey, J., O'Neill, H., Foston, M., Myles, D.A., Ragauskas, A., Evans, B.R., 2010. Breakdown of Cell Wall Nanostructure in Dilute Acid Pretreated Biomass. Biomacromolecules. 11, 2329-2335.

Piot, O., Autran, J.-C., Manfait, M., 2000. Spatial distribution of protein and phenolic constituents in wheat grain as probed by confocal raman microspectroscopy. J. Cereal Sci. 32, 57-71.

Prückler, M., Siebenhandl-Ehn, S., Apprich, S., Höltinger, S., Haas, C., Schmid, E., Kneifel, W., 2014. Wheat bran-based biorefinery 1: Composition of wheat bran and strategies of functionalization. LWT – Food Sci. Technol. 56, 211-221.

Rhodes, D.I., Sadek, M., Stone, B.A., 2002. Hydroxycinnamic acids in walls of wheat aleurone cells. J. Cereal Sci. 36, 67-81.

Rhodes, D.I., Stone, B.A., 2002. Proteins in walls of wheat aleurone cells. J. Cereal Sci. 36, 83-101.

Rosa-Sibakov, N., Poutanen, K., Micard, V., 2015. How does wheat grain, bran and aleurone structure, impact their nutritional and technological properties? Trends Food Sci. Technol. 41, 118-134.

Saadi, A., Lempereur, I., Sharonov, S., Autran, J.C., Manfait, M., 1998. Spatial distribution of phenolic materials in durum wheat grain as probed by confocal fluorescence spectral imaging. J. Cereal Sci. 28, 107.114.

Santala, O.K., Nordlund, E.A., Poutanen, K.S., 2013. Treatments with xylanase at high (90%) and low (40%) water content have different impacts on physicochemical properties of wheat bran. Food Bioprocess. Technol. 6, 3102-3112.

Swennen, K., Courtin, C.M., Lindemans, G.C.J.E., Delcour, J.A., 2006. Large-scale production and characterization of wheat bran arabinoxylooligosaccharides. J. Sci. Food Agric. 86, 1722-1731.

Van Craeyveld, V., Holopainen, U., Selinheimo, E., Poutanen, K., Delcour, J.A., Courtin, C.M., 2009. Extensive dry ball milling of wheat and rye bran leads to *in situ* production of arabinoxylan oligosaccharides through nanoscale fragmentation. J. Agric. Food Chem. 57, 8467-8473.

Van Craeyveld, V., Dornez, E., Holopainen, U., Selinheimo, E., Poutanen, K., Delcour, J.A., Courtin, C.M., 2010. Wheat bran AX properties and choice of xylanase affect production of wheat bran-derived arabinoxylan-oligosaccharides. Cereal Chem. 87, 283-291.

Warren, F.J., Gidley, M.J., Flanagan, B.M., 2016. Infrared spectroscopy as a tool to characterize starch-ordered structure – a joint FTIR-ATR, NMR, XRD and DSC study. Carbohydr. Polym. 139, 35-42.

Xiong, F., Yu, X.R., Zhou, L., Wang, F., Xiong, A.S., 2013. Structural and physiological characterization during wheat pericarp development. Plant Cell Rep. 32, 1309-1320.

Xu, F., Shi, Y.-C., Wang, D., 2013. X-ray scattering studies of lignocellulosic biomass: A review. Carbohydr. Polym. 94, 904-917.

Yan, X., Ye, R., Chen, Y., 2015. Blasting extrusion processing: The increase of soluble fiber content and extraction of soluble fiber polysaccharides from wheat bran. Food Chem. 180, 106-115.

Table 1.1 Morphology and heterogeneity of mature wheat bran as discovered by light microscopy.[1]

Major findings	References
The testa with its thicker outer cuticularized layer, color layer, and thinner inner cutin layer were identified. The color layer was shown to be composed of two cellular layers and were oriented, so the cells crossed at a 45° angle. The testa and pigment layer were shown to be resistant to sulphuric acid treatment. The nucellar epidermis cell morphology was imaged.	Bradbury et al., 1956
The aleurone inner wall layer and portions of the anticlinal wall and periclinal wall near the nucellar epidermis remained intact after 12 days of germination.	Fulcher et al., 1972
The outer cuticle thickness, the degree to which the pericarp cells were crushed during maturation, and the amount/size of protein bodies in subaleurone cells could affect water penetration rate into the endosperm.	Moss, 1973
The aleurone cell wall and nucellar epidermis were the only bran structures immunolabelled with xylanase and were partially degraded by xylanase. The ferulic acid monomer ester linkage on AX did not hinder xylanase efficiency. This is confirmed in the hydrolysis of the aleurone layer.	Beaugrand et al., 2004a
The cellular structure of the pericarp and testa was not changed and the aleurone structure was lost after xylanase treatment of destarched wheat bran.	Beaugrand et al., 2004b
Wheat bran milled to 1687 µm showed intact bran structure, 520 µm bran showed isolated pericarp and aleurone layers, and 77 µm bran lost its organized cell wall cell structure. The amount of strongly bound water in cell wall nanopores and through hydrogen bonding was the same for each bran particle size. The amount of weakly bound water held between bran particles and bran layers was greater for wheat bran of larger particle size.	Jacobs et al., 2015
Hydrothermal treatment of destarched bran at 180 °C and 200 °C resulted in coloration of the aleurone layer due to the Mallard reaction and oxidation of lipids.	Merali et al., 2015
Bran treated with a NaOH/urea solvent resulted in the dissolution of each layer except the outer and inner pericarp. The color layer was lost indicating the testa was dissolved. Intact cross cells and outer pericarp cells were imaged.	Mense and Shi, 2018

[1]AX = arabinoxylans.

Table 1.2 Morphology and heterogeneity of mature wheat bran as discovered by fluorescence microscopy.[1]

Major findings	References
During germination, the periclinal wall facing the endosperm was hydrolyzed first followed by the anticlinal cell wall, and lastly the periclinal wall facing the nucellar epidermis.	Fulcher et al., 1972
β-D-glucans were imaged using Congo Red that showed their presence in the aleurone periclinal walls near the endosperm and nucellar epidermis. The double cuticle of the testa was imaged using Nile Blue A with the outer cuticle appearing to be thicker.	Fulcher and Wood, 1982
UV-induced autofluorescence of isolated aleurone cell walls deceased but persisted in intensity after 1 M NaOH treatment. This indicated that some phenolic compounds are not ester-linked to AX but may be covalently linked to proteins.	Rhodes et al., 2002
UV induced autofluorescence of isolated aleurone cell walls remained after hydrogen fluoride/pyridine treatment. This indicated that some phenolic compounds may be covalently linked with protein.	Rhodes and Stone, 2002
The outer pericarp was three layers thick. Aleurone layer cells contained fluorescent granular inclusions.	Antoine et al., 2003
Xylanase simultaneously hydrolyzed AX from both periclinal walls of isolated aleurone allowing for quicker penetration into the anticlinal cell wall. AX was visualized by UV autofluorescence.	Beaugrand et al., 2005
Exhaustive ball milling of wheat bran resulted in the complete loss of wheat bran tissue structure as visualized with Calcofluor and Acid Fuchsin staining.	Van Craeyveld et al., 2009
Wheat bran extensibility and stiffness were positively and negatively correlated respectively with both moisture and temperature.	Hemery et al., 2010
Confocal immunomicroscopy was used to determine the location of several proteins throughout the wheat bran layers. Oxalate oxidase was distributed throughout the outer pericarp, xylanase inhibitor protein 1 was located in the nucellar epidermis adjacent to the aleurone layer, and pathogenesis-related protein 4 was located in the aleurone and also in the testa.	Jerkovic et al., 2010
Xylanase treatment separated the aleurone from the nucellar epidermis. After xylanase hydrolysis, the aleurone cell walls remained intact while the nucellar epidermis was completely degraded as visualized by Calcofluor and Acid Fuchsin staining.	Van Craeyveld et al., 2010
AX in bran was imaged using inactive fluorescently labeled xylanase. AX was stained in the testa, nucellar epidermis, and aleurone but not the pericarp. It is less time intensive and complex than the immunolabeling technique.	Dornez et al., 2011a
A xylanase probe, immunolabeling of AX, and Calcofluor and Acid Fuchsin staining were unable to image AX and β-glucan in the pericarp. Phenolic acids likely contributed to autofluorescence,	Dornez et al., 2011b

which overwhelmed the staining. Most of the AX was found to be in the aleurone and nucellar epidermis.	
UV-autofluorescence showed that ferulic acid was more concentrated in the anticlinal walls of the aleurone than the periclinal. The periclinal walls near the endosperm were stained more intensively with Calcofluor, indicating a higher concentration of β-glucan, than in the anticlinal walls.	Jääskeläinen et al., 2013
A bran mixture with 40% water resulted in more protein released during mixing than bran with 90% water. Endoxylanase treatment had little effect on the level of protein in the mixtures as visualized using Calcofluor and Acid Fuchsin stain. The aleurone cell wall structure was still intact after xylanase treatment.	Santala et al., 2013
Pearling wheat kernels removed bran from the rounded portions of the kernel more so than the flat regions as visualized with epifluorescence microscopy.	De Brier et al., 2015
A fluorescently labelled xylanase probe showed strong intensity for the aleurone and subaleurone layers around the crease. Calcofluor staining was observed in the aleurone layer around the crease.	Escarnot et al., 2015
Ball milling treatment resulted in the purest AX extract and lye appeared to dissolve most material as imaged using the immunolocalization of AX	Hell et al., 2015
After hydrothermal pretreatment at 180 °C and 200 °C, the blue autofluorescence at a neutral pH was reduced indicating a possible decrease in lignin content. A reduction in green autofluorescence at alkaline pH indicated a decrease in ferulic acid content.	Merali et al., 2015
Neutral protease did not significantly hydrolyze proteins within the aleurone cells but mainly solubilized proteins in the subaleurone and carbohydrate-hydrolyzing enzymes did not increase protein solubilization as imaged using a Calcofluor and Acid Fuchsin stain. The aleurone cell wall structure remained intact after treatment with protein and carbohydrate (high in xylanase activity) hydrolyzing enzymes. The seed coat and pericarp autofluoresced orange and light green/yellowish respectively.	Arte et al., 2016

[1]AX = arabinoxylan; CSLM = Confocal laser scanning microscopy; intermediate layer = cross cells + tube cells, + testa + nucellar epidermis.

Table 1.3 Morphology and heterogeneity of mature wheat bran as discovered by SEM.[1]

Major findings	References
The outer surface of the aleurone cell contents had rough and smooth textures.	Bacic and Stone, 1981a
Fissures were found to be present between cells of the pericarp layer where the cell walls come together.	Lee and Atkey, 1984
The nucellar lysate, an amorphous layer between the aleurone and nucellar epidermis, was reported.	Evers and Reed, 1988
Field-emission scanning electron microscopy found that after a pericarp and aleurone rich wheat bran fraction were fed to a rat the pericarp fraction was unaffected while the aleurone cell walls were partially degraded.	Harris et al., 2005
ESEM was used to image bran treated with LIBS. The outer pericarp was removed initially showing damaged cross and tube cells perpendicular to each other. The inner pericarp was removed next exposing the unaltered testa. Next, the testa was removed exposing the partially damaged nucellar epidermis. The nucellar epidermis and the periclinal wall near the nucellar epidermis were removed together indicating their firm attachment. The damaged aleurone layer was left.	Martelli et al., 2009
The multiple layers of the outer pericarp were shown. The cross cells and tube cells of the inner pericarp were imaged that showed more intercellular spaces between tube cells than the cross cells.	Jerkovic et al., 2010
Bran treated with blasting extrusion processing induced the formation of holes on the residual bran and it appeared course.	Yan et al., 2015
Bran treated with a NaOH/urea solvent resulted in the dissolution of each layer except the outer and inner pericarp. The structure of the cross cells were still intact after treatment.	Mense and Shi, 2018

[1]ESEM = Environmental scanning electron microscopy; LIBS = Laser-induced breakdown spectroscopy; and SEM = Scanning electron microscopy.

Table 1.4 Morphology and heterogeneity of mature wheat bran as discovered by TEM.[1]

Major findings	References
The outer- and inner-cuticles of the testa were imaged. The inner cuticle lacked substructure while the outer cuticle appeared to have a thin underlying cuticle layer.	Morrison, 1975
The aleurone cell wall was bilayered with a thin inner wall adjacent to the cell contents which was transversed by plasmodesmata. The aleurone cell granules were surrounded by lipids. The cell contents also contained mitochondria and plastids.	Morrison et al., 1975
The aleurone cell wall was bilayered with a thin inner wall adjacent to the lumen and a thick outer wall with a distinct middle lamella when stained with uranyl acetate and lead citrate. Plasmodesmata were present in the cell wall.	Bacic and Stone 1981a
A boundary was present between the aleurone inner and outer cell wall layers. The aleurone cell wall structure was destroyed with 8M urea followed by 0.5M potassium hydroxide treatment which released a mass of microfibrils which comprised the wall structure.	Bacic and Stone, 1981b
The aleurone inner and outer wall layers had different polysaccharide distributions as evidenced with PATAg staining. Water extraction (24 h, 60 °C) was also found not to alter the PATAg stained inner and outer wall layers of the aleurone cell wall.	Beaugrand et al., 2004b
Indirect immunogold labelling of feruloylated AX with pAb anti-5-O-Fer-Ara, stained with uranyl acetate showed that no heterogeneity existed in the distribution of feruloylated AX for periclinal and anticlinal walls.	Philippe et al., 2007

[1]TEM = Transmission electron microscopy; PATAg = Periodic acid-thiocarbohydrazide silver proteinate reagent; and AX = arabinoxylan.

Table 1.5 Solid-State ^{13}C CP/MAS NMR resonance assignments of wheat bran.[1,2]

Peak	Chemical Shift, ppm	Wheat bran
1	170-174	Carbonyl carbons of esters/amides (acetate groups of glucuronic acid in hemicellulose, carbonyl groups of cutin and lipids, and amide carbons of proteins)
Not identified	153	Oxygen substituted aromatic carbons in lignin, 4-O-etherified syringyl residues in lignin
Weak signals	110-160	Aromatic carbons
Weak signals	120-140	Aromatic carbons of phenolic moieties in cutin, olefinic carbons in lipids, guaiacyl lignin units
2	109	C-1 of L-arabinofuranose in arabinoxylans
3	105	C-1 of D-glucopyranose in cellulose
4	102-103 (shoulder)	C-1 of D-xylose in arabinoxylans, and C-1 of D-glucopyranose in starch
See peaks 2, 3, 4	90-120	Di-O-alkyl carbons
5	88-89 (shoulder)	C-4 of crystalline cellulose
6	82-85 (shoulder)	C-4 carbons of amorphous cellulose, starch, and xylan
7	73, 75 (doublet)	Overlapping signals due to C-2, C-3, C-5 carbons of glucans and C-2 and C-3 of xylans
8	65 (shoulder)	C-6 of crystalline cellulose
9	62	C-6 carbons of amorphous cellulose and starch
10	56	Methoxy groups of mostly hemicellulose possibly minor contribution from lignin
See peaks 5, 6, 7, 8	65-90	O-alkyl carbons
Not identified	41	Protein side-chain carbons
11	28-32	Bulk methylene in cutin (hydrocarbon chains) and lipids
12	21-22	Alkyl groups of acetyl
See peaks 11, 12	0-45	Alkyl carbon peaks

[1]Resonances assigned based on Ha et al. 1997; Gauthier et al. 2002; Locci et al. 2008.
[2]Peak numbers are shown in Fig. 1.1.

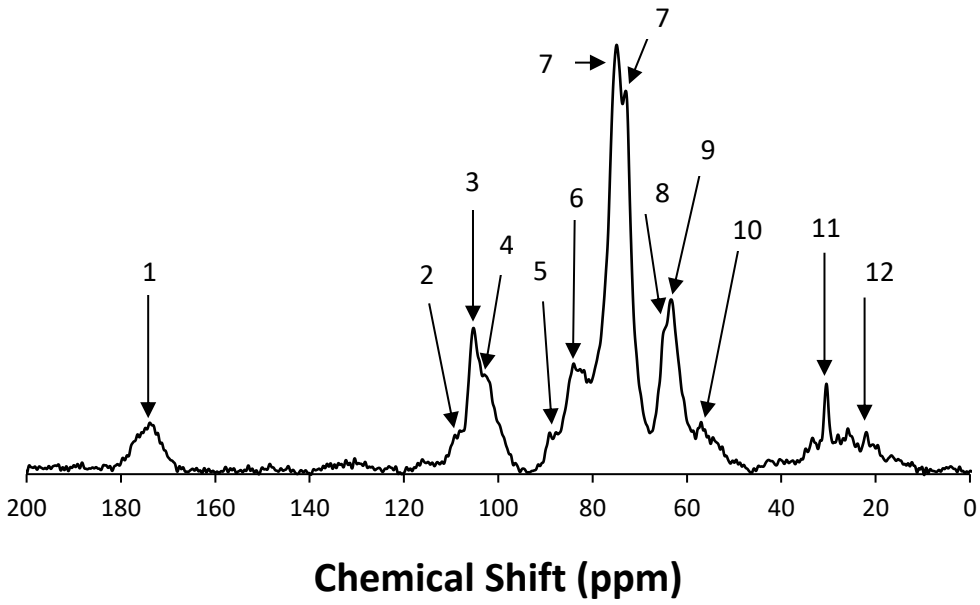

Figure 1.1 Solid-state ^{13}C CP/MAS NMR of hard white winter wheat bran analyzed at ~25% moisture. The resonance of each peak is assigned in Table 1.5.

Chapter 2 - Physical structure of wheat bran and its dissected layers

Abstract

The objectives of this work were to 1) determine the physical structure of untreated wheat bran and the differences in physical structure between its dissected layers; 2) evaluate how bran hydration affected bran crystallinity and polymer order; and 3) determine how enzymatic treatment of wheat bran affected its physical structure. For the first time, X-ray diffraction (XRD), small angle X-ray scattering (SAXS), and solid-state ^{13}C cross-polarization magic-angle spinning nuclear magnetic resonance (^{13}C CP/MAS NMR) were used to study the physical structure of wheat bran and its dissected layers. The XRD and solid-state ^{13}C CP/MAS NMR both confirmed the presence of crystalline cellulose in untreated bran, enzymatically treated bran, and dissected bran layers. Most of the crystalline cellulose was present in the outer pericarp with a much lower proportion in the intermediate layer. The aleurone layer was completely amorphous. The treatment of destarched and deproteinized bran (DSDPB) with the Updegraff reagent removed amorphous material, leaving its crystalline cellulose structure intact. Hydration of the outer pericarp increased the signal intensity of its XRD diffractogram and CP/MAS NMR spectrum and indicated a possible increase in polymer order. The SAXS confirmed that cell wall polymers, possibly cellulose microfibrils, increased in size as a result of hydration. The cell walls of each layer exhibited birefringence due to the orientation of cell wall components. Birefringence was observed in amorphous cell walls such as in the aleurone layer.

Introduction

To understand the functional and nutritional properties of wheat bran and better use of wheat bran in food, it is critical to understand the physical structure of wheat bran. Structure and composition determine how grain is processed as well as its nutritional value.[1,2] Knowledge of wheat bran physical structure and how it is assembled will increase our understanding of how to take it apart or change its structure via processes such as dry milling, extrusion, and enzymatic hydrolysis.[2] The disintegration of or change in wheat bran structure can aid in making it a more nutritious product[2] thus increasing its value and utilization as a food ingredient. In this case, more nutritious means achieving a desired physiological response and increased bioaccessibility and bioavailability of nutrients.[2]

Approximately 90 million tons of wheat bran is produced by the flour milling industry each year.[3] Wheat bran is a good source of fiber with the majority existing as insoluble fiber.[4] In wheat bran, non-starch polysaccharides such as glucuronoarabinoxylans, cellulose, and mixed linked (1-3), (1-4) β-D glucan make up 46% of the wheat bran with protein and lignin contributing 10-20% and 4-8% to the bran respectively.[5] The recommended dietary fiber intakes are not being met by the majority of the population.[4] Consumption of more food products containing wheat bran would help people achieve the dietary fiber intake recommendations.[4] Epidemiological studies have shown that bran consumption lowers the risk of diabetes and heart disease, decreases gastrointestinal transit time, increases fecal weight, alleviates constipation and diarrhea, improves gut health, and reduces glycemic response.[4,6,7] Cell wall polysaccharides, in particular those that constitute dietary fiber,[7] are responsible in part for these health effects with arabinoxylans providing the most potential for health and functional benefits as they are the main

non-starch polysaccharide representing 40% of destarched and deproteinized wheat bran.[2,8] The difficulty in deconstruction and utilization of functional wheat bran components, such as arabinoxylans, comes from the complexity of the cell wall. These polymers are held in the cell wall through non-covalent bonds and covalent cross linkages.[9] The assembly of the main cell wall polymers and their hierarchical structure (cellulose, hemicellulose, protein, lignin) in biomass plant cell walls is unknown.[10,11] Cellulose molecules form hierarchically assembled microfibrils that are 2-4 nm in diameter and likely consist of 18 individual cellulose chains that are comprised of crystalline and amorphous domains.[11,12] Cellulose microfibrils aggregate together and with other cell wall polymers through physical association (hydrogen bonding via hydroxyl groups) to form microfibril aggregates (100-1000 nm in diameter).[11] Cell wall polymers interact differently at different hierarchical levels.[11] Small angle X-ray scattering (SAXS) and X-ray diffraction (XRD) can be used to study polymer structure at different structural levels with minimal sample preparation.[11] These instruments could be used to evaluate how various processing treatments effect cell wall physical structure to determine optimal processing methods.[10]

X-ray diffraction is a non-invasive technique that can assess crystallinity and long-range order where there is periodicity to the structure in the sub nanometer dimensions.[11,13,14,15] X-ray diffraction is used to study structure of the inter atomic length scale and can be used to probe the crystalline and semi-crystalline structure of carbohydrate polymers,[14] such as cellulose crystallinity, crystalline orientation, conformation, and domain size.[10] A disadvantage of XRD is that polymers not contributing to molecular order (amorphous protein, hemicellulose, lignin, and cellulose) can affect the diffractogram.[16,17] Small angle X-ray scattering is used to study electron density at the colloidal dimension (mesoscopic length scale) between the atomic and microscopic

structures (tens and several thousand Å), which corresponds with cellulose microfibril structure features.[14,18,19] Small angle X-ray scattering is commonly used to study polymer morphology.[20]

Solid-state ^{13}C cross-polarization magic-angle spinning nuclear magnetic resonance (^{13}C CP/MAS NMR) is a non-invasive technique that can analyze the structure of plant materials without the isolation and solubilization, which can change the structure.[21,22] The ^{13}CP/MAS NMR increases the signal to noise ratio of carbons in rigid domains (such as crystalline cellulose)[22] providing molecular structure information at the sub nm level.[13,23] The ^{13}C CP/MAS NMR allows for structural characterization even when the sample contains other polymers of less interest[16] providing a means to study plant cell walls without altering their structure.[24] The C4 resonance is commonly used to evaluate cellulose structure. The amorphous and crystalline carbons give different resonances due to the ability of NMR to differentiate chemically equivalent carbons if they are in different magnetic environments, e.g. from packing or conformational differences.[25,26]

Non-invasive techniques such as solid-state NMR[26], XRD[11], and SAXS[27] can be used to explore the physical structure of biopolymers in food and how they are impacted by various processes such as hydrothermal, acid, and enzymatic hydrolysis and alkaline dissolution. The ^{13}C CP/MAS NMR has been used to determine wheat bran composition and in particular the presence of crystalline structure in intact wheat bran.[21,22,28] The XRD and SAXS have not been previously used to study wheat bran structure. The ^{13}C CP/MAS NMR, XRD, and SAXS have never been used to study the physical structure of dissected bran layers. In this study, we dissected wheat bran and isolated outer pericarp (OP), intermediate layer (IL), and aleurone layer (AL). The objectives were to 1) determine the physical structure of untreated wheat bran and the differences in physical structure between its dissected layers; 2) evaluate how bran hydration

impacted bran crystallinity and polymer order; 3) determine how enzymatic treatment of wheat bran affected its physical structure.

Materials and methods

Materials

A hard red winter wheat (variety Everest) was obtained from the Kansas Foundation Seed Project (Manhattan, KS) and milled using the Buhler method for hard wheat. The bran fraction was collected.

Stargen II (Genencor, Palo Alto, CA), an α-amylase and glucoamylase blend,[29] was used to hydrolyze adhering starch of wheat bran. Stargen II had an enzyme activity of 570 GAU/g (Glucoamylase Unit/g). One GAU was the amount of enzyme that could release one gram of reducing sugar (glucose) per hour from soluble starch substrate under standard assay conditions. Protex 14L (Genencor, Palto Alto, CA), a neutral bacterial thermostable protease, was added to hydrolyze bran protein. Protex 14L had an enzyme activity of 160 units/g. One unit was the amount of enzyme that produced 200 µg of tyrosine-equivalent trichloracetic acid soluble peptides per minute from a casein substrate under standard assay conditions (pH = 6.5, 35 ˚C).

Preparation of wheat bran

The Buhler experimental mill MLU202 (Buhler Inc., Switzerland) was set up to mill hard wheat according to AACC 26-21.02.[30] A feed rate of 80 g of wheat/min was used to obtain a

76% flour extraction. The wheat bran, once collected, was ground using a Ross table top roll stand (serial # 915, size 9x6; Oklahoma City, OK) (20/22 corrugations per square inch; 2.5:1 differential) to a 200 µm particle size. The roll gap was set to 0.003 in. The bran was milled 2X and then sifted using a Great Western Sifter for 2 min over a sieve stack of 300 µm > 200 µm > 132 µm > Pan. The overs from the 300 µm screen were milled twice more and then sifted. This process was repeated until all bran passed through the 300 µm screen. The particle size distribution of milled wheat bran was determined on a standard Tyler Ro-tap sieve shaker (W. S. Tyler, Mentor, OH), utilizing various screen sizes as described below in the particle size distribution section.

The 200 µm bran will be referred to as untreated bran (UB). Destarched bran (DSB) was prepared by making a 12.5% (w/v) mixture of bran (50 g) and water (350 mL) with the pH adjusted to 4.0 with 0.5 N HCl. Stargen II (80 µL) was added. The mixture was stirred at 35 °C for 15 h, at which time, the undissolved pellet (bran) was collected by centrifuging the mixture at 21,100 × g for 15 min. The pellet was collected, and the supernatant discarded. A fresh 12.5% (w/v) mixture was prepared (by diluting to volume) using the pellet and its pH was adjusted to 4.0 using 0.5 N HCl, after which a second dose of Stargen II (80 µL) was added. The mixture was stirred at 35 °C for another 15 h to complete the starch hydrolysis and the pellet was collected by centrifuging the mixture. The pellet was washed three times with water (250 mL each time), centrifuging after each wash to remove the water solubles. The washed pellet was freeze dried.

Destarched and deproteinized bran (DSDPB) was prepared using the procedure for DSB up to the point where the wheat bran was washed. After the removal of the water solubles from the starch digestion, a fresh 12.5% (w/v) mixture was prepared (by diluting to volume) and the

pH was adjusted to 7.5 using 0.5 N NaOH. Protex 14L was added (2.5 mL) and incubated at 65 °C for 5 h with continuous stirring. The pH was kept at 7.5 with additions of 0.5 N NaOH. The pellet was collected by centrifuging the mixture at 21,100 × g for 15 min, discarding the supernatant. The pellet was washed three times (250 mL each time) using centrifugation to remove the water after each washing and was subsequently freeze dried.

The outer pericarp (OP), intermediate layer (IL), and aleurone layer (AL) were isolated from the bran layer of Everest wheat kernels using a modified method.[31] Kernels were soaked in 50% ethanol for 16 h, after which the germ, crease, and endosperm were removed using a scalpel. The modification was that the germ was removed after soaking and not before. First, the OP was removed, and then the AL was scraped away from the IL with the aid of a 20X dissection microscope leaving the IL. The outer pericarp was composed of the epidermis and hypodermis layers. The IL was composed of the inner pericarp (cross cells and tube cells), testa, and nucellar layer. The layers were air dried and stored in a desiccator before analysis.

Updegraff treated destarched and deproteinized bran (DSDPB)

DSDPB (2 g) was added to the Updegraff reagent (30 mL) (acetic acid, nitric acid, water; 8:1:2 v/v).[32] The sample was heated at either 50 °C or 100 °C for 30 min. After heating, the sample was cooled to room temperature, centrifuged at 21,100 × g for 15 min and the supernatant was discarded. The pellet was washed with 40 mL of water 3 times and then 20 mL acetone 3 times with centrifuging in between using the same settings as previously mentioned. The supernatant was discarded after washing. The pellet was dried under vacuum at room temperature.

General analytical methods

The moisture contents of the samples were determined by oven drying for 1 h at 130 °C (AACCI Approved Method 44-15.02). The starch content of the UB, DSB, and DSDPB was determined using a Total Starch Assay kit from Megazyme (AACCI Method 76-13.01) (Wicklow, Ireland). Protein content was determined by nitrogen combustion (N% × 5.70) using AACCI method 46-30.01.

Total sugars analysis

Sulfuric acid (2.0 mL, 12 M) was added to 20 mg of UB, DSB, DSDPB, OP, IL, AL, and the insoluble fraction of DSDPB treated with Updegraff reagent and subsequently placed in a 35 °C water bath for 30 min and then diluted to a 2 M sulfuric acid concentration by adding 10 mL of deionized water. The test tubes were then placed in an oven set at 100 °C for 2 h. After cooling to 25 °C, the samples were diluted 100× with deionized water. Samples were filtered through a 0.45 µm filter (Thermo Scientific 30mm nylon syringe filter) before injection into the High-Performance Anion-Exchange Chromatograph (HPAEC). Total sugars were analyzed using a HPAEC (Dionex ICS-3000, Dionex Corp., Sunnyvate, CA, USA) equipped with a pulsed amperometric detector, a guard column, a CarboPacTM PA1 analytical column, and an AS-DV autosampler. Eluent A was 150 mM NaOH and eluent D was 15 mM NaOH. The gradient program was as followed for a 45 min run: 100% of eluent D at 0 min, 100% eluent A at 15 min, and 100% eluent D at 30 min. The separations were carried out at 25 °C with a flow rate of 1

mL/min. The column was then equilibrated with eluent D for 15 min. Arabinose, galactose, glucose, and xylose (Sigma-Aldrich Inc., St. Louis, MO, USA) were used as standards. Arabinose and xylose were injected at a concentration of 0.0526 mg/mL and glucose and galactose were injected at a concentration of 0.0631 mg/mL. Data analysis was performed using Chromeleon 6.8 (Thermo Fisher Scientific, Waltham, MA).

Particle size distribution

The particle size distribution of the untreated wheat bran was determined using a modified AACC 66-20.01 Ro-Tap Sieve Shaker method (AACCI, 2009). The milled bran was analyzed in triplicate. One hundred grams of untreated bran (14% MB) was weighed and sifted for 5 min with 2 pan cleaners per sieve. The data was recorded as the overs of the 350, 212, 180, 106, 53, and < 53 μm screens.

Solid-state ^{13}C CP/MAS NMR analysis

High-resolution solid-state ^{13}C cross-polarization magic-angle spinning nuclear magnetic resonance (^{13}C CP/MAS NMR) analysis of bran was carried out at Bo = 9.4 T on a Bruker AVANCE III 400 WB spectrometer as previously described.[33] The samples were analyzed at both ~25% moisture after conditioning in a saturated NaCl solution environment for 1 week before analysis and 50% moisture. A 4 mm probe was used for analysis at ~25% moisture (which was damaged) and was then replaced by a 7 mm probe, which was used to analyze the samples hydrated to 50% moisture. The corresponding ^{13}C resonance frequency was 100.6 MHz.

Samples were packed in a 7 mm ZrO_2 rotor and spun at the magic angle (54.7°) at a spin rate of 6 kHz. ^{13}C CP/MAS NMR spectra were recorded with a contact time of 1.2 ms and a recycle delay of 2 s. The chemical shifts were referenced to tetramethylsilane (TMS) at 0 ppm. Typically, 8000 to 12000 transients were accumulated for the ^{13}C spectra.

X-ray diffraction analysis

X-ray diffraction (XRD) analysis of bran was conducted (D8, Bruker, Germany) as previously described.[33] The samples (UB and dissected layers) were analyzed at both ~25% moisture after conditioning in a saturated NaCl solution environment for 1 week before analysis and 50% moisture. The samples were exposed to the X-ray beam at 200 mA and 40 kV. The scanning region of the diffraction angle (2θ) was from 5° to 40° with a step size of 0.02° and a count time of 0.8 s. Samples were stored at 4 °C for analysis.

The Updegraff reagent treated bran samples were analyzed using a multi-purpose X-ray diffractometer (PANalytical Empyrean, The Netherlands). It was operated at 35 kV and 20 mA with a 2θ range of 2-35, 0.006° step size, 40 seconds/step, 255 active channels, 10 mm mask, and 0.02 rad soller slit on a diffracted beam side. The anti-scatter slit size was 1/8 degree and the aperture size was 1/16 degree for 27 mm front loaded samples. X-rays were produced using a copper X-ray tube (λ = 1.54 Å). A large nickel beta filter was used to remove beta scattering. A PIXcel 3D-Medpix3 1x1 PASS detector was used. The samples were analyzed at ~12% moisture.

The crystallinity index of the OP (analyzed at ~25% and 50% moisture) and the bran treated with the Updegraff reagent at 100 °C were determined as previously described.[19] Peak

fitting was performed using an Igor software package (Igor Pro, Wavemetrics, Lake Oswego, OR) as previously described.[19] The cross-section dimensions of the cellulose microfibrils were estimated using the Scherrer equation[19] (1) for the 1-10 and 200 lattice planes of cellulose Iβ. The cross-section dimensions of the cellulose microfibrils (nm), L (hkl); the Scherrer constant (0.94), k; the X-ray wavelength, λ; the full-width at half-maximum of the hkl, B(hkl); and the Bragg angle, 2θ were used to calculate the cross-section dimensions of the cellulose microfibrils.

$$\boldsymbol{L(hkl)} = \frac{\boldsymbol{k \times \lambda}}{\boldsymbol{B(hkl) \times cos\theta}} \qquad \textbf{(1)}$$

SAXS analysis

Small-angle X-ray scattering (SAXS) measurement of bran was performed using a Bruker NanoStar SAXS instrument equipped with a Vantec 2000 detector and pin-hole collimation for point focus geometry as previously described.[34] The samples were analyzed at both ~25% moisture after conditioning in a saturated NaCl solution environment for 1 week before analysis and 50% moisture. The X-ray source was a rotating copper anode (0.1 nm filament) operating at 50 kV and 30 W, fitted with cross coupled Göbel mirrors, resulting in Cu Kα radiation wavelength of 1.5418 Å. The optics and sample chamber were under vacuum to minimize air scattering. The power-law exponent values were calculated by determining the slope of the region in which experimental data for all the different samples followed a linear trend in the log I versus log q plot.

Light microscopy

Bran layers were observed in water using an optical microscope with a digital camera (model BX51, Olympus Co., Tokyo, Japan) under polarized light with and without a 530 nm first order waveplate.

Statistical analysis

Each sample was measured in replicate (n = 2) and means and standard deviations were reported. Means were compared using one-way ANOVA to test for significance followed by a Tukey HSD test for significance between means at a $P < 0.05$ (KaleidaGraph 4.1, Reading, PA).

Results and discussion

Solid-state ^{13}C CP/MAS NMR analysis of wheat bran

Solid-state NMR spectra of wheat bran and its dissected layers are shown in **Fig. 2.1**. The carbonyl carbon resonance (174 ppm) in UB (**Fig. 2.1A**) was probably from the AL, which had the most intense carbonyl carbon signal (**Fig. 2.1D**) followed by the IL (**Fig. 2.1C**) and OP (**Fig. 2.1B**). This signal indicates the presence of protein, lipids, cutin, and glucuronic acid from arabinoxylan.[22] The C-1 cellulose resonance (105 ppm) was not resolved in UB and the AL (**Fig. 2.1**). It was most intense for the OP followed by the IL (**Fig. 2.1**). Cellulose appeared to be most concentrated in the OP and least concentrated in the AL (**Fig. 2.1**), which coincides with the non-

starch glucose amounts in **Table 2.1** and is in agreement with previous research.[35] Crystalline cellulose resonances [89 ppm (C-4) and 65 ppm (C-6)] were identified in UB with the highest intensity found in the OP followed by the IL (**Fig. 2.1**). They were absent in the AL (**Fig. 2.1**), which would be expected because of the low amount of cellulose present in the layer.[35] The C-1 xylan resonance (103 ppm), indicating the presence of arabinoxylan, was a shoulder for UB and the AL (**Fig. 2.1**). It was the most resolved and intense for the OP and IL indicating a higher concentration in those layers (**Fig. 3.1**), which corresponds with the arabinoxylan percentage in **Table 2.1** and is in agreement with previous work.[35] The alkyl carbon signals (0-45 ppm), specifically bulk methylene from cutin and lipids at 30 ppm, were less intense for OP compared to UB, IL, and AL (**Fig. 2.1**). The resonance at 30 ppm was most intense and resolved for IL, possibly due to the testa layer and its outer and inner cuticle being present. This layer also was rich in pigments, which may have contributed to the resonance in this region. In comparison, a hard white winter wheat bran sample was analyzed under the same conditions (~25% moisture) using the same solid-state NMR (**Fig. 1.1**) and a strong resonance was seen at 30 ppm. This indicated that the chemical shift at 30 ppm was likely from the cuticle layers and not from pigmentation. The alkyl carbon signals were also intense for AL (**Fig. 2.1**), which was expected as it has the highest lipid content of any layer.[36] The AL had more intense methoxy group (56 ppm) and protein (41 ppm) resonances than both the OP and IL (**Fig. 2.1**). The protein signal at 41 ppm was absent in the UB, OP, and IL (**Fig. 2.1**) and both the DSB (**Fig. 2.2A**) and DSDPB (**Fig. 2.2B**) spectrum. The DSDPB spectrum showed a decrease in signal intensity at 174 ppm (carbonyl carbon region) compared to DSB (**Fig. 2.2**) and a corresponding decrease in protein content (**Table 2.1**). This resonance is comprised primarily of carbonyl carbons from proteins. The AL was the only layer with a strong carbonyl carbon resonance indicating that most of the

protein was likely removed from this layer after the protease treatment (**Fig. 2.1**). Protein concentration appeared to be highest for the AL, which corresponds with the composition data compiled in previous work.[37] According to protein composition data using a reference[37] the pericarp had a protein content of 5.1%, the testa was 5.7% protein, and the aleurone was comprised of 22.9% protein. The untreated, α-amylase and protease treated, and dissected bran samples did not show a signal for lignin at 153 ppm (**Fig. 2.1 and Fig. 2.2**).[21] For each sample, the aromatic range was weak (120-160 ppm) (**Fig. 2.1 and Fig. 2.2**).

The broad C-1 resonance from semi-crystalline A-type starch (96-104 ppm)[16] and the C-1 resonance from mixed-linkage β-glucan could contribute to the assigned arabinoxylan and cellulose resonance at 103 and 105 ppm respectively (**Fig. 2.1 and 2.2**). Therefore, the overlapping cellulose and arabinoxylan C-1 signals (105 and 103 ppm respectively) shown in UB (**Fig. 2.1**) were more resolved and intense following α-amylase and α-amylase + protease treatment per DSB and DSDPB samples respectively (**Fig. 2.2**). The increased intensity of the C-1 cellulose signal (105 ppm) in the enzyme treated samples compared to UB could be due to the removal of starch, protein, and water solubles thereby increasing its effective concentration. For the enzymatically treated samples, the C-1 cellulose signal was more intense than the C-1 arabinoxylan signal (**Fig. 2.2**) although the percentage of arabinoxylan was greater (**Table 2.1**). The ^{13}C CP-MAS NMR increases the signal to noise ratio of carbons in rigid domains (such as crystalline cellulose),[16] which may partially explain the difference in signal intensity. The shoulder (103 ppm) for the C-1 of xylan was more resolved than was the resonance at 109 ppm (C-1 of arabinose) for both DSB and DSDPB (**Fig. 2.2**). This would be expected as xylan is the sugar comprising the backbone of arabinoxylan. The resonances for C-4 and C-6 crystalline cellulose were present as shoulders at 89 and 65 ppm respectively for both DSB and DSDPB.

The enzymatically treated bran samples showed a more resolved and intense crystalline cellulose signal compared to UB (**Fig. 2.1 and Fig. 2.2**). The amount of cellulose may have been concentrated by the removal of starch, protein, and water solubles (**Table 2.1**).

Hydration to 50% moisture slightly decreased UB (**Fig. 2.3A**) signal intensity compared to UB (**Fig. 2.1A**) when analyzed at ~25% moisture, whereas the OP hydrated to 50% (**Fig. 2.3B**) signal intensity slightly increased compared to the OP analyzed at ~25% moisture (**Fig. 2.1B**). In particular, the OP hydrated to 50% moisture C-4 and C-6 crystalline cellulose and C-1 cellulose resonances were more intense and resolved (**Fig. 2.3B**) compared to the OP analyzed at ~25% moisture (**Fig. 2.1B**). The increase in signal intensity could possibly be due to the more ordered orientation of the cell wall polymers when hydrated. The objective of tempering wheat, a period of time that allows water to distribute throughout the kernel, before milling is to soften the endosperm and toughen the bran.[38] Our results suggest a possible connection between the increased cellulose signal intensity and the "toughening" effect upon tempering.

SAXS analysis of wheat bran

The SAXS data (**Fig. 2.4A and B**) show the SAXS intensities as a function of q (magnitude of the scattering wave vector)[39] for untreated and dissected bran layers plotted double logarithmically. The SAXS intensity measured within the q range used for this analysis corresponding the 17-71 Å length scale would be expected to result from cellulose microfibrils[19] and other cell wall components such as adjacent arabinoxylan, mixed-linkage β-glucan, and protein. The power-law exponent values (**Table 2.2**) in the $0.014 < q < 0.056$ $Å^{-1}$ range of the AL, IL, and OP curves (**Fig. 2.4A**) analyzed at ~25% moisture, corresponding to a size range of

17-71 Å, were larger than those of the samples hydrated to 50% moisture. This indicated that a more densely compacted structure was measured compared to the samples hydrated to 50%.[19] Upon hydration of the AL, IL, and OP samples (**Fig. 2.4B**) to 50% moisture, the power-law exponent values (**Table 2.2**) in the $0.014 < q < 0.020$ $Å^{-1}$ range, corresponding to a size range of 50-71 Å, were smaller than those of the samples measured at ~25% moisture. This indicated that the structures detected, which could include cellulose microfibrils and adjacent arabinoxylan, mixed-linkage β-glucan, and protein increased in size upon hydration. The increase in size as a result of hydration to 50% moisture could be mostly attributed to the hydration of the components adjacent to the cellulose microfibrils while the cellulose structures were not hydrated but increased in order. Interestingly, the power-law exponent value of the UB sample showed minimal change due to the increased hydration to 50% (2.1 to 2.5) (**Table 2.2**). The composite bran (UB) is comprised of a variety of structures compared to the isolated layers, which may attenuate the effect of hydration as analyzed using SAXS.

XRD analysis of wheat bran

The OP hydrated to ~25% moisture (**Fig. 2.5B**) showed a characteristic crystalline cellulose diffraction pattern and provided another confirmation of the presence of crystalline cellulose in wheat bran. The 2θ peaks at 15.0°, 22.5°, and 35.0° corresponded to the (1-10), (200), and (004) planes of cellulose I, respectively, as previously identified.[40] The crystallinity index of the OP measured at ~25% moisture was 16.0% (**Table 2.3**). The cellulose microfibril cross-section dimensions for the 200 lattice plane from the OP at ~25% moisture was 2.4 nm (**Table 2.3**), which falls within the range reported for most plant biomass (2-4 nm).[11] The IL

(Fig. 5C) showed some cellulose crystallinity with a weak peak at 22.5° 2θ, whereas, the AL (**Fig. 2.5D**) was completely amorphous as expected. The amorphous nature of the aleurone layer was likely due to the lack of cellulose present in the layer[35] and not due to unusually amorphous cellulose. The XRD data showed UB to be mostly amorphous at ~25% moisture (**Fig. 2.5A**), which was expected due to the majority of amorphous polymers present. The hydration of UB to 50% moisture resulted in the defining of its characteristic cellulose peak at 22.5° 2θ (**Fig. 2.5a**), although its overall signal intensity decreased compared to analysis at ~25% moisture. The intensity of the peak at 22.5° 2θ slightly increased for the OP hydrated to 50% (**Fig. 2.5b**) compared to analysis at ~25% moisture. Correspondingly, the crystallinity index of the 50% moisture sample increased slightly compared to the sample analyzed at ~25% moisture from 16.0% to 18.7% respectively (**Table 2.3**). The increased sharpness of the peak at 22.5° 2θ for UB hydrated to 50% could be a result of OP hydration. The intensity of the hydrated AL (**Fig. 2.5d**) diffractogram also increased, while the IL (**Fig. 2.5C and c**) showed little change between moisture treatments. The cellulose microfibril cross-section dimensions for the 1-10 and 200 lattice planes from the OP hydrated to 50% moisture were 2.4 and 3.0 nm respectively (**Table 2.3**). The cellulose microfibril cross-section dimensions for the most intense peak at 22.5° 2θ (L_{200}) was larger compared to the OP analyzed at ~25% moisture (**Table 2.3**). The sharper XRD signals on increased hydration are not necessarily due to an increase in the cellulose crystallinity or larger cellulose microfibril diameters but could reflect the preferential hydration of non-cellulosic polysaccharides from cellulose microfibril surfaces without any change in underlying cellulose crystallinity within microfibrils.

Updegraff treated DSDPB

DSDPB and DSDPB treated at 50 °C with the Updegraff reagent were amorphous (**Fig. 2.6A and B**) as confirmed by XRD analysis of the insoluble material. Treatment at 100 °C with the Updegraff reagent gave a diffractogram characteristic of crystalline cellulose (**Fig. 2.6C**), which was confirmed by the composition data in **Table 2.1**. The insoluble material was 97% cellulose **(Table 2.1**), which constituted 21.71±0.11% of the DSDPB sample (db). At 100 °C, most of the amorphous components of the DSDPB were hydrolyzed leaving the crystalline cellulose structure intact. Crystalline cellulose was resistant to the Updegraff reagent when treated for 30 min at 100 °C. The crystallinity index of the insoluble material was 25.0%. The microfibril cross-section dimensions for the 1-10 and 200 lattice planes were 2.5 and 2.8 nm, respectively (**Table 2.3**). The XRD data of the dissected layers showed that the OP was where the crystalline cellulose was most concentrated with a slight amount in the intermediate layer. The material resistant to hydrolysis likely belonged to the pericarp bran layer.

Light microscopy

The cell walls of OP (**Fig. 2.7A**), IL (**Fig. 2.7C**), and AL (**Fig. 2.7E**) all exhibited birefringence when viewed under polarizing light. The presence of crystalline cellulose alone did not affect cell wall birefringence as the AL exhibited birefringence (**Fig. 2.7E**). The use of the 530 nm waveplate created a magenta-colored background with birefringent polymers appearing as blue and yellow (**Fig. 2.7B, 2.7D, and 2.7F**). The use of the first order waveplate can assist in

determining the optical sign of a birefringent specimen (positive or negative)[41] and can make birefringent features become more apparent relative to the non-birefringent structures. The optical sign of the birefringence was then determined. The cell wall polymer orientation of the OP (**Fig. 2.7B**) and IL (**Fig. 2.7D**) gave a negative sign of birefringence while the AL (**Fig. 2.7F**) was positively birefringent. The OP and IL birefringence appeared yellow when the cell walls were oriented in a northeast-southwest direction (**Fig. 2.7**) and blue when oriented southeast-northwest (data not shown). The AL cell wall birefringence exhibited a blue color when oriented northeast-southwest and yellow was observed when oriented so that the cell walls were southeast-northwest (**Fig. 2.7**). This could suggest differences in the cell wall polymer orientation[39] between the OP and IL and AL.

Conclusion

The use of solid-state ^{13}C CP/MAS NMR, XRD, and SAXS to analyze the physical structure of wheat bran and its dissected layers was reported for the first time. The ^{13}C CP/MAS NMR spectra showed that the outer pericarp had the highest cellulose concentration of the bran layers. Arabinoxylan was found to be concentrated in the outer pericarp and intermediate layer. The presence of cutin from the testa was identified in the alkyl carbon region of the spectrum of the intermediate layer. The protein and carbonyl carbon resonances were most intense for the aleurone layer indicating that protein was most concentrated there.

The ^{13}C CP/MAS NMR and XRD confirmed the presence of crystalline cellulose in untreated wheat bran, enzymatically treated bran, and its dissected layers. Most of the crystalline cellulose was present in the outer pericarp, which had a crystallinity index of 16.0%. A much

lower proportion was in the intermediate layer. The aleurone layer was found to be completely amorphous. Treatment of destarched and deproteinized bran with the Updegraff reagent removed amorphous material, leaving crystalline cellulose structure intact as confirmed by XRD.

SAXS confirmed that cell wall polymers increased in size due to hydration from ~25% to 50% moisture. The increase in size as a result of hydration to 50% moisture could be mostly attributed to the hydration of the components adjacent to the cellulose microfibrils while the cellulose structures were not hydrated but possibly increased in order. Hydration of the outer pericarp from ~25% to 50% moisture slightly increased the signal intensity of its cellulose XRD diffractogram and CP/MAS NMR spectrum, which could indicate a possible increase in polymer order. Although this could reflect the preferential hydration of non-cellulosic polysaccharides from cellulose microfibril surfaces without any change in underlying cellulose crystallinity within microfibrils. These findings could explain the "toughening" effect tempering has on wheat bran that prevents bran from fracturing into small particles during milling. The cell walls of each layer exhibited birefringence due to the orientation of cell wall components. This birefringence was independent of the presence of crystalline cellulose. The use of a first order waveplate indicated the possibility of a different polymer orientation in the aleurone layer compared to the outer pericarp and intermediate layer.

Conflicts of interest

There are no conflicts to declare.

Acknowledgements

We thank Dr. Jon Faubion for his help editing the manuscript and Dr. Christopher Sorensen for helpful discussions on the SAXS data. This is contribution no. 18-197-J from the Kansas Agricultural Experiment Station.

References

1 A.-S., Jääskeläinen, U. Holopainen-Mantila, T. Tamminen and T. Vuorinen, Endosperm and aleurone cell structure in barley and wheat as studied by optical and raman microscopy, *J. Cereal Sci.*, 2013, **57**, 543-550.

2 N. Rosa-Sibakov, K. Poutanen and V. Micard, How does wheat grain, bran and aleurone structure, impact their nutritional and technological properties?, *Trends Food Sci. Technol.*, 2015, **41**, 118-134.

3 E. Arte, K. Katina, U. Holopainen-Mantila and E. Nordlund, Effect of hydrolyzing enzymes on wheat bran cell wall integrity and protein solubility, *Cereal Chem.*, 2016, **93**, 162-171.

4 L. Stevenson, F. Phillips, K. O'Sullivan and J. Walton, Wheat bran: its composition and benefits to health, a European perspective, *Int. J. Food Sci. Nutr.*, 2012, **63**, 1001-1013.

5 C. Maes and J.A. Delcour, Alkaline hydrogen peroxide extraction of wheat bran non starch polysaccharides, *J. Cereal Sci.*, 2001, **34**, 29-35.

6 L. Dykes and L.W. Rooney, Phenolic compounds in cereal grains and their health benefits, *Cereal Foods World.*, 2007, **52**, 105-111.

7 J.L. Ward, K. Poutanen, K. Gebruers, V. Piironen, A.-M. Lampi, L. Nystrom, A.M. Andersson, P. Aman, D. Boros, M. Rakszegi, Z. Bedo and P.R. Shewry, The HEALTHGRAIN cereal diversity screen: concepts, results, and prospects, *J. Agric. Food Chem.*, 2008, **56**, 9699-9709.

8 K. Swennen, C.M. Courtin, G. Lindemans and J.A. Delcour, Largescale production and characterization of wheat bran arabinoxylooligosaccharides, *J. Sci. Food Agric.*, 2006, **86**, 1722-1731.

9 J. Beaugrand, D. Reis, F. Guillon, P. Debeire and B. Chabbert, Xylanase-mediated hydrolysis of wheat bran: Evidence for subcellular heterogeneity of cell walls, *Int. J. of Plant Sci.*, 2004, **165,** 553-563.

10 F. Xu, Y.-C. Shi and D. Wang, X-ray scattering of lignocellulosic biomass: A review, *Carbohydr. Polym.*, 2013, **94**, 904-919.

11 M. Martínez-Sanz, M.J. Gidley and E.P. Gilbert, Application of X-ray and neutron angle scattering techniques to study the hierarchical structure of plant cell walls: A review, *Carbohydr Polym.*, 2015, **125**, 120-134.

12 S. Pérez and D. Samain, Structure and engineering of celluloses, *Adv. Carbohydr. Chem. Biochem.*, 2010, **64**, 25-116.

13 M.J. Gidley and S.M. Bociek, ^{13}C CP/MAS NMR studies of amylose inclusion complexes, cyclodextrins, and the amorphous phase of starch granules: relationships between glycosidic linkage conformation and solid-state ^{13}C chemical shifts, *J. Am. Chem. Soc.*, 1988, **110**, 3830-3829.

14 A.M. Donald, K.L. Kato, P.A. Perry and T.A. Waigh, Scattering studies of the internal structure of starch granules, *Starch/Stärke*., 2001, **53**, 504-512.

15 F.J. Warren, M.J. Gidley and B.M. Flanagan, Infrared spectroscopy as a tool to characterize starch-ordered structure – a joint FTIR-ATR, NMR, XRD and DSC study, *Carbohydr. Polym.* 2016, **139**, 35-42.

16 B.M. Flanagan, M.J. Gidley and F.J. Warren, Rapid quantification of starch molecular order through multivariate modelling of ^{13}C CP/MAS NMR spectra, *Chem. Commun.*, 2015, **51**, 14856.

17 O.D. Bernardinelli, M.A. Lima, C.A. Rezende, I. Polikarpov and E.R. deAzevedo, Quantitative ^{13}C MultiCP solid-state NMR as a tool for evaluation of cellulose crystallinity index measured directly inside sugarcane biomass, *Biotechnol. Biofuels.*, 2015, **8**, 110.

18 E. Dündar, Y. Turan and A.E. Blaurock, Large scale structure of wheat, rice and potato starch revealed by ultra small angle X-ray diffraction, *Int. J. of Biol. Macromol.*, 2009, **45**, 206-212.

19 M. Martínez-Sanz, P. Lopez-Sanchez, M.J. Gidley and E.P. Gilbert, Evidence of differential interaction mechanism of plant cell wall matrix polysaccharides in hierarchically-structured bacterial cellulose, *Cellulose*, 2015, **22**, 1541-1563.

20 R.J. Young and P.A. Lovell, Introduction to Polymers, 2011, 3rd ed., Taylor and Francis Group, LLC: Boca Raton.

21 M.-A. Ha, W.G. Jardine and M.C. Jarvis, Solid-state ^{13}C NMR of cell walls in wheat bran, *J. Agric. Food Chem.*, 1997, **45**, 117-119.

22 E. Locci, S. Laconi, R. Pompei, P. Scano, A. Lai and F.C. Marincola, Wheat bran biodegradation by Pleurotus ostreatus: A solid-state carbon-13 NMR study, *Bioresour. Technol.*, 2008, **99**, 4279-4284.

23 A. Lopez-Rubio, B.M. Flanagan, E.P. Gilbert and M.J. Gidley, A novel approach for calculating starch crystallinity and its correlation with double helix content: A combined XRD and NMR study, *Biopolymers.*, 2008, **89**, 761-768.

24 T.J. Foster, S. Ablett, M.C. McCann and M.J. Gidley, Mobility-Resolved ^{13}C-NMR spectroscopy of primary plant cell walls, *Biopolymers.*, 1996, **39**, 51-66.

25 T. Liitiä, S. L. Maunu, B. Hortling, T. Tamminen, O. Pekkala and A. Varhimo, Cellulose crystallinity and ordering of hemicelluloses in pine birch pulps as revealed by solid-state NMR spectroscopic methods, *Cellulose*, 2003, **10**, 307-316.

26 M. Foston, Advances in solid-state NMR of cellulose, *Curr. Opin. Biotechnol.*, 2014, **27**, 176-184.

27 J. Blazek and E.P. Gilbert, Application of small-angle x-ray and neutron scattering techniques to the characterization of starch structure: A review, *Carbohydr. Polym.*, 2011, **85**, 281-293.

28 A. Gauthier, S. Derenne, L. Dupont, E. Guillon, C. Largeau, Dumonceau and M. Aplincour, Characterization and comparison of two lingo-cellulosic substrates by ^{13}C CP/MAS NMR, XPS, conventional pyrolysis and thermochemolysis, *Anal. Bioanal. Chem.*, 2002, **373**, 830-838.

29 Z. Li, L. Cai, Z. Gu and Y.-C. Shi, Effects of granule swelling on starch saccharification by granular hydrolyzing enzyme, *J. Agric. Food Chem.*, 2014, **62**, 8114-8119.

30 AACC International, Approved Methods of the American Association of Cereal Chemists, 2000, 10th Ed, The Association: St. Paul, MN.

31 C. Barron, A. Surget and X. Rouau, Relative amounts of tissues in mature wheat (Triticum aestivum L.) grain and their carbohydrate and phenolic acid composition, *J. Cereal Sci.*, 2007, **45**, 88-96.

32 D.M. Updegraff, Semimicro determination of cellulose in biological materials, *Analytical Biochemistry.*, 1969, **32**, 420-424.

33 C. Wei, B. Xu, F. Qin, H. Yu, C. Chen, X. Meng, L. Zhu, Y. Wang, M. Gu and Q. Liu, C-type starch from high-amylose rice resistant starch granules modified by antisense RNA inhibition of starch branching enzyme, *J. Agric. Food Chem.*, 2010, **58**, 7883-7388.

34 J. Cai, Y. Yang, J. Man, J. Huang, Z. Wang, C. Zhang, M. Gu, Q. Liu and C. Wei, Structural and functional properties of alkali-treated high-amylose rice starch, *Food Chem.*, 2014, **145**, 245-253.

35 C. Antoine, S. Peyron, F. Mabille, C. Lapierre, B. Bouchet, J. Abecassis and X. Rouau, Individual contribution of grain outer layers and their cell wall structure to the mechanical properties of wheat bran, *J. Agric. Food Chem.*, 2003, **51**, 2026-2033.

36 Y. Pomeranz, Wheat: Chemistry and Technology, 1988, 3rd ed., Am. Assoc. Cereal Chem., St. Paul, MN.

37 K. Khan and P.R. Shewry, Wheat: Chemistry and Technology, 2009, 4th ed., St. Paul, MN AACC.

38 E. Posner and A.N. Hibbs, Wheat Flour Milling, 2005, 2rd ed., Am. Assoc. Cereal Chem., St. Paul, MN.

39 C.M. Sorensen, C. Oh, P.W. Schmidt and T.P. Rieker, Scaling description of the structure factor of fractal soot composites, *Physical Review E.*, 1998, **58**, 4666-4672.

40 Y. Murata, S. Kubo, E. Togawa, S.F.B.M. Ramle, O. Sulaiman, Hashim, W.A. Ibrahim, A. Kosugi, A. Hirooka and H. Abe, Detection of vascular bundles using cell wall birefringence on exposure to polarized light, *Ind. Crops Prod.*, 2015, **65**, 190-197.

41 S. Kobayashi, L.J. Hobson, J. Sakamoto, S. Kimura, J. Sugiyama, T. Imai and T. Itoh, Formation and structure of artificial cellulose spherulites via enzymatic polymerization, *Biomacromolecules*, 2000, 1, 169-173.

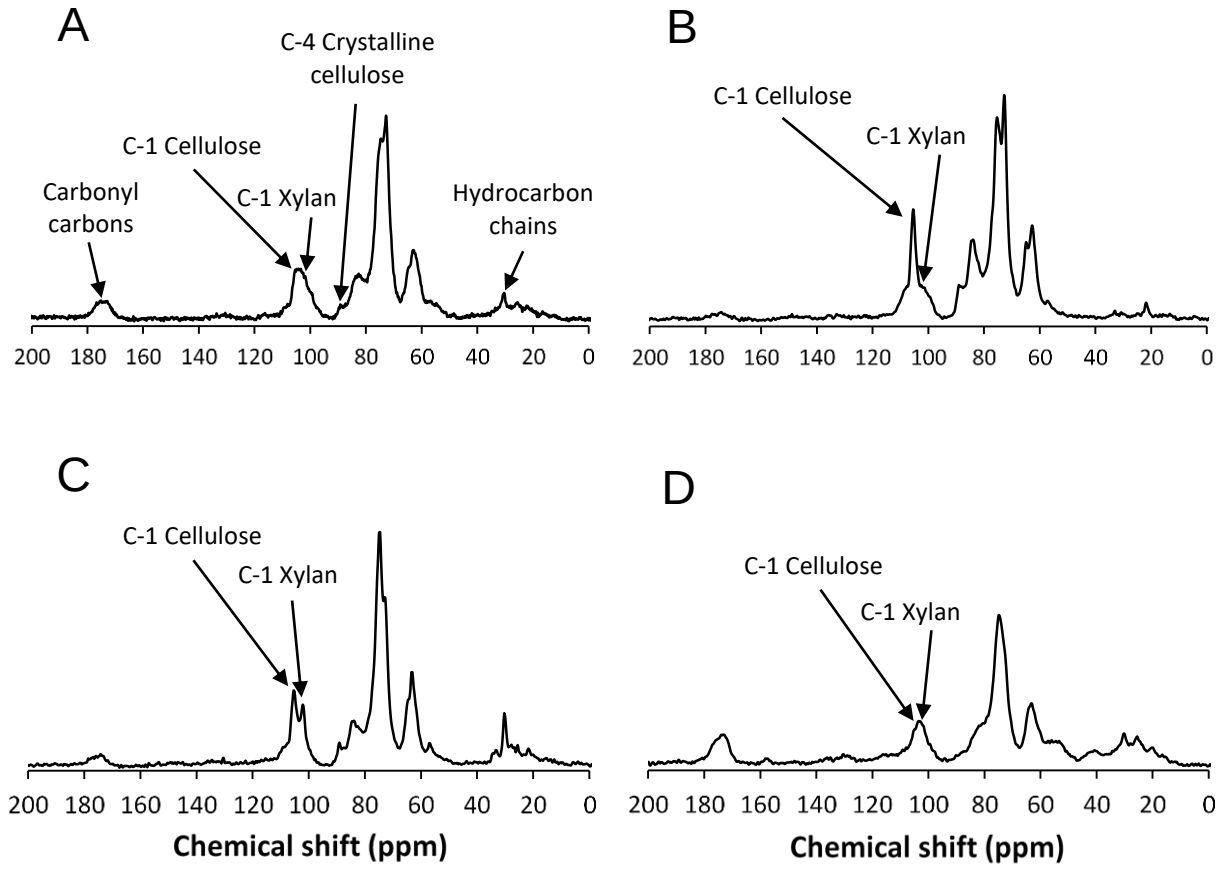

Figure 2.1 Solid-state ^{13}C CP/MAS NMR spectra of (A) untreated bran (UB), (B) outer pericarp (OP), (C) intermediate layer (IL), and (D) aleurone layer (AL) hydrated to ~25% moisture.

Outer pericarp = epidermis + hypodermis; intermediate layer = cross cells + tube cells + testa + nucellar layer. Resonances identified using references[21,22,28]

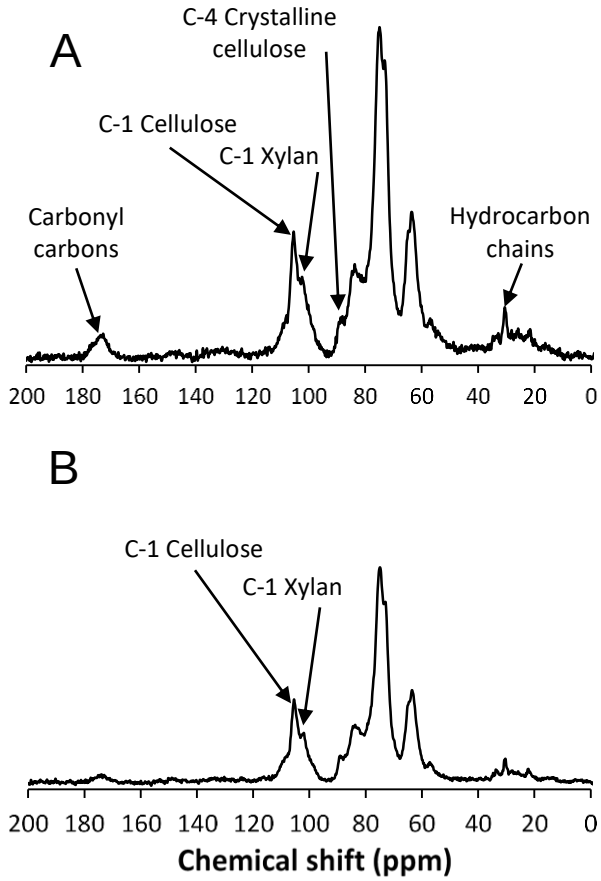

Figure 2.2 Solid-state ^{13}C CP/MAS NMR spectra of (A) destarched bran (DSB), and (B) destarched and deproteinized bran (DSDPB) hydrated to ~25% moisture.

Resonances identified references[21,22,28]

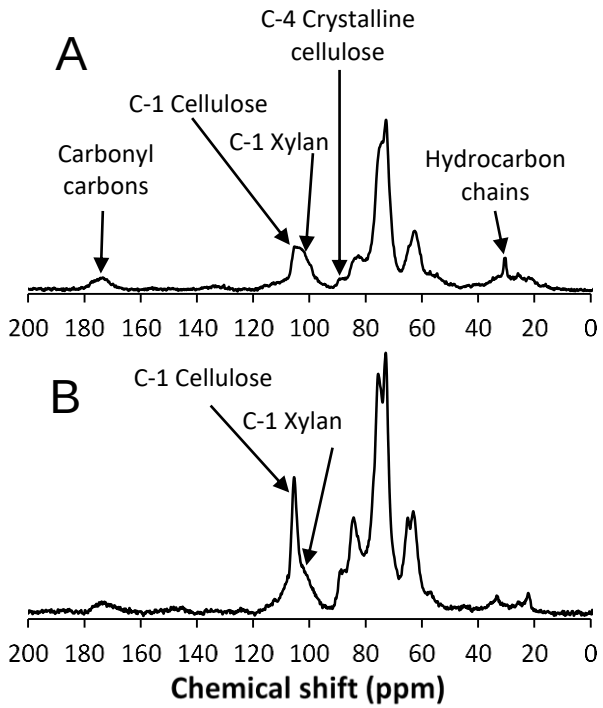

Figure 2.3 Solid-state ^{13}C CP/MAS NMR spectra of (A) untreated bran (UB), and (B) outer pericarp (OP) hydrated to 50% moisture.

Resonances identified using references[21,22,28]

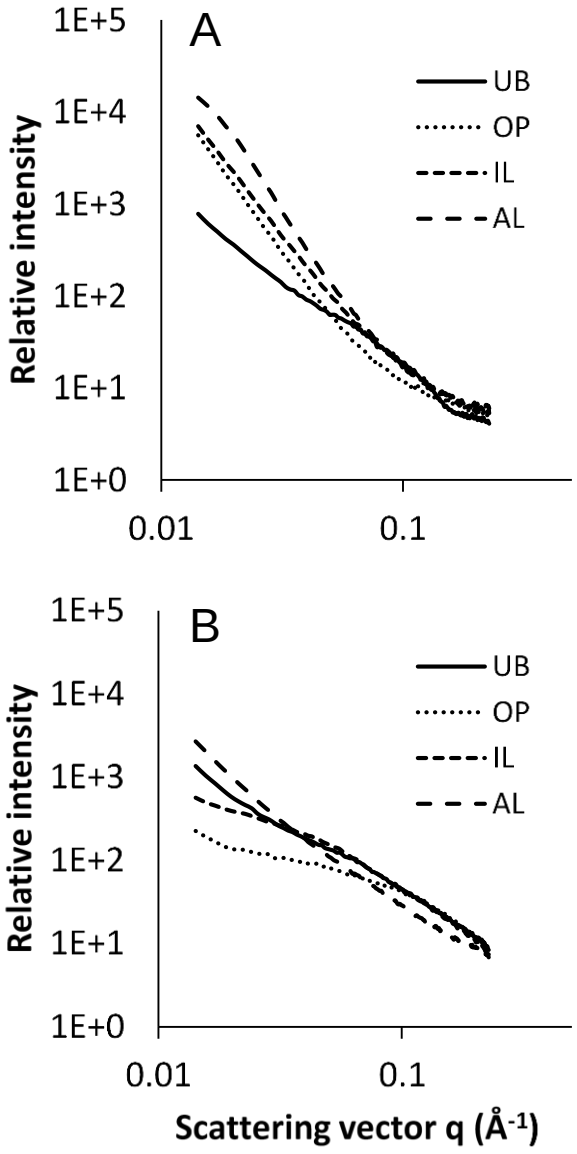

Figure 2.4 Small-angle X-ray scattering of untreated bran and dissected bran layers (A) hydrated to ~25% moisture, and (B) hydrated to 50% moisture.

UB = untreated bran; OP = outer pericarp; IL = intermediate layer; AL = aleurone layer.
Outer pericarp = epidermis + hypodermis; intermediate layer = cross cells + tube cells + testa + nucellar layer.

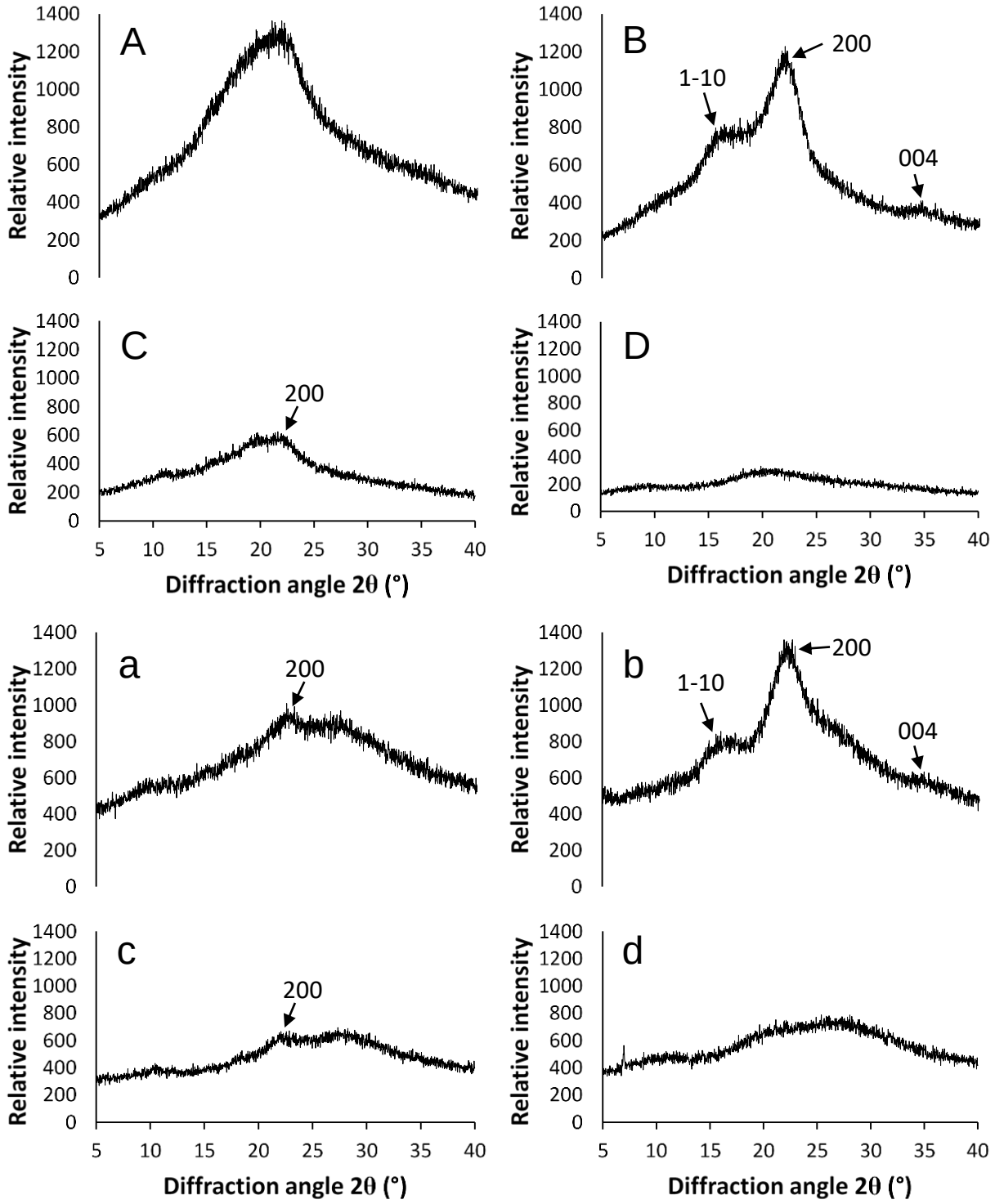

Figure 2.5 X-ray diffraction of (A, a) untreated bran (UB), (B, b) outer pericarp (OP), (C, c) intermediate layer (IL), and (D, d) aleurone layer hydrated to ~25% moisture (A, B, C, D) and hydrated to 50% moisture (a, b, c, d).

Outer pericarp = epidermis + hypodermis; intermediate layer = cross cells + tube cells + testa + nucellar layer. (1-10), (200), and (004) are planes of cellulose I crystals at 15.0°, 22.5°, and 35.0° respectively.[40]

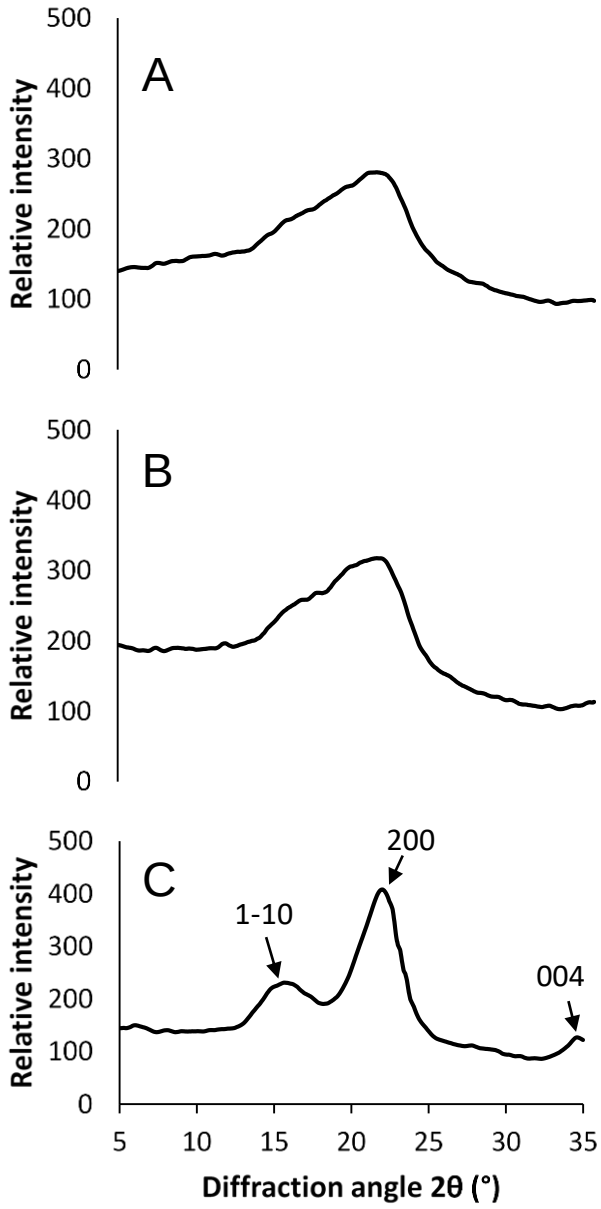

Figure 2.6 X-ray diffraction of (A) destarched and deproteinized bran (DSDPB), (B) destarched and deproteinized bran treated with Updegraff reagent at 50 °C, and (C) destarched and deproteinized bran treated with Updegraff reagent at 100 °C analyzed at ~12% moisture.

(1-10), (200), and (004) are planes of cellulose I crystals at 15.0°, 22.5°, and 35.0° respectively.[40]
Data collected using XRD at Kansas State University.

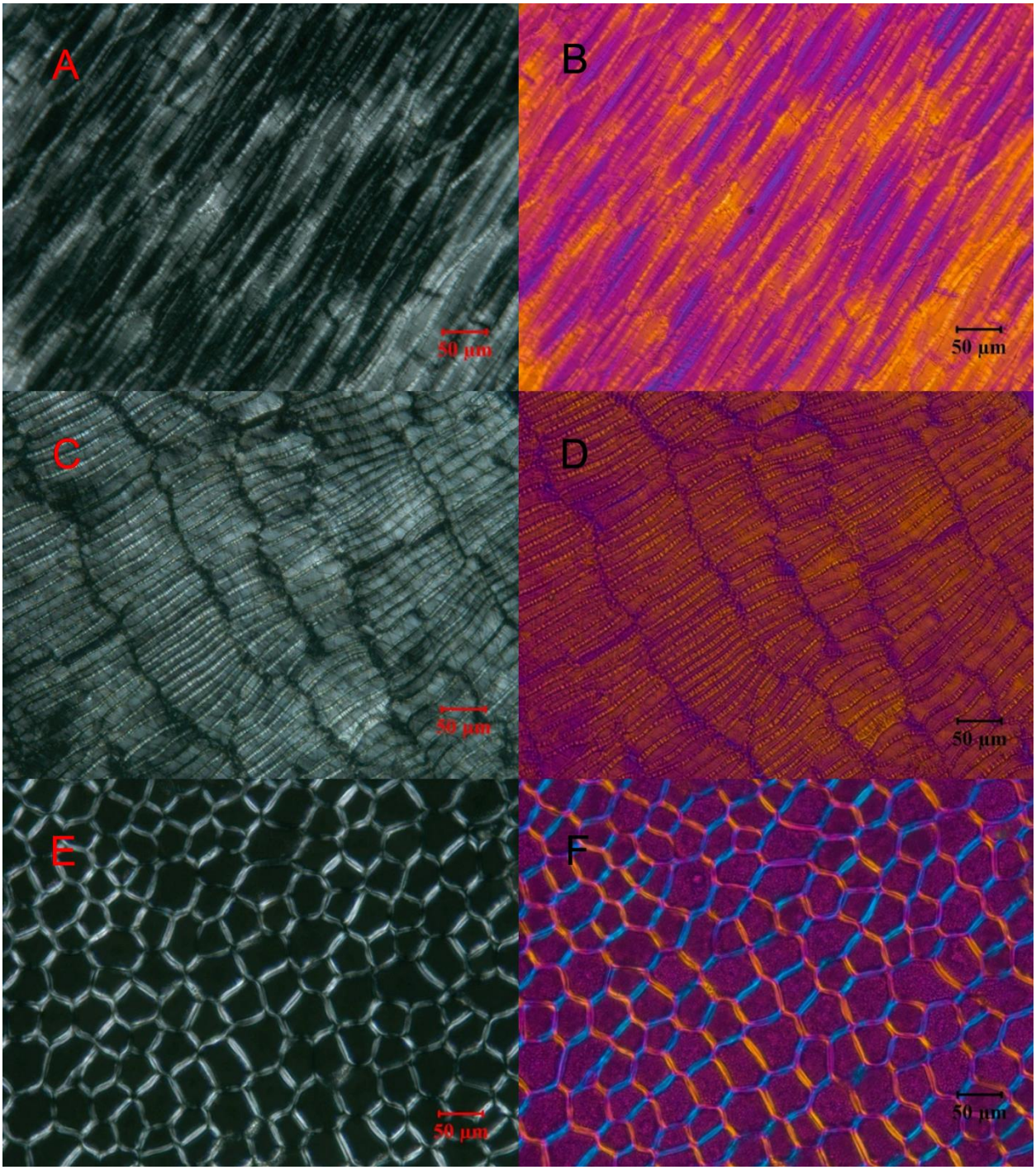

Figure 2.7 Polarized light images of (A) outer pericarp (OP), (C) intermediate layer (IL), and (E) aleurone layer (AL), and polarized light with a first order waveplate images of (B) outer pericarp (OP), (D) intermediate layer (IL), and (F) aleurone layer (AL).

Outer pericarp = epidermis + hypodermis; intermediate layer = cross cells + tube cells + testa + nucellar layer. Scale bar = 50 µm.

Table 2.1 Composition percentage (expressed in dry basis) of untreated bran (UB), destarched bran (DSB), destarched and deproteinized bran (DSDPB), outer pericarp (OP), intermediate layer (IL), aleurone layer (AL), and insolubles from Updegraff reagent treatment of DSDPB[1]

Composition (%)	UB	DSB	DSDPB	OP	IL	AL	Insolubles from Updegraff treatment of DSDPB
Arabinose	11.1±0.1	21.7±0.4	23.1±0.4	27.2±0.6	16.1±0.6	8.0±0.1	0
Xylose	16.6±0.0	26.6±0.1	30.0±0.6	23.4±0.3	29.6±0.3	13.6±0.1	3.1±0.2
Arabinoxylan[2]	24.4	42.5	46.7	44.5	40.2	19.0	2.7
A/X Ratio[3]	0.67	0.82	0.77	1.2	0.54	0.59	0
Glucose (starch + β-glucan + cellulose)	42.3±0.0	32.6±0.7	31.5±0.4	43.9±0.5	37.9±2.1	17.0±0.9	96.9±1.5
Starch[4]	15.9±0.1	2.4±0.4	0.1±0.0	0[4]	0[4]	0[4]	0[4]
β-glucan[5]	n.d.[8]	n.d.[8]	n.d.[8]	9.3[5]	6.3[5]	15.6[5]	n.d.[8]
Cellulose[6]	n.d.[8]	n.d.[8]	n.d.[8]	34.6[6]	31.6[6]	1.4[6]	96.9[7]
Protein	14.4±0.1	10.2±0.2	4.9±0.1	n.d.[8]	n.d.[8]	n.d.[8]	n.d.[8]

[1]The values express means ± standard deviations, n = 2.
[2]Arabinoxylan % = 0.88 × (arabinose % + xylose %).
[3]A/X = arabinose / xylose ratio.
[4]The dissected bran layers (OP, IL, AL) and the insoluble fraction from Updegraff treatment of DSDPB were assumed to contain no starch.
[5]β-glucan values were determined using data from reference.[35]
[6]Cellulose % = glucose % - starch % - β-glucan %.
[7]The glucose % in the insoluble fraction after Updegraff reagent treatment was assumed to be comprised of cellulose.[32]
[8]n.d., not determined.
Outer pericarp = epidermis + hypodermis; intermediate layer = cross cells + tube cells + testa + nucellar layer.

Table 2.2 Power-law coefficients in the q range 0.014-0.056 $Å^{-1}$ (analysis at ~25% moisture) and 0.014-0.020 $Å^{-1}$ (analysis at 50% moisture) for the untreated wheat bran (UB), outer pericarp (OP), intermediate layer (IL), and aleurone layer (AL)[1]

Sample	~25% moisture	50% Moisture
UB	2.1	2.5
OP	3.6	1.9
IL	3.4	1.9
AL	3.9	2.7

[1]The corresponding q range was selected by determining the region in which experimental data for all the different samples followed a linear trend in the log I versus log q plots, refer to Fig. 4A and B.

Table 2.3 Crystallinity index and cross-section dimensions of the cellulose microfibrils for outer pericarp (OP) analyzed at ~25% moisture and 50% moisture; and untreated wheat bran (UB) treated with the Updegraff reagent at 100˚C[1,2]

Sample	Crystallinity Index (%)	$L_{(1-10)}$ (nm)	$L_{(200)}$ (nm)
OP ~25% moisture	16.0	nd[1]	2.4
OP 50% moisture	18.7	2.4	3.0
Updegraff treated UB ~12% moisture	25.0	2.5	2.8

[1]nd = not determined; the peak was not defined enough for analysis.
[2]Crystalline dimensions referred to the cellulose Iβ crystalline planes.

Chapter 3 - Dissolution of wheat bran by NaOH/urea solutions and structure of soluble materials

ABSTRACT

Wheat bran is an abundant low-cost by-product of the wheat milling industry that can be used as a renewable resource for the production of biofuels, chemicals, feed, and food ingredients. In this study, destarched and deproteinized wheat bran (DSDPB) was treated with a mixture of either 7 or 9% sodium hydroxide and 12% urea solvent and structure of the extracted polymers was investigated. Three and 6 cycle dissolution schemes, were examined involving the repeated cooling of the solvent bran mixture to -12.6 °C and then agitating it at 25 °C. When 7% NaOH/12% urea (6 cycle) was applied to DSDPB, 84.1% of the material was solubilized including 89.8% of the arabinoxylans (AX). The high molecular weight fraction constituted 62.9% of the AX originally in the DSDPB. This procedure recovered more wheat bran arabinoxylans for characterization than any previous study using alkaline dissolution. The percent solubilization and its molecular weight significantly increased with more dissolution cycles. The material insoluble in NaOH/urea contained crystalline cellulose, which may have provided the cell wall with structure, along with crosslinks, to prevent complete solubilization. Enzymatic treatment of the high molecular weight fraction provided evidence of carbohydrate-protein conjugation.

INTRODUCTION

Wheat bran is a low value by-product of the dry wheat milling industry[1] and represents 14-19% of the wheat kernel.[2] Bran can be procured in large amounts with approximately 90 million tons produced each year.[3] The use of wheat bran in a biorefinery would provide for the opportunity to turn bran into renewable energy, chemicals, and increase its use in food products.[4] In addition to starch (14-25%) and protein (13-18%), bran is comprised of non-starch polysaccharides (~46% of the wheat bran), which are comprised of 70% arabinoxylans (AX), 24% cellulose, and 6% (1,3) (1,4)-β-glucan.[2] Naturally, much research has been conducted on the extraction and utilization of AX.[5] It has many functional properties and could potentially be used as a food ingredient and in biofuels, chemicals, cosmetics and pharmaceuticals.[5] Arabinoxylans can function as a film former, thickener, emulsifier, stabilizer, and binder.[5] Food products containing wheat bran are mostly found in the bakery and cereal product segment of the industry (60% market share) followed by savory snacks, baby food, chilled food, dairy food, and sauces, dressings, and condiments (each with a ~4-6% market share).[6] Arabinoxylan extracted from wheat bran is often used as a baking additive.[6]

Arabinoxylans in wheat bran, the structure of which has been previously described,[5,7] is largely not extractable in water[7] and that water unextractability could be due to covalent or non-covalent associations with each other and with other cell wall components such as protein, cellulose, and lignin.[8,9] The effect of physical entanglement versus covalent linkages on AX extraction is not completely known.[10,11] Structural details such as the presence of diferulate linkages, uronic acid covalent linkages as part of the AX side chain, hydrogen bonding,

substitution pattern, substitution level (arabinose/xylose, A/X ratio), molecular weight, and ether linkages affect AX extractability.[7,11,12,13,14]

The dissolution of cellulose, one of the main cell wall components, could lead to a more complete dissolution of wheat bran. Cadoxen (cadmium oxide in ethylenediamine) was a solvent developed to dissolve up to 99% of the cellulose in biomass materials without developing undesirable sugar side products.[15] The downside is that it's toxic.[15] To avoid using a very toxic solvent, Zhang and co-workers pioneered the work on dissolution of cellulose using a precooled (-5 to -20 °C) aqueous solution of sodium hydroxide (6-10%) and urea (2-20%), sodium hydroxide/thiourea, or lithium hydroxide/urea.[16,17,18] A two-step method was developed to conserve energy where the solvent is cooled to 0 °C.[19] The mechanism for how the solvent works has been described in previous research.[18,19,20]

In this study, we applied the NaOH/urea solvent to solubilize wheat bran and determined the structure of soluble materials. Understanding the chemical and physical structure of wheat bran would broaden its use in the food, chemical, and biofuels industries. More knowledge about how bran is assembled will aid in developing more bran based products though effective means of processing.[21] Wheat bran processing may include changing the particle size, enzymatic, hydrothermal, and acid hydrolysis and alkaline dissolution. There is a need to understand bran physical structure so the factors that affect its solubility and dissolution can be determined. Specific objectives of this study were to 1) evaluate the amount of wheat bran dissolved using a NaOH/urea solvent; 2) determine the physical structure and chemical composition of both the

precipitated and undissolved fractions; 3) enzymatically treat the precipitated bran fraction to probe for the existence of protein/carbohydrate conjugation in the cell wall structure.

EXPERIMENTAL SECTION

Materials. A hard red winter wheat (variety Everest) was obtained from the Kansas Foundation Seed Project (Manhattan, KS). Urea, hydrochloric acid, 200 proof ethanol, sodium hydroxide solution, and sodium hydroxide pellets were all analytical grade (Sigma Aldrich, St. Louis, MO). Termamyl 120L (Novozymes, Franklinton, NC), a thermostable α-amylase, that had an enzyme activity of 120 KNU-T/g (Kilo Novo α-amylase units/g) was used to remove starch from bran. One KNU is the amount of α-amylase that can dextrinize 5.26 g starch (dry basis) per hour under standard conditions (pH = 7.1 at 37 ˚C). Protex 14L (Genencor, Palto Alto, CA), a thermostable bacterial neutral protease, with an enzyme activity of 160 units/g was used to remove protein from bran. One unit is the amount of enzyme that produces 200 µg of tyrosine-equivalent trichloracetic acid soluble peptides per minute from a casein substrate under standard assay conditions (pH = 6.5, 35 ˚C). Multifect PR 6L (Genencor, Palto Alto, CA), a bacterial alkaline protease, that had an enzyme activity of 580,000 DU/g was used to treat bran solubles. This enzyme activity assay is based on the ability of the protease to cleave p-nitroanilide from a synthetic peptide substrate. Multifect CX 12L (Genencor, Palto Alto, CA), an endoxylanase from Trichoderma reesei, with an activity of 30,450 ABX/g (Acid Birchwood Xylanase units/g) was used to treat bran solubles. The activity is determined by the release of reducing sugars by the action of xylanase on a birchwood xylan substrate. Avicel PH 101 microcrystalline cellulose (FMC Corp., Philadelphia, PA) with a DP of 350 was used.

Preparation of Wheat Bran. Everest wheat bran was obtained by milling the wheat using the Buhler method for hard wheat. The Buhler experimental mill MLU202 (Buhler Inc., Uzwil, Switzerland) was set up to mill hard wheat per AACC 26-21.02.[22] A feed rate of 80 g of wheat/min was used to obtain a 76% flour extraction. The wheat bran was further milled to a smaller particle size using a single blue Ross roll stand (Ross, Oklahoma City, OK) with a differential of 2.5:1, 0.5-inch spiral, 24 corrugations per inch pitch, and a grinding action of dull:dull. The roll gap was set to 0.003 in. The bran was milled 2X and then sifted using a Great Western Sifter for 2 min over a sieve stack of 300 µm > 200 µm> 132 µm > Pan. The overs from the 300 µm screen were milled twice more and then sifted. This process was repeated until all bran passed through the 300 µm screen. The milled bran will be referred to as untreated bran.

Particle Size Distribution. The particle size distribution of the untreated bran was determined using a modified AACC 66-20.01 Ro-Tap Sieve Shaker method. The milled bran was analyzed in triplicate. Next, 100 g of untreated bran (14% MB) was weighed and sifted for 5 min with 2 pan cleaners per sieve. The data were recorded as the overs of the 350, 212, 180, 106, 53, and < 53 µm screens (**Table 3.1**).

Protein and Starch Digestion. Untreated bran (50 g) was added to water (350 mL) to make a 12.5% w/v bran in water mixture, and the pH was 6.6. Termamyl 120L (0.6% based on bran weight) was added to the mixture. The mixture was heated at 90 °C for 120 min with continuous stirring, cooled to 65 °C, and the pH measured (6.1). The pH was adjusted to 7.5 with 0.5 N NaOH and a neutral bacterial thermostable protease was added (Protex 14L) (2.5 mL) and

incubated at 65 °C for 5 h with continuous stirring. The pH was maintained at 7.5 using 0.5 N NaOH. The enzymes were then denatured by heating the solution to 100 °C for 15 min. The destarched and deproteinised bran was separated from the water solubles by centrifuging the mixture at 12,100 × g, 15 min, at 4 °C. The bran was then washed three times with water (250 mL each time) to remove any residual water solubles. Washed bran was freeze dried. The supernatant containing the water solubles was discarded. The bran material after starch and protein removal was the destarched and deproteinized bran (DSDPB).

Three Cycle Bran Dissolution. A modified procedure was used (**Figure 3.1**) to examine the effects of NaOH concentration on dissolution of DSDPB.[23] The 2 solvents were tested separately. A solution of 7% (1.75 M) sodium hydroxide and 12% (2.00 M) urea and a second solvent composed of 9% (2.25 M) sodium hydroxide and 12% (2.00 M) urea. Dissolved fractions denoted with an A refer to the 7% NaOH/12% urea solution and the fractions denoted with a B refer to the 9% NaOH/12% urea solution. Both were brought to -12.6 °C in a -20 °C freezer until ice crystals started to form. At the desired temperature, bran (2 g) was added to the solution to make a 0.5% (w/w) bran mixture, which was then homogenized (Pro Scientific Inc. 350, Oxford, CT) at 750 rpm for 10 min, and stirred at 25 ˚C for 12 h, cooled to -12.6 °C (until light ice formation) in a -20 °C freezer, homogenized again, and then stirred for 12 h at 25 ˚C. The cooling, homogenizing, and stirring process was performed three times, hence the name 3 cycle bran dissolution. The order of DSDPB addition, either before or after cooling the NaOH/urea solvent to -12.6 °C, did not affect the amount dissolved.

Six Cycle Bran Dissolution. A modified procedure was used (**Figure 3.1**) to examine the effects of the number of dissolution cycles on dissolution of DSDPB.[23] A solution of 7% (1.75 M) sodium hydroxide and 12% (2.00 M) urea was brought to -12.6 °C in a -20 °C freezer until ice crystals started to form. When at the desired temperature, 2 g DSDPB was added to the solution, creating a 0.5% w/w mixture. The mixture was homogenized (Pro Scientific Inc. 350, Oxford, CT) at 750 rpm for 10 min. The mixture was then stirred at 25 ˚C for 12 h after, which it was cooled to -12.6 °C (until light ice formation) in a -20 °C freezer, homogenized at 750 rpm for 10 min, and stirred at 25 ˚C for another 12 h. The cooling, homogenizing, and stirring process of the mixture was performed six times, hence the name 6 cycle bran dissolution. Dissolved fractions denoted with a C refer to the 6 cycle dissolution.

At this point, both dissolution procedures were the same except for the number of cycles. The mixture was then centrifuged at 12,100 × g for 10 min at 4 °C to separate the material insoluble in NaOH/urea (P1A/P1B/P1C) from the NaOH/urea solubles (S1A/S1B/S1C) (**Figure 3.1**). The insoluble fraction (P1) was washed with water to remove salts and then freeze dried. The entire procedure was replicated (n = 2).

The soluble fraction (S1) was neutralized to pH 7 with 2 N HCl and then centrifuged at 27,200 × g for 15 min at 4 °C to remove any HMW material insoluble at pH 7 (P2A/P2B/P2C) (**Figure 3.1**). The P2 fraction was washed with water and freeze dried. The total solubles at pH 7 (S2A/S2B/S2C) were then adjusted to 80% ethanol with 200 proof ethanol and stirred for 30 min followed by 12 h at 25 ˚C without stirring. This resulted in the precipitation of HMW material insoluble in 80% ethanol (P3A/P3B/P3C) (**Figure 3.1**). The P3 fraction was separated using

filtration, washed three times with 80% ethanol solution to remove remaining salts, then dissolved in water and freeze dried. The low molecular weight (LMW) material soluble in 80% ethanol (S3A/S3B/S3C) was discarded. The composition of P1, P2, and P3 fractions were determined using high-performance anion-exchange chromatography (HPAEC). The molecular weight distributions of the P3 fractions were determined by gel permeation chromatography (GPC).

A dissolution was performed to confirm the solvents ability to dissolve crystalline cellulose. Avicel PH 101 microcrystalline cellulose (FMC Corp., Philadelphia, PA) with a DP of 350 was dissolved as follows. A 7% sodium hydroxide and 12% urea solution was cooled to until ice crystals started to form (-12.6 °C). Cellulose was then added to make a mixture of 4% (5 g db) microcrystalline cellulose by weight in replicate (n = 2). The mixture was stirred vigorously for 10 min, cooled to -12.6 °C, and stirred for 10 min. The cooling and stirring of the mixture was repeated twice. After dissolution, it was centrifuged (12,100 × g, 2 min, 4 °C). The pellet was washed with 50% ethanol three times with centrifuging in between. The resulting sample was washed once with 100% ethanol and centrifuged using the same conditions as previously mentioned. The pellet was dried in a vacuum oven (MTI Corporation, Richmond, CA) at 50 °C for 1 h. The dry weight of the material was recorded.

Enzymatic Treatment of the HMW Material Insoluble in 80% Ethanol (P3C). The P3C fraction was dissolved in the HPLC mobile phase overnight with constant stirring to make a 1 mg/mL solution. An alkaline protease (Multifect PR 6L) was added (1 µl/g P3C) and incubated for 5 h at 55 °C. Next, the sample was directly injected into the GPC. This treatment will be

referred to as PP3C. A blank containing only the protease was injected to insure no interference with the P3C molecular weight determination.

The P3C fraction was dissolved in the HPLC mobile phase overnight with constant stirring (adjusted to pH = 5.0 with 0.5 N HCl) to make a 1 mg/mL solution. An endoxylanase (Multifect CX 12L) was added (1 µl/g P3C) and incubated for 5 h at 55 °C. After that, the sample was directly injected into the HPLC for molecular weight analysis. This treatment will be referred to as XP3C. A sample containing only the endoxylanase was injected to insure no interference with the P3C molecular weight determination.

A 1.0% w/w solution of P3C (0.15 g in 14.85 g HPLC mobile phase) was made and treated with Multifect PR 6L and in a separate solution with Multifect CX 12L as detailed above. After the enzyme treatment, the solution was cooled to 25 °C and adjusted to 80% ethanol with 200 proof ethanol and stirred for 30 min followed by 12 h at 25 °C without stirring. This resulted in the precipitation of HMW material insoluble in 80% ethanol [(protease treated P3C insoluble in 80% ethanol; PP3CP) and (endoxylanase treated P3C insoluble in 80% ethanol; XP3CP)]. The precipitate was separated using filtration, washed 3X with 80% ethanol solution to remove remaining salts, then dissolved in water and freeze dried. The composition of the precipitate was then determined.

Light Microscopy. The DSDPB and material insoluble in NaOH/urea (P1C) were observed in water using an optical microscope with a digital camera (model BX51, Olympus Co., Tokyo, Japan).

Scanning Electron Microscopy (SEM). The DSDPB and material insoluble in NaOH/urea (P1C) were imaged using SEM. The samples were coated with gold-palladium in a sputter coater, and then viewed using SEM (S-3500N, Hitachi Science System, Ltd, Tokyo, Japan). The operation was at a voltage of 5.0 kV and 300× magnification.

Infrared Spectroscopy. Fourier transform infrared (FTIR) spectroscopic data were collected in the region of 600-4000 cm-1 using a FTIR spectrometer (Spectrum 100, PerkinElmer, Waltham, MA). The microcrystalline cellulose, P1C, and DSDPB samples were made into disks and scanned 64 times at a resolution of 2 cm-1 and transmission spectra were recorded.

X-ray Diffraction. The material insoluble in NaOH/urea (P1C) was analyzed using a multi-purpose X-ray diffractometer (PANalytical Empyrean, The Netherlands). It was operated at 40 kV and 20 mA with a 2Θ range of 2-35, 0.006 ° step size, 40 seconds/step, 255 active channels, 10 mm mask, and 0.02 rad soller slit on a diffracted beam side. The anti-scatter slit size was 1/8 degree and the aperture size was 1/16 degree for 27 mm front loaded samples. X-rays were produced using a copper X-ray tube. A large nickel beta filter was used to remove beta scattering. A PIXcel 3D-Medpix3 1x1 PASS detector was used.

Gel Permeation Chromatography (GPC). To determine the amount of HMW material insoluble in 80% ethanol (P3) dissolved in the mobile phase, 40 mg was dissolved in the mobile phase (40 mL) overnight with constant stirring. Next, they were centrifuged at 12,100 × g for 15

min at 4 ˚C. The supernatant was decanted and the tube was washed with ethanol and centrifuged again using the same settings as before. After the ethanol was decanted, the previously tared tube was dried in a vacuum oven at 30 ˚C and subsequently weighed to determine the weight of the insolubles. For a normal GPC analysis, much smaller amounts of the P3 fractions (~5 mg) were dissolved in the mobile phase overnight with constant stirring at a concentration of 1 mg/mL. After that, they were filtered through a 30 mm nylon 0.45 μm syringe filter (Thermo Fisher Scientific, Waltham, MA) before injection. The molecular weight distribution was determined by a GPC (Agilent, Santa Clara, CA) using a triple detection system. A Viscotek 270 dual detector (light scattering plus viscometer) (Malvern PANalytical, Almelo, The Netherlands) and Viscotek VE3580 refractive index detector (Malvern PANalytical, Almelo, The Netherlands) on an Agilent Technologies 1100 series liquid chromatograph (Agilent, Santa Clara, CA) equipped with an autosampler and diode array detector (DAD). The DAD was set at 280 nm. The dn/dc value of the P3 fraction was 0.142. The light scattering detector, which consisted of a right angle light scattering (RALS) and low angle light scattering (LALS) detector, was calibrated using a pullulan standard (P-800, 80.5 × 104 weight average molecular weight) (Shodex Standard, Kawasaki, Japan). The mobile phase was water in 100 mmol sodium nitrate and 0.03% sodium azide. The flow rate was 1 mL/min with a run time of 30 min and injection volume of 100 μL. Samples passed through a pre-column and two SEC columns (Suprema pre-column, 10 μm, 8 × 50 mm; Suprema 3000 Å, 10 μm, 8 × 300 mm; Suprema 100 Å, 100 μm, 8 × 300 mm) (Phenomenex, Torrence, CA). Data analysis was performed using OmniSEC 4.7 (Malvern PANalytical, Almelo, The Netherlands).

Total Sugars Analysis. Sulfuric acid (2.0 mL, 12 M) was added to 0.02 g of the untreated bran, DSDPB, P1, P2, and P3 fractions. The solutions were placed in a 35 °C water bath for 30 min and then diluted to 2 M sulfuric acid adding 10 mL of deionized water. The test tubes were then placed in an oven set at 100 °C for 2 h. After cooling to 25 °C, the samples were diluted 100x with deionized water. Samples were filtered through a 0.45 µm filter (Thermo Scientific 30mm nylon syringe filter) and were analyzed using a high-performance anion-exchange chromatograph (HPAEC) (Dionex ICS-3000, Dionex Corp., Sunnyvate, CA, USA) equipped with a pulsed amperometric detector, a guard column, a CarboPacTM PA1 analytical column, and an AS-DV autosampler. Eluent A was 150 mM NaOH and eluent D was 15 mM NaOH. The gradient program was as follows: 100% of eluent D at 0 min, 100% eluent A at 15 min, and 100% eluent D at 30 min. The column was then equilibrated with eluent D for 15 min. The separations were carried out at 25 °C with a flow rate of 1 mL/min. Arabinose, galactose, glucose, and xylose (Sigma-Aldrich Inc., St. Louis, MO, USA) were used as standards. Arabinose and xylose were injected at a concentration of 0.0526 mg/mL and glucose and galactose were injected at a concentration of 0.0631 mg/mL. Data analysis was performed using Chromeleon 6.8 (Thermo Fisher Scientific, Waltham, MA).

Starch, Protein, and Moisture Determination. The starch content of the DSDPB was determined using the Total Starch Assay Procedure (Megazyme, Wicklow, Ireland). Protein content was determined by nitrogen combustion (N% × 5.70) using AACCI method 46-30.01.[22] Ash content was determined using AACCI method 08-03.01.[22] The moisture contents of the samples were determined by oven drying for 1 h at 130 °C (AACCI method 44-15.02).[22]

Ferulic Acid Determination. Ferulic acids were hydrolyzed, extracted and quantified from DSDPB and extracted and quantified in the fraction soluble at pH 7 (S2C) using a modified procedure.[24] The procedure was performed in duplicate. The cited procedure[24] used 1 g of material in 40 mL 2 M NaOH and this study used 10% of those amounts. Ethyl acetate (10 mL × 3) was used to extract the ferulic acid instead of ethyl ether (40 mL × 3).

The DSDPB (0.1 g) was hydrolyzed with 4 mL of 2 M NaOH at 25 °C for 4 h under a continuous nitrogen flow. Ferulic acid was extracted at pH 2 with ethyl acetate (10 mL × 3). The extracts were pooled and evaporated under nitrogen. The residue was dissolved in 5 mL of methanol. The extract was then injected into the reversed-phase HPLC for quantification.

The total solubles at pH 7 (S2C) from the six cycle bran dissolution procedure (under nitrogen) (**Figure 3.1**) was extracted 3 times with ethyl acetate. The extracts were pooled and evaporated under nitrogen. The residue, dissolved in 5 mL of methanol was then injected into the reversed-phase HPLC for quantification.

The chromatographic separation and quantification of the ferulic acid present in the DSDPB and the bran dissolution fraction was carried out using a modified method.[23] The alteration was that only cinnamic acid derivatives were analyzed. An Agilent Technologies 1100 series liquid chromatograph (Agilent, Santa Clara, CA) equipped with an autosampler and diode array detector (DAD) was used. The mobile phase was acetonitrile (mobile phase A) and 2% acetic acid in water (v/v) (mobile phase B). The flow rate was 1.0 mL/min. The column was a Phenomenex Kinetex C18 (100 × 4.60 µm; 6µm) (Phenomenex, Torrance, CA). The analysis

was performed at room temperature. All samples were filtered through a 30 mm nylon 0.45 µm syringe filter (Thermo Fisher Scientific, Waltham, MA) before injection. The injection volume was 10 µL and peaks were monitored at 320 nm for ferulic acid. The mobile phase gradient was: 100% B to 85% B in 30 min, 85% B to 50% B in 20 min, 50% B to 0% B in 5 min and 0% B to 100% B in 5 min. There was 10 min of post run for reconditioning. The ferulic acid peak was identified by comparing the retention time to that of a ferulic acid standard. The ultraviolet (UV) absorption from a ferulic acid standard (Sigma-Aldrich Inc., St. Louis, MO) of varied concentration (1, 0.5, 0.25, 0.125, and 0.0625 mg/mL) was used to determine the concentration. Data analysis was performed using OpenLAB CDS ChemStation Edition (Agilent Technologies, Santa Clara, CA).

Statistical Analysis. Each sample was measured in replicate (n = 2) and means and standard deviations were reported. Means were compared using one-way ANOVA to test for significance followed by the Tukey HSD test for significance between means at a $P < 0.05$ (KaleidaGraph 4.1, Reading, PA).

RESULTS AND DISCUSSION

Dissolution Fraction Yields. The amount of DSDPB dissolved using the NaOH/urea solvent increased with more dissolution cycles. DSDPB solubility in NaOH/urea significantly increased from the 3 cycle (81.2%, S1A) to the 6 cycle (84.1%, S1C) dissolution process (**Table 3.2**). Bran solubility in NaOH/urea decreased when the NaOH% increased from 7 to 9% in the NaOH/urea solvent suggesting that higher NaOH concentrations decreased the stability of the

dissolution mixture (**Table 3.2**). The order of DSDPB addition, either before or after cooling the NaOH/urea solvent to -12.6 °C, did not affect the amount dissolved. The HMW material insoluble at pH 7 (P2) yield decreased with both more dissolution cycles and increased NaOH% (**Table 3.2**). The HMW material insoluble in 80% ethanol (P3) yield increased significantly with more dissolution cycles but decreased when the NaOH% of the solvent was increased (**Table 3.2**). The amount of DSDPB solubilized was directly related to the amount of HMW material insoluble in 80% ethanol (P3). Predictably, the LMW material soluble in 80% ethanol (S3) increased with NaOH% suggesting that bran polysaccharides were dissolved into lower molecular weight sugars by the higher NaOH% (**Table 3.2**).

Six Cycle Dissolution Fraction Composition. After a 6 cycle dissolution, the fraction insoluble in NaOH/urea (P1C) contained 10.2% of the AX from DSDPB, which means 89.8% of the AX [**1.** (100 - 10.2%)] and 97% of the esterified ferulic acid originally present in the DSDPB was solubilized (**Table 3.3**). The material insoluble in NaOH/urea (P1C) was composed mostly of glucose (67.5%), likely belonging to cellulose, and AX (25%) (**Table 3.3**). Maes and Delcour (2002) dissolved approximately 67% of the AX present in their destarched deproteinized bran. The P3C fraction constituted 62.9% of the original DSDPB AX for analysis (**Table 3.3**). Bran water unextractable arabinoxylans were recovered for analysis by varying degrees in the prior literature; 45%;[2] ~43%;[25] 53%;[26] 40%;[27] ~47%;[28] 18.5%**;**[29] and 42.5%.[30] Compared to the current study, most of these extraction methods were shorter (2 h to 16 h), used higher temperatures (20 °C to 95 °C), and used lower alkaline concentrations. The extraction methods that did use a higher alkaline concentration (25% NaOH[28] and 24% KOH[30]) used significantly shorter dissolution times (2 h to 4 h). Extraction time, temperature, and alkaline concentration

are important parameters effecting arabinoxylan extraction from wheat bran. Compared to existing literature, the NaOH/urea solvent recovered more wheat bran arabinoxylans for characterization than has any previous study using alkaline dissolution.

Microscopy images of DSDPB, milled to a particle size of ~200 µm (**Table 3.1**), showed that the aleurone, nucellar layer, testa, and pericarp cell wall structures were intact as imaged using light microscopy and SEM (**Figures 3.2A, and C**). The material insoluble in NaOH/urea (P1C) was comprised of the outer pericarp and inner pericarp cells, which was confirmed using both light microscopy and SEM (**Figures 3.2B and D**). The cross cells and outer pericarp cell wall structures appeared to be intact (**Figures 3.2B and D**). The material insoluble in NaOH/urea (P1C) FTIR spectrum more closely resembled the microcrystalline cellulose standard than it did DSDPB (**Figure 3.3**), which would be expected as P1C was 67.5% glucose. The absence of the 1738 cm^{-1} absorbance band in the P1C fraction spectrum implied that ester links associated with both AX ester links with hydroxycinnamic acids and lipidic material of the testa layer were dissolved from the DSDPB (**Figure 3.3**).[31] The absorbance bands at 1640 cm^{-1} and 1541 cm^{-1}, related to absorbed water and protein content respectively,[31] were greatly reduced in the P1C fraction spectrum compared to DSDPB (**Figure 3.3**). The weak absorbance bands at 1204, 1317, 1332, and 1369 cm^{-1}, used for identifying cellulose,[31] appeared at the same frequencies for the DSDPB, P1C, and microcrystalline cellulose samples (**Figure 3.3**). There were no shifts in these frequencies between the material insoluble in NaOH/urea (P1C) and microcrystalline cellulose, which indicated that no physical interactions between cellulose and other cell wall polymers were detected. The broad absorbance band at 1023 $cm^{-1}$and its two shoulders at 1155 cm^{-1} and 897 cm^{-1} were common to each spectrum and were associated with glyosidic linkages of

arabinoxylan, cellulose, and β-glucan (**Figure 3.3**).[31] The A/X ratio in the material insoluble in NaOH/urea (P1C) was 1.04 (**Table 3.3**) similar to those reported for the outer bran layers of the pericarp; 1.14;[32] 1.19;[33] and 1.13.[34] A previous study,[10] dissolved 79% of the outer pericarp by sequentially extracting with alkaline solvents of increasing strength before and after a delignification step resulting in a residue that was 69% glucose and 25% AX (A/X of 1.13). Their reported residue composition was similar to the P1C fraction in the current study. After imaging the P1C sample using light microscopy and SEM, it was confirmed that the inner and outer pericarp were the insoluble materials (**Figures 3.2B and D**). Ferulic acid is the dominant hydroxycinnamic acid and constitutes 95% (w/w) of esterified phenolic groups.[35] Ferulic acid esterified to AX did not appear to prevent bran dissolution because only ~3% was left in the material insoluble in NaOH/urea (P1C) (**Table 3.3**). Most (89.8%) of the arabinoxylans were extracted along with most of the esterified ferulic acid, suggesting that most of the AX was held in the cell wall by ester bonds and crosslinks (**Table 3.3**). The remaining polymers in the material insoluble in NaOH/urea (P1C) could result from physical or covalent association with each other and other cell wall components such as protein, cellulose, and lignin.[7,8,9,12] X-ray diffraction patterns of the material insoluble in NaOH/urea (P1C) showed that the remaining cellulose was crystalline (**Figure 3.4**). The crystalline cellulose structure resisted solubilization and possibly provided the cell wall with structure, which prevented the complete solubilization of the AX and protein. This possibly kept the cell walls intact as imaged in **Figures 3.2B and D**. The crystalline nature of the cellulose, along with crosslinking may prevent complete solubilization of wheat bran. The diffractogram exhibited a cellulose II pattern (**Figure 3.4**), which was reported for regenerated cellulose after NaOH/urea treatment[19] although the dissolution solvent dissolved pure crystalline cellulose (**Table 3.2**). The molecular weight of the

remaining crystalline cellulose in the material insoluble in NaOH/urea (P1C) could be too large for dissolution.

Molecular Weight of HMW Material Insoluble in 80% Ethanol (P3). The dissolution solubles that precipitated out in 80% ethanol (P3C) had a greater A/X ratio (0.93) than DSDPB (0.86) (**Table 3.3**) suggesting that this solvent solubilized AX from lower A/X ratio regions (aleurone and nucellar layer) into LMW sugars that remained soluble in 80% ethanol (S3C) while the precipitate was localized from higher A/X ratio regions of the DSDPB. The P3C fraction was the HMW portion of the total solubles at pH 7 (S2C) (**Figure 3.5A**). The area under the curve for the GPC chromatogram of the S2C fraction (not shown) was mostly comprised of intense refractive index (RI) and ultraviolet (UV) peaks of low molecular weight that matched the retention time of glucose. The molecular weight distribution of P3C was 11,020,467 to 64,224 weight average molecular weight. The RALS indicated a broad, asymmetric, and homogeneous molecular weight distribution (**Figure 3.5A**) as previously reported.[28] The RI showed that the sugar molecular weight distribution was shifted towards HMW while the UV showed a greater concentration of LMW proteins (**Figure 3.5A**).

The P3C fraction had the largest molecular weight, suggesting that materials with higher molecular weight were solubilized after 6 cycle dissolution compared to 3 cycle dissolution. Fewer dissolution cycles were used to obtain the P3A and P3B fractions, which resulted in a significantly lower molecular weight (**Table 3.4**) and consequently a lower percentage of DSDPB dissolved (**Table 3.2**) compared to more dissolution cycles used to obtain P3C. The P3 molecular weight was not affected by increased NaOH% in the NaOH/urea solvent (**Table 3.4**).

Increasing the concentration of sodium hydroxide from 7% (P3A, **Figure 3.6A**) to 9% (P3B, **Figure 3.6B**) did not affect molecular weight (**Table 3.4**) although it has been reported that stronger alkaline concentrations lowered the molecular weight of extracted xylan, decreasing the amount of medium molecular weight extract and increasing the LMW extract.[36] The molecular weight of the P3 fractions from largest to smallest were: P3C > P3B ~ P3A (**Table 3.4**). The dissolution cycles appeared to play a larger role in the current study. Many different molecular weights have been reported for water unextractable AX.[2,9,25,26,27,28,29,30,36,37,38,39] The differing molecular weight values could be due to a variety of variables such as type and concentration of alkaline extraction solvent, extraction conditions and time, and the method of molecular weight determination.

Enzymatic Hydrolysis of HMW Material Insoluble in 80% Ethanol (P3C). Both the protease treated P3C (PP3C) and endoxylanase treated P3C (XP3C) showed a decrease in HMW material and increase in LMW material for both their RI and UV curves compared to P3C (**Figure 3.5**). The observed molecular weight shifts for both detectors after individual protease and endoxylanase treatment could be an indication that there was carbohydrate-protein conjugation in P3C. The protease and endoxylanase treatments decreased the amount of both HMW protein and AX insoluble in 80% ethanol (**Table 3.3**), which confirmed the conclusions described above from the GPC chromatograms in **Figure 3.5**. The protease and endoxylanase treatments decreased the amount of HMW AX insoluble in 80% ethanol by 18% and 49% respectively (**Table 3.3**). The molecular weight of PP3C (**Figure 3.5B**) was little changed compared with P3C (**Table 3.4**), possibly due to the low percentage of protein in the P3C fraction (6.2%, **Table 3.3**). The molecular weight of XP3C (**Figure 3.5C**) was significantly

decreased compared to the P3C fraction (**Table 3.4**). It has been reported that endoxylanase treatment of water extractable AX resulted in a decrease in HMW AX and increase in LMW AX,40 which is in agreement with the data presented in this study.

CONCLUSION

More than 80% of destarched and deproteinized bran may be dissolved in the NaOH/urea solvent and the molecular weight of the dissolution solubles precipitated in 80% ethanol increased with more dissolution cycles. The percentage of arabinoxylans (63%) present in the high molecular weight material insoluble in 80% ethanol originally in the starting material (destarched and deproteinized bran) was the most recovered for characterization compared to existing literature using an alkaline solvent. This solvent exhibited a promising application to solubilize cell wall polymers with functional properties. X-ray diffraction of the material insoluble in NaOH/urea showed that the remaining cellulose was crystalline. Along with crosslinks, the crystalline cellulose may have provided the cell wall with structure to prevent the complete solubilization of the arabinoxylan and protein. In addition, enzymatic treatment of the high molecular weight material insoluble in 80% ethanol provided evidence of carbohydrate-protein conjugation.

ACKNOWLEDGEMENTS

We thank Mr. Ian Andree of the Kansas State University Geology Department for his help running the X-ray diffraction samples, Dr. Jon Faubion of the Department of Grain Science

for his help editing the manuscript, and Dr. Donghai Wang of the Department of Biological and Agricultural Engineering for the use of FTIR. This is contribution no. 18-185-J of the Kansas Agricultural Experiment Station.

REFERENCES

(1) Apprich, S.; Tirpanalan, Ö.; Hell, J.; Reisinger, M.; Böhmdorfer, S.; Siebenhandl-Ehn, S.; Novalin, S.; Kneifel, W. Wheat bran-based biorefinery 2: valorization of products. *Food Sci. and Tech.* **2014,** 56, 222-231.

(2) Maes, C.; Delcour, J.A. Structural characterization of water extractable and water unextractable arabinoxylans in wheat bran. *J. Cereal Sci.* **2002,** 35, 315-326.

(3) Arte, E.; Katina, K.; Holopainen-Mantila, U.; Nordlund, E. Effect of hydrolyzing enzymes on wheat bran cell wall integrity and protein solubility. *Cereal Chem.* **2016,** 93, 162-171.

(4) Reisinger, M.; Tirpanalan, Ö.; Prückler, M.; Huber, F.; Kneifel, W.; Novalin, S. Wheat bran biorefinery – a detailed investigation on hydrothermal and enzymatic treatment. *Bioresour. Technol.* **2013,** 144, 179-185.

(5) Jacquemin, L.; Mogni, A.; Zeitoun, R.; Guinot, C.; Sablayrolles, C.; Saulnier, L.; Pontalier, P-Y. Performance evaluation of a semi-industrial production process of arabinoxylans from wheat bran. *Process Biochem.* **2015,** 50, 605-613.

(6) Prückler, M.; Siebenhandl-Ehn, S; Apprich, S; Höltinger, S; Haas, C; Schmid, E; Kneifel, W. Wheat bran-based biorefinery 1: Composition of wheat bran and strategies of functionalization. *LWT – Food Sci. Technol.* **2014,** 56, 211-221.

(7) Maes, C.; Delcour, J.A. Alkaline hydrogen peroxide extraction of wheat bran non starch polysaccharides. *J. Cereal Sci.* **2001,** 34, 29-35.

(8) Manisseri, C.; Gudipati, M. Bioactive xylo-oligosaccharides from wheat bran soluble polysaccharides. *Food Sci. and Tech.* **2010,** 43, 421-430.

(9) Sun, Y.; Cui, S.W.; Gu, X.; Zhang, J. Isolation and structural characterization of water unextractable arabinoxylans from Chinese black-grained wheat bran. *Carbohydr. Polym.* **2011,** 85, 615-621.

(10) DuPont, M.S.; Selvendran, R.R. Hemicellulosic polymers from the cell walls of beeswing wheat bran: part 1, polymers solubilized by alkali at 2°. *Carb. Res.* **1987,** 163, 99-113.

(11) Kiszonas, A.M.; Fuerst, P.; Morris, C.F. Wheat arabinoxylan structure provides insight into function. *Cereal Chem.* **2013,** 90, 387-395.

(12) Izydorczyk, M.S.; Biliaderis, C.G. Cereal arabinoxylan advances in structure and physiochemical properties. *Carbohydr. Polym.* **1995,** 28, 33-48.

(13) Beaugrand, J.; Crônier, D.; Thiebeau, P.; Schreiber, L.; Debeire, P.; Chabbert, B. Structure, chemical composition, and xylanase degradation of external layers isolated from developing wheat grain. *J. Agric. Food Chem.* **2004a,** 52, 7108-7117.

(14) Beaugrand, J.; Reis, D.; Guillon, F.; Debeire, P.; Chabbert, B. Xylanase-mediated hydrolysis of wheat bran: Evidence for subcellular heterogeneity of cell walls. *Int. J. of Plant Sci.* **2004b,** 165 (4), 553-563.

(15) Ladisch, M.R.; Ladisch, C.M.; Tsao, G.T. Cellulose to sugars: new path gives quantitative yield. *Science* **1978**, 201, 743-745.

(16) Cai, J.; Zhang, L. Rapid dissolution of cellulose in LiOH/Urea and NaOH/Urea aqueous solutions. *Macromol. Biosci.* **2005,** 5, 539-548.

(17) Cai, J.; Zhang, L. Unique gelation behavior of cellulose in NaOH/Urea aqueous solution. *Biomacromolecules.* **2006,** 7, 183-189.

(18) Cai, J.; Zhang, L.; Chang, C.; Cheng, G.; Chen, X.; Chu, B. Hydrogen-bond-induced inclusion complex in aqueous cellulose/LiOH/Urea solution at low temperature. *ChemPhysChem.* **2007,** 8, 1572-1579.

(19) Qi, H.; Yang, Q.; Zhang, L.; Liebert, T.; Heinze, T. The dissolution of cellulose in NaOH-based aqueous system by two-step process. *Cellulose* **2011,** 18, 237-245.

(20) Cai, J.; Zhang, L.; Liu, S.; Liu, Y.; Xu, X.; Chen, X.; Chu, B.; Guo, X.; Xu, J.; Cheng, H.; Han, C.C.; Kuga, S. Dynamic self-assembly induced rapid dissolution of cellulose at low temperatures. *Macromolecules.* **2008,** 41, 9345-9351.

(21) Rosa-Sibakov, N.; Poutanen, K.; Micard, V. How does wheat grain, bran and aleurone structure, impact their nutritional and technological properties? *Trends Food Sci. Technol.* **2015,** 41, 118-134.

(22) AACC International. Approved Methods of Analysis, 11th Ed. Method 08-03.01, 44-15.02, 46-30.01. AACC International, St. Paul, MN, U.S.A.

(23) Qi, H.; Chang, C.; Zhang, L. Effects of temperature and molecular weight on dissolution of cellulose in NaOH/urea aqueous solution. *Cellulose* **2008,** 15, 779-787.

(24) Kim, K.-H.; Tsao, R.; Yang, R.; Cui, S.W. Phenolic acid profiles and antioxidant activities of wheat bran extracts and the effect of hydrolysis conditions. *Food Chemistry* **2006,** 95, 466-473.

(25) Annison, G.; Choct, M.; Cheetham, N.W. Analysis of wheat arabinoxylans from a large-scale isolation. *Carbohydr. Polym.* **1992,** 19 (3), 151-159.

(26) Bergmans, M.E.F.; Beldman, G.; Gruppen, H.; Voragen, A.G.J. Optimization of the selective extraction of (glucurono)arabinoxylans from wheat bran: Use of barium and calcium hydroxide solution at elevated temperatures. *J. Cereal Sci.* **1996,** 23, 235-245.

(27) Schooneveld-Bergmans, M.E.F.; Beldman, G.; Voragen, A.G.J. Structural features of (glucurono) arabinoxylans extracted from wheat bran by barium hydroxide. *J. Cereal. Sci.* **1999b,** 29, 63-75.

(28) Hollmann, J.; Lindhauer, M.G. Pilot-scale isolation of glucuronoarabinoxylans from wheat bran. *Carbohydr. Polym.* **2005,** 59, 225-230.

(29) Zhou, S.; Liu, X.; Guo, Y.; Wang, Q.; Peng, D.; Cao, L. Comparison of the immunological activities of arabinoxylans from wheat bran with alkali and xylanase-aided extraction. *Carbohydr. Polym.* **2010,** 81, 784-789.

(30) Zhang, Y.; Pitkanen, L.; Douglade, J.; Tenkanen, M.; Remond, C.; Joly, C. Wheat bran arabinoxylans: Chemical structure and film properties of three isolated fractions. *Carbohydr. Polym.* **2011,** 86, 852-859.

(31) Barron, C.; Rouau, X. FTIR and Raman signatures of wheat grain peripheral tissues. *Cereal Chem.* **2008,** 85 (5), 619-625.

(32) Brillouet, J.M. Investigation of the structure of a heteroxylan from the outer pericarp (beeswing bran) of wheat kernel. *Carbohydr. Res.* **1987,** 159 (1), 109-126.

(33) Antoine, C.; Peyron, S.; Mabille, F.; Lapierre, C.; Bouchet, B.; Abecassis, J.; Rouau, X. Individual contribution of grain outer layers and their cell wall structure to the mechanical properties of wheat bran. *J. Agric. Food Chem.* **2003,** 51 (7), 2026-2033.

(34) Barron, C.; Surget, A.; Rouau, X. Relative amounts of tissues in mature wheat (Triticum aestivum L.) grain and their carbohydrate and phenolic acid composition. *J. Cereal Sci.* **2007,** 45, 88-96.

(35) Parker, M.L.; Ng, A.; Waldron, K.W. The phenolic acid and polysaccharide composition of cell walls of bran layers of mature wheat (Triticum aestivum L. cv. Avalon) grains. *J. Sci. Food Agric.* **2005,** 85, 2539-2547.

(36) Merali, Z.; Collins, S.R.A.; Elliston, A.; Wilson, D.R.; Kasper, A.; Waldron, K.W. Characterization of cell wall components of wheat bran following hydrothermal pretreatment and fractionation. *Biotechnol. Biofuels.* **2015,** 8, DOI 10.1186/s13068-015-0207-1.

(37) Shiiba, K.; Yamada, H.; Hara, H.; Okada, K.; Nagao, S. Purification and characterization of two arabinoxylans from wheat bran. *Cereal Chem.* **1993,** 70, 209-214.

(38) Schooneveld-Bergmans, M.E.F.; van Dijk, Y.M.; Beldman, G.; Voragen, A.G.J. Physicochemical characteristics of wheat bran glucuronoarabinoxylans. *J. Cereal Sci.* **1999a,** 29, 49-61.

(39) Swennen, K.; Courtin, C.M.; Lindemans, G.; Delcour, J.A. Largescale production and characterization of wheat bran arabinoxylooligosaccharides. *J. Sci. Food Agric.* **2006,** 86, 1722-1731.

(40) Courtin, C.M.; Delcour, J.A. Relative activity of endoxylanases towards water-extractable and water-unextractable arabinoxylan. *J. Cereal Sci.* **2001,** 33, 301-312.

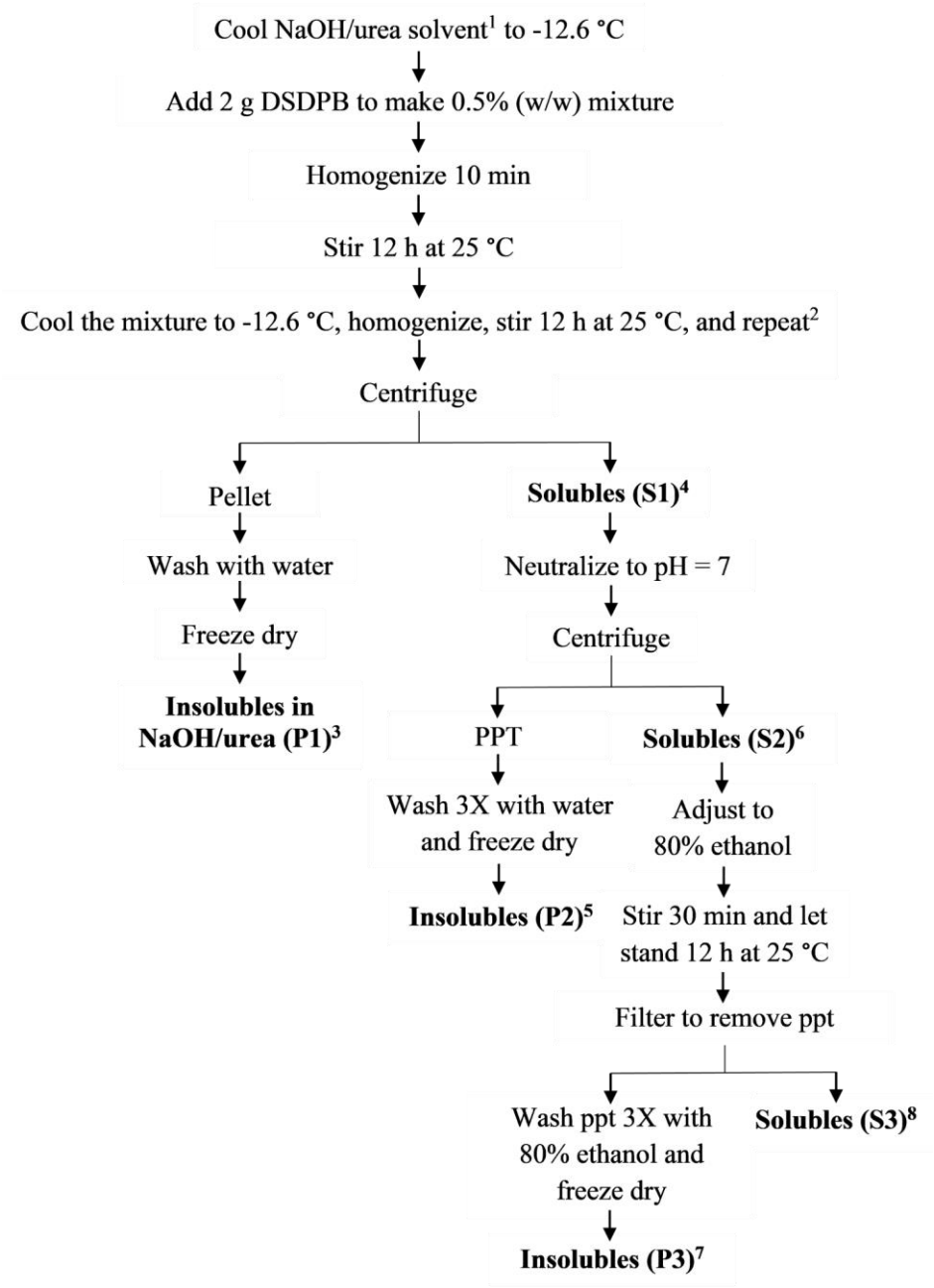

Figure 3.1 NaOH/urea solvent wheat bran dissolution procedure.*

[1]Either a 7% NaOH/12% urea or 9% NaOH/12% urea solvent.
[2]3 cycle dissolution, performed step 3 times; 6 cycle dissolution, performed step 6 times.
[3]P1 = material insoluble in NaOH/urea.
[4]S1 = NaOH/urea solubles.
[5]P2 = high molecular weight material insoluble at pH 7.
[6]S2 = total solubles at pH 7.
[7]P3 = high molecular weight material insoluble in 80% ethanol.
[8]S3 = low molecular weight material soluble in 80% ethanol.
*A = 3 cycle dissolution using 7% NaOH/12% urea solvent.
*B = 3 cycle dissolution using 9% NaOH/12% urea solvent.
*C = 6 cycle dissolution using 7% NaOH/12% urea solvent.

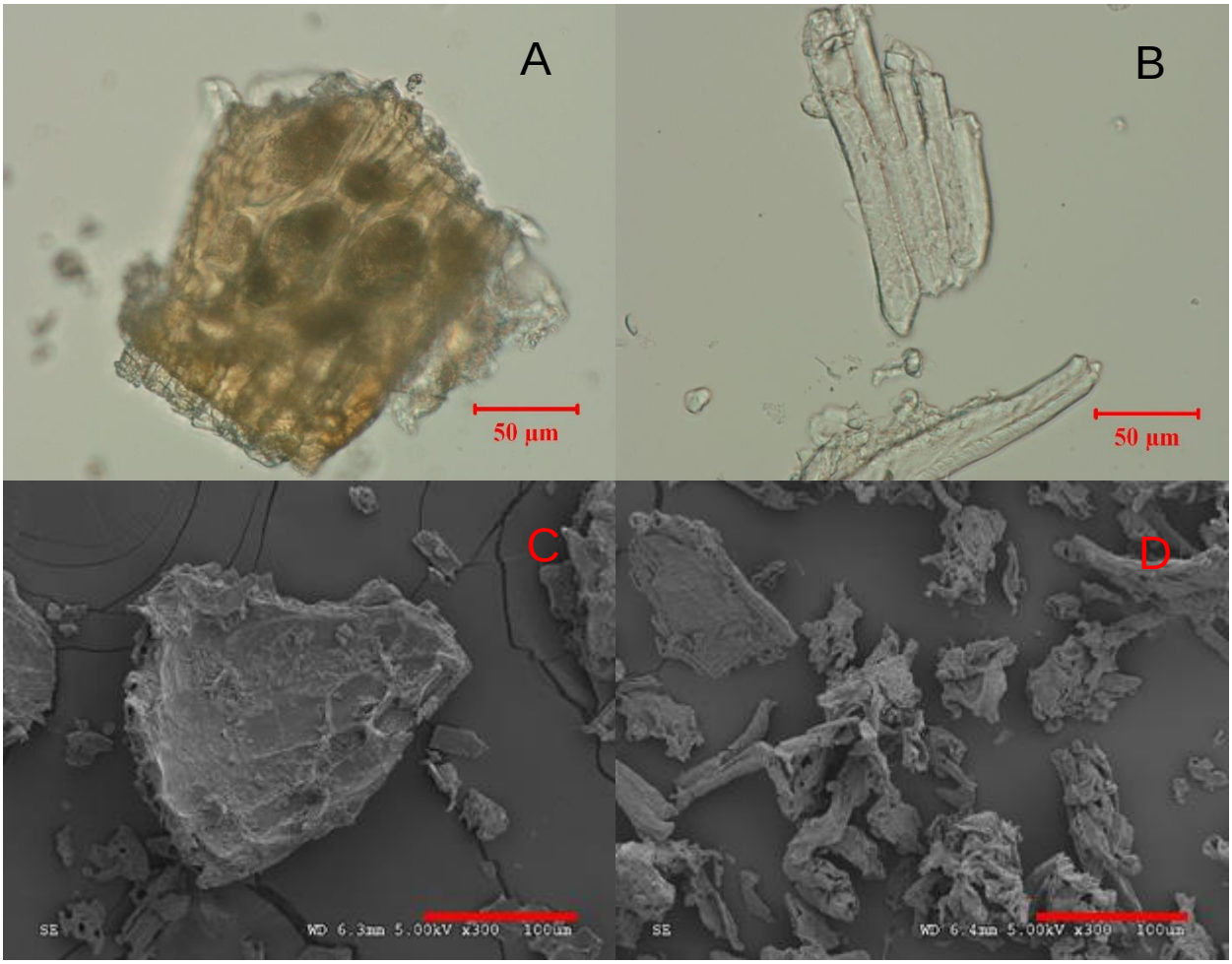

Figure 3.2 Microscopy images of DSDPB and material insoluble in NaOH/urea in Figure 3.1.

A and C = destarched and deproteinized bran (DSDPB); B and D = material insoluble in NaOH/urea (P1C); A and B = light microscopy at 40× magnification with 50 µm scale bars; C and D = scanning electron microscopy at 300× magnification with 100 µm scale bars.

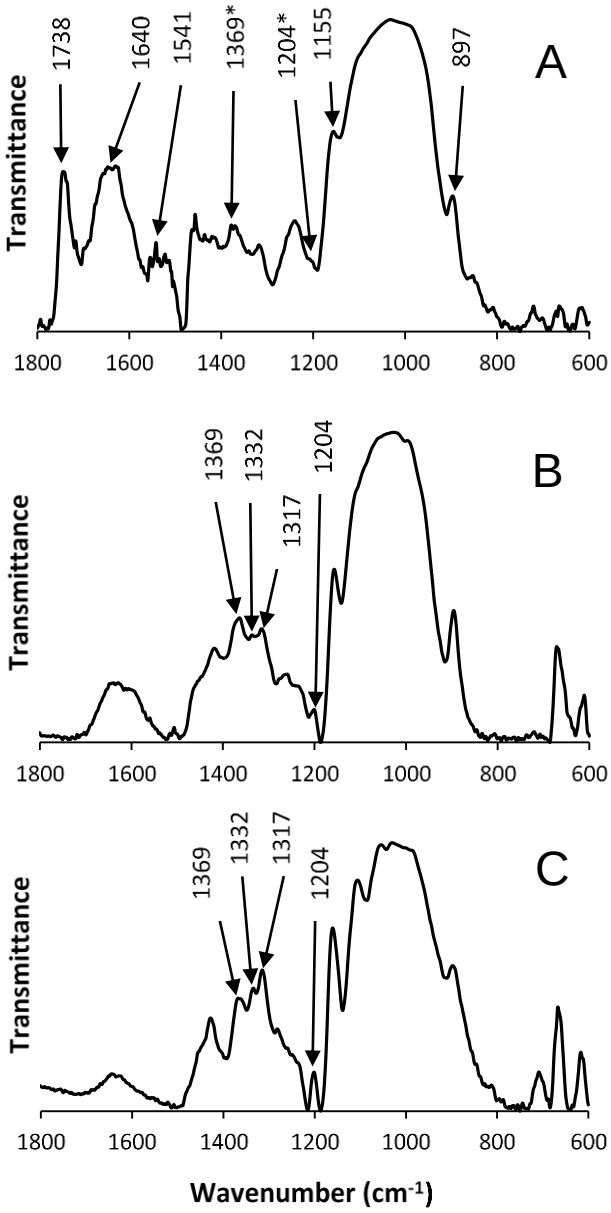

Figure 3.3 FTIR spectra of bran dissolution fractions in Figure 3.1 and microcrystalline cellulose.

A = destarched and deproteinized bran (DSDPB); B = material insoluble in NaOH/urea (P1C); C = microcrystalline cellulose.
*1369 and 1204 cm^{-1} refer to signals used to identify cellulose along with 1317 and 1332 cm^{-1} which are labeled in B and C.

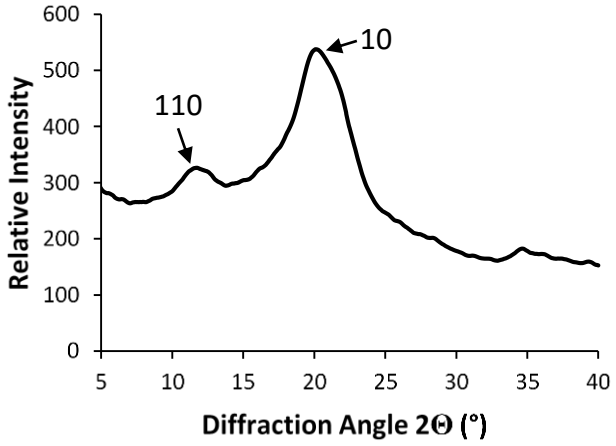

Figure 3.4 X-ray diffraction pattern of partially crystalline material insoluble (P1C) in 6 cycle dissolution using 7% NaOH/12% urea solvent (see Figure 3.1).

P1C cellulose II diffraction peaks; 110, 10, and 200 planes corresponded to 2Θ = 12.0 °, 19.9 ° and 22.1 ° respectively.[19] The 200 plane was not resolved.

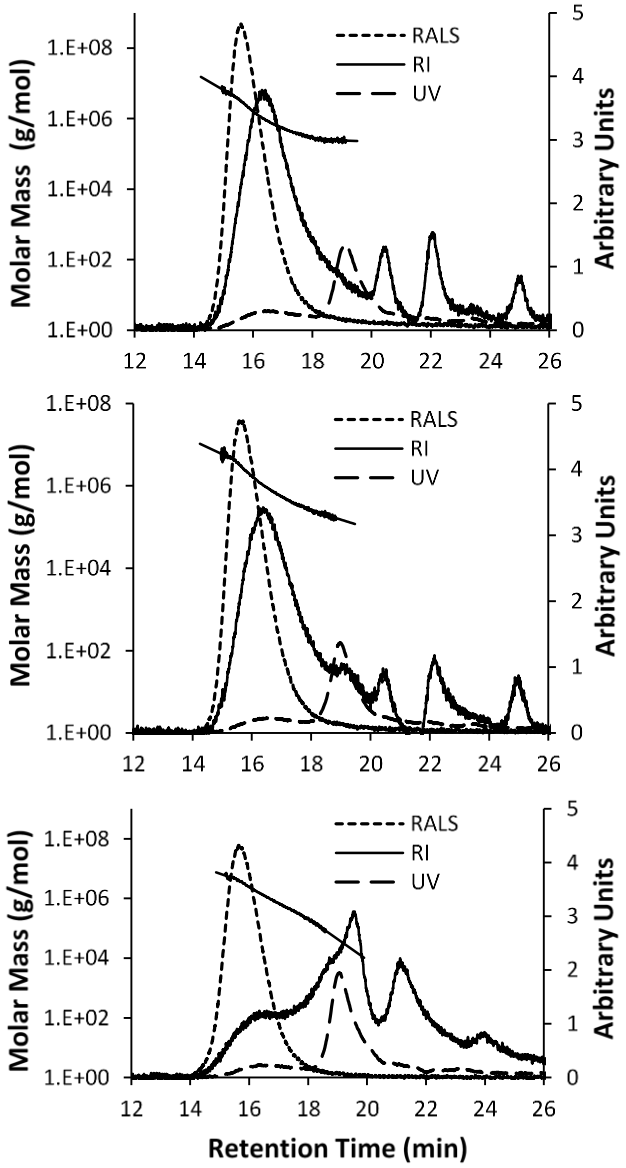

Figure 3.5 Molecular weight distribution of high molecular weight material insoluble in 80% ethanol in 7% NaOH/12% urea solvent using a 6 cycle dissolution (A; P3C in Figure 3.1) treated with a protease (B) or endoxylanase (C).

A = P3C; B = protease treated P3C (PP3C); C = endoxylanase treated P3C (XP3C).
The right angle light scattering, RALS; refractive index, RI; ultraviolet, UV; and molecular weight distribution curves (g/mol) are shown.

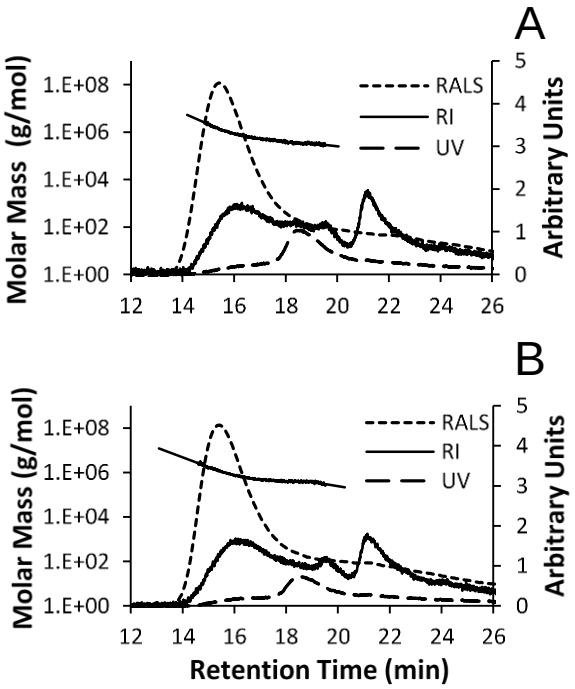

Figure 3.6 Molecular weight distribution of high molecular weight material insoluble in 80% ethanol in 7% NaOH/12% urea solvent (A) and 9% NaOH/12% urea solvent (B) using 3 cycle dissolution (P3A and P3B in Figure 3.1).

The right angle light scattering, RALS; refractive index, RI; ultraviolet, UV; and molecular weight distribution curves (g/mol) are shown.

Table 3.1 Particle size distribution of untreated bran as determined by a modified AACC 66-20.01 ro-tap sieve shaker method.[1]

Bran particle size distribution	
Micron opening	Average (%) held over
350	0.2±0.1
212	43.3±0.4
180	17.1±0.2
106	16.6±0.4
53	16.9±0.4
0	5.9±0.5

[1]Two pan cleaners were used per sieve; n = 3.

Table 3.2 Yield (%) of insoluble (P1) and soluble (S1) materials in a mixture of NaOH/urea solvent; materials soluble in the NaOH/urea solvent but insoluble at pH 7 (P2) and materials soluble at pH 7 (S2); and materials soluble at pH 7 but insoluble in 80% ethanol (P3) and materials soluble in 80% ethanol (S3) (see Figure 3.1).[1,2]

			From DSDPB (%)[3]		From S1 (%)		From S2 (%)	
Treatment	Cycle[4]	Sample notation	P1[4]	S1[4]	P2[4]	S2[4]	P3[4]	S3[4]
7%NaOH/ 12% urea	3	A	18.8±0.3b	81.2±0.3b	7.1±0.7b	74.1±1.0b	38.0±1.0b	36.1±0.0a
9%NaOH/ 12% urea	3	B	20.1±0.8b	80.0±0.8b	6.9±0.8b	73.0±1.6b	35.8±0.1b	37.2±1.5a
7%NaOH/ 12% urea	6	C	15.9±1.2a	84.1±1.2a	5.9±0.8a	78.2±1.9a	42.6±1.6a	35.6±3.5a
7%NaOH/ 12% urea[5]	-	-	0.79±0.9	99.12±0.7	-	-	-	-

[1]All percentages are based on the 2.0 g of DSDPB.
[2]Numbers in the same column followed by a letter in common are not significantly different at $p < 0.05$; $n = 2$.
[3]DSDPB = destarched and deproteinized bran.
[4]P1% = (P1 g/2.0 g) × 100; S1% = 100-P1%; P2% = (P2 g/2.0 g) × 100; S2% = S1% – P2%; P3% = (P3 g/2.0 g) × 100; S3% = S2% – P3%.
[5]Microcrystalline cellulose dissolution.

Table 3.3 Chemical composition of the material insoluble (P1C) in 6 cycle dissolution using 7% NaOH/12% urea solvent; high molecular weight material soluble in the solvent but insoluble at pH 7 (P2C); high molecular weight material soluble at pH 7 but insoluble in 80% ethanol (P3C); protease treated P3C insoluble in 80% ethanol (PP3CP); and endoxylanase treated P3C insoluble in 80% ethanol (XP3CP) (see Figure 3.1).

Composition (%)[1]	DSDPB[2]	P1C	P2C	P3C	PP3CP	XP3CP
Arabinose	20.7±0.2	14.6±0.7	4.9±0.4	31.9±1.7	26.0±0.2	24.7±1.0
Xylose	24.2±0.4	14.1±0.5	52.9±1.2	34.3±1.9	31.4±0.6	27.0±1.0
Glucose	28.5±0.6	67.5±1.3	37.7±0.9	21.9±1.3	22.8±0.8	26.2±0.9
Cellulose	27.5[3]	67.5±1.3[4]	37.7±0.9[4]	21.9±1.3[4]	22.8±0.8[4]	26.2±0.9[4]
Galactose	1.4±0.1	1.0±0.0	0.5±0.1	2.1±0.0	1.4±0.1	1.5±0.0
AX[5]	39.5	25.3	50.9	58.3	50.5	45.5
A/X Ratio[6]	0.86	1.04	0.09	0.93	0.83	0.91
% AX from DSDPB	100	10.2	7.6	62.9	51.5	32.3
Protein	9.4±0.2	2.6±0.7	-	6.2±0.9	2.3±0.5	3.2±0.7
Ash	5.1±0.1	-	-	-	-	-
Starch	1.0±0.1	-	-	-	-	-
Ferulic acid (µg/g)	3530±4.8	102±3.5[7]	-	-	-	-

[1]Expressed as weight percentage (dm) of DSDPB and respective precipitate fractions, n = 2.
[2]DSDPB, destarched and deproteinized bran.
[3]Cellulose% = glucose% – starch%.
[4]Cellulose% = glucose%.
[5]AX = arabinoxylan = 0.88 × (%arabinose + %xylose).
[6]A/X = arabinose/xylose ratio.
[7]P1C ferulic acid (µg/g) = DSDPB ferulic acid (3530) - S2C ferulic acid (3428) = 102; S2C = total solubles at pH 7.

Table 3.4 Weight average molecular weight (Mw) of high molecular weight material soluble in 6 cycle dissolution using 7% NaOH/12% urea solvent at pH 7 but insoluble in 80% ethanol (P3C) and high molecular weight materials soluble at pH 7 but insoluble in 80% ethanol treated with protease (protease treated P3C) or endoxylanase (endoxylanase treated P3C); and high molecular weight materials soluble in 3 cycle dissolution using 7% NaOH/12% urea solvent (P3A) or 9% NaOH/12% urea solvent (P3B) at pH 7 but insoluble in 80% ethanol (see Figure 3.1).[1,2]

Sample	Solvent	Cycle	Mw (g/mol)
P3C	7% NaOH/ 12% urea	6	1,156,326a
Protease treated P3C	-	-	1,081,961a
Endoxylanase treated P3C	-	-	180,324b
P3A	7% NaOH/ 12% urea	3	661,816c
P3B	9% NaOH/ 12% urea	3	670,567c

[1]The Mw values are the average of two replicates each within 20% of each other; n = 2.
[2]Numbers followed by a letter in common are not significantly different at $p < 0.05$.

Chapter 4 - Hydrothermal treatment and enzymatic hydrolysis of wheat bran and their effects on physical structure

ABSTRACT

Wheat bran was enzymatically and hydrothermally treated to solubilize the bran fraction. Unlike previous research, in this study, the starch and protein were kept and not removed before xylanase treatment. This could make the process more economical due to the increased product yield. The retained protein and glucose containing polymers could provide functional benefits in addition to the arabinoxylan (AX). Wheat bran hydrolyzed with thermostable α-amylase at 95°C for 2h at pH 6.7, protease at 70°C for 3h at pH 6.3, and xylanase at 50°C for 24h at pH 5.5 was the recommended treatment for the production of solubles because of high bran and AX solubilization without 140°C treatment. The combined solubles had a viscosity of 23 cP (10% w/w solids) and a molecular weight between ~600 and 20,000. The percentage of AX solubilized from wheat bran was 50% and the percentage of AX in the solubles was 23%. A cooking step (> 95°C) followed by xylanase was required before the aleurone layer structure was completely lost and disorganized. X-ray diffraction, small angle X-ray scattering, solid-state NMR, and light microscopy were used to study the physical structure of the insoluble bran fractions. The pericarp structure was not affected by enzymatic or hydrothermal treatments.

Wheat bran is comprised of several layers which are as follows from outer to inner; epidermis, hypodermis, cross cells, tube cells, testa, nucellar layer, and aleurone layer (Benamrouche et al. 2002). Wheat bran is abundant in hemicellulose (~40% of destarched wheat bran) (Beaugrand et al. 2004a), protein (13-19.5%) (Arte et al. 2016), and dietary fiber (43-53%) (Rose and Inglett 2010). The number of wheat bran containing products launched has increased from 52 in 2001 to 798 in 2011 (Prückler et al. 2014). Research exploring the structural factors limiting solubilization and processing of wheat bran into heathy ingredients would widen its usage in the food industry and would increase the value of this cheap by-product of flour milling.

Extracting bran components to produce a functional product and maximize the amount solubilized to provide an economically feasible product requires an understanding of wheat bran structure. Wheat bran consists of cell walls which are comprised of non-starch polysaccharides such as arabinoxylan (AX) and (1-3, 1-4)-β-glucan along with protein and lignin in a matrix with cellulose microfibrils (Beaugrand et al. 2004b; Beaugrand et al. 2004a). Covalent linkages and physical interactions between polymers, the presence of lignin (Benamrouche et al. 2002), highly substituted AX (Van Craeyveld et al. 2010), ferulic dimers (Beaugrand et al. 2004a), ether linkages (Beaugrand et al. 2004a), and the exclusion of enzymes (Beaugrand et al. 2004b) can limit hydrolysis.

The starch and protein contents, often removed during the wheat bran solubilization processes, could be retained to add value and increase the yield of wheat bran solubles. For example, wheat bran proteins from the aleurone layer can be used as ingredients in bread making, controlling enzymatic browning, and nutritional fortification (Balandrán-Quintana et al. 2015). The solubilized wheat bran starch, cellulose, and β-glucan could possibly be used in baking to increase flour water absorption, add sweetness and color, substitute sucrose, and

provide fermentable sugars for yeast. Arabinoxylans may function as a thickener, emulsifier, binder, and film-former (Jacquemin et al. 2015). Arabinoxylans are known to have positive physiological effects acting as a prebiotic in oligosaccharide form (Pareyt et al. 2011). Furthermore, the minimization of hydrolysis is crucial because high molecular weight proteins have better functionality (Arte et al. 2016) and polysaccharide fractions (fructooligosaccharides, galactooligosaccharides, and xylooligosaccharides) can function as prebiotics and are of commercial interest (Immerzell et al. 2014).

Xylanase hydrolysis affects the percentage of AX solubilized, AX molecular weight, and arabinose to xylose ratios (A/X) (Benamrouche et al. 2002; Beaugrand et al. 2004b; Maes et al. 2004; Van Craeyveld et al. 2010; Santala et al. 2011). Xylanase hydrolysis depleted 50% of the wheat bran AX (Benamrouche et al. 2002; Beaugrand et al. 2004b). Similarly, Van Craeyveld et al. (2010) reported that 32-55% of wheat bran AX were solubilized by xylanase treatment. Destarched and deproteinized wheat bran was treated with xylanase solubilizing up to 45% of water unextractable AX (Maes et al. 2004). Xylanase was localized to regions of the wheat bran with low A/X ratios (Beaugrand et al. 2004b) which corresponded to findings that AX yield increased when xylanase hydrolyzed AX with low A/X compared with high A/X (Van Craeyveld et al. 2010). As expected, the aleurone layer was fully destroyed while the pericarp and testa layers were not visibly changed after xylanase treatment of destarched wheat bran (Beaugrand et al. 2004b). The percentage of AX solubilized increased with incubation time and dosage while the molecular weight of the solubles decreased as the xylanase dosage increased (Maes et al. 2004). In agreement, Santala et al. (2011) reported that both increased xylanase incubation time (24 h vs. 4 h) and dosage shifted the molecular weight towards smaller polymers.

The effect of starch and protein solubilization on wheat bran dissolution has been evaluated (Benamrouche et al. 2002; Maes and Delcour 2002; Swennen et al. 2006; Santala et al. 2013; Arte et al. 2006). The removal of starch and protein solubilized 51-55% of the wheat bran dry matter (Maes and Delcour 2002; Swennen et al. 2006). Interestingly, neutral protease treatment was not effective at releasing and hydrolyzing aleurone cell protein but that most of the reported wheat bran protein hydrolysis was from the adhered subaleurone layer (Arte et al. 2016). Enzymes with xylanase, β-glucanase, β-glucosidase, polygalacturonase, cellulase, and endoglucanase activity did not aid in the release of proteins from aleurone cells or increase protein solubilization (Arte et al. 2016). Similarly, xylanase treatment did not significantly affect the molecular weight of solubilized proteins (Santala et al. 2013). In contrast, xylanase treatment released protein from the aleurone cells solubilizing 3% of wheat bran dry matter in protein (Benamrouche et al. 2002).

Hydrothermal pretreatment (121 °C for 15 min) of wheat bran before xylanase incubation decreased the amount of monomers released from the AX polymer (Van Craeyveld et al. 2010). Wheat bran treated using a microwave found that hydrothermal pretreatment at 130 °C released 36% of the wheat bran solids (Rose and Inglett 2010). Reisinger et al. (2013) hydrothermally treated wheat bran and reported that between temperatures 140-180 °C around 60% of glucose, 20-65% xylose, 30-80% arabinose, and 30-70% protein was released. The percent of solids released from wheat bran depended on the instrument used for heating, temperature, and treatment time.

In this study, wheat bran was subjected to hydrothermal treatments. Starch and protein were kept and not removed before endoxylanase treatment. In addition, the physical structure of wheat bran was studied to understand the limitations of the hydrothermal and enzymatic

treatments on solubilizing wheat bran. The specific objectives were; 1) determine the effect of hydrothermal, xylanase, α-amylase, and protease treatment on AX yield and the molecular weight and viscosity of the soluble fraction containing all bran components from the treatments and 2) determine the effect of hydrothermal and enzymatic treatment on the physical structure of the insoluble wheat bran fraction.

MATERIALS AND METHODS

Materials. Hard red winter wheat bran, referred to as untreated wheat bran (UB), was obtained from the Hal Ross flour mill (Kansas State University, Manhattan, KS). Hydrochloric acid, nitric acid, and acetic acid were all analytical grade (Sigma Aldrich, St. Louis). A thermostable α-amylase (TS α-amylase) (Termamyl 120L) and an intermediate thermostable α-amylase (ITS α-amylase) (BAN 480L) were obtained from Novozymes (Franklinton, NC). Multifect CX 12L, an endoxylanase from Trichoderma reesei, and FoodPro PNL, a neutral protease, were obtained from Danisco (Copenhagen Denmark).

The TS α-amylase had an enzyme activity of 120 KNU-T/g (Kilo Novo α-amylase Units/g). The ITS α-amylase had an enzyme activity of 480 KNU-B/g (Kilo Novo α-amylase Units/g). One KNU was the amount of enzyme that can dextrinize 5.26 g starch (dry basis) per hour under standard conditions (pH = 7.1 at 37 °C). The protease had an enzyme activity of 1,600 AZO/g. The endoxylanase had an activity of 30,450 ABX/g (Acid Birchwood Xylanase Units/g). The activity is determined by the release of reducing sugars by the action of xylanase on a birchwood xylan substrate.

Wheat Bran Preparation. A portion of the UB was further milled to a smaller particle size using a single blue Ross roll stand with a differential of 2.5:1, 0.5 inch spiral, 24 corrugations/in. pitch, and a grinding action of dull:dull (Ross, Oklahoma City, OK). The milled bran will be referred to as ground wheat bran (GB). A portion of the GB was ball milled for 24 h at ~70 rpm and will be referred to as ball milled wheat bran (BMB).

Particle Size Distribution. The particle size distribution was determined using a modified AACC 66-20.01 Ro-Tap Sieve Shaker method (AACCI, 2009). The UB and GB were analyzed in triplicate. One hundred grams of UB and GB (14% MB) were weighed and sifted for 6 min with 2 pan cleaners per sieve. The data was recorded as the overs of the 2000, 1400, 1000, 600, 210, and < 210 µm screens for UB and as the overs of the 350, 210, 180, 53, and < 53 µm screens for GB.

Hydrothermal Treatment of Wheat Bran. The bran mixtures were hydrothermally treated at various temperatures (25 °C, 70 °C, 95 °C) and incubation times (1.5 h and 3 h) (**Figure 6.1**). In addition, a bran mixture was treated at 140 °C for 40 min in a PARR reactor (PARR Instrument Co., Moline, IL) (1 L vessel). The 40 min treatment time at 140 °C was used because the PARR reactor could not hold the temperature any longer. A 5% w/v mixture of UB (10 g db) and water (190 mL) was prepared and the pH measured before hydrothermal treatment. This is a normal mixture of bran and water as most are between 5-14.3% w/v for hydrothermal and enzymatic treatment (Maes and Delcour 2002; Swennen et al. 2006; Rose and Inglett 2010; van den Borne et al. 2012; Reisinger et al. 2013; Arte et al. 2016).

After treatment, the samples were cooled to room temperature and the pH was measured again. The supernatant was removed by centrifuging at 21,100 x g for 10 min. The undissolved bran was washed 3 times with water (100 mL each time) to remove all solubles and lastly with

ethanol (200 mL) to flush out water. The physical structure of the undissolved bran was evaluated using bright field microscopy. The undissolved bran was subsequently vacuum dried at 60 °C and then weighed to determine the percentage of bran solubilized. The supernatant was spray dried. A spray dryer (Büchi Mini Spray Dryer B-290, New Castle, DE) was used to dry the bran solubles after hydrothermal and enzymatic treatment. The inlet temperature was set to 150 °C, aspirator to 100%, air flow to 30 mm, the pump to 10%, and nozzle cleaning at 1. The spray dried material was used to determine composition, molecular weight, and viscosity data. The procedure describing the separation of the undissolved bran (pellet) from the supernatant and preparation of both for analysis was applied to the following experiments after xylanase hydrolysis of wheat bran: xylanase hydrolysis; intermediately thermostable α-amylase + xylanase; thermostable α-amylase + xylanase; thermostable α-amylase + protease + xylanase; and hydrothermal treatment + xylanase treatment.

Xylanase Hydrolysis of Wheat Bran. The effect of xylanase on wheat bran arabinoxylan solubilization was studied (**Figure 6.2**). A 5% w/v mixture of UB (10 g db) and water (190 mL) was prepared and the pH measured. Next, the pH was adjusted to 5.5 using 0.5N HCl. The UB was then treated with xylanase (1000 ABX, 28 µL) for 24 h at 55 °C. The data from this treatment will be referred to as xylanase.

Intermediately Thermostable and Thermostable α-amylase and Xylanase Hydrolysis of Wheat Bran. A separate set of experiments were performed to determine the effect of α-amylase treatment on soluble and insoluble bran components. The UB was first treated with either an ITS α-amylase or a TS α-amylase followed by xylanase. First, a 5% w/v mixture of UB (10g db) and water (190 mL) was prepared without pH adjustment (pH = 6.4). ITS α-amylase was added (8.6 KNU, 15 µL) (**Figure 6.3**) and incubated at 70 °C for 2 h or TS α-

amylase was added (8.6 KNU, 60 µL) (**Figure 6.4**) and incubated at 95 °C for 2 h. The TS α-amylase dosage was chosen based upon Maes and Delcour (2002) and the ITS α-amylase dosage was set so the same enzyme units were added per gram of UB compared to TS α-amylase. The mixture was then cooled to 55 °C and the pH was adjusted to 5.5. A 1000 ABX dosage of xylanase (28 µL) was then added and incubated for 24 h. The data from these treatments will be referred to as TS α-amylase + xylanase and ITS α-amylase + xylanase.

Thermostable α-amylase, Protease, and Xylanase Hydrolysis of Wheat Bran. Finally, three types of enzymes were used to treat UB [TS α-amylase + protease + xylanase] (**Figure 4.1**). The protease was added to determine its effect on soluble and insoluble bran components. A 5% w/v mixture of UB (10g db) and water (190 mL) was prepared and the pH was checked. To limit the amount of salts added into the mixture the pH was not adjusted. TS α-amylase was added (8.6 KNU, 60 µL) and incubated at 95 °C for 2 h. The mixture was cooled to 55 °C and a protease was added (48 AZO, 25 µL) and mixed for 3 h. This dosage was within the recommended dosage range according to its product data sheet. The protease was denatured by heating the mixture to 100 °C for 30 min. The mixture was then cooled to 55 °C and the pH was adjusted to 5.5. A 1000 ABX dosage of xylanase (28 µL) was then added and incubated for 24 h at 55 °C. The data from this treatment will be referred to as TS α-amylase + protease + xylanase.

Hydrothermal Treatment Followed by Xylanase Treatment. The effect of hydrothermal treatment on the degree of arabinoxylan hydrolysis by xylanase treatment was evaluated. A 5% w/v mixture of UB (10 g db) and water (190 mL) was prepared and the pH measured. The bran mixtures were hydrothermally treated at either 140 °C for 40 min or 95 °C for 3 h. The mixture was cooled to room temperature and the pH was measured again and adjusted to 5.5 using 0.5 N HCl. The UB was then treated with a xylanase (1000 ABX, 28 µL)

for 24 h at 55 °C. The data from these treatments will be referred to as 95 °C + xylanase and 140 °C + xylanase.

Neutral Protease Treatment of UB, GB, and BMB. The effect of wheat bran particle size on the degree of protein solubilization by protease treatment. A 5% w/v mixture of bran (UB, GB, or BMB) (10 g db) and water (190 mL) was prepared and the pH measured. Without pH adjustment, protease was added (48 AZO, 25 µL) and mixed for 3 h at 55 °C. After treatment, the samples were cooled to room temperature and the pH was measured again. The supernatant was removed by centrifuging at 21,100 × g for 10 min. The undissolved bran was washed 3 times with water (100 mL each time) to remove all solubles and lastly with ethanol (200 mL) to flush out water. All solubles were discarded. The undissolved bran was subsequently vacuum dried at 60 °C and then weighed to determine the percentage of bran solubilized and the protein content of the insoluble fraction was determined.

Updegraff Treated Wheat Bran. The effect of hydrothermal treatment (25 °C vs. 140 °C) of UB on Updegraff reagent insolubles was determined. The Updegraff reagent can hydrolyze biological plant material leaving the crystalline cellulose intact at 100 °C. Untreated wheat bran (0.5 g bran/9.5 g water, 5% w/w) was treated at 25 °C or 140 °C for 40 min and then freeze dried. The 140 °C treated sample was heated in a PARR reactor (PARR Instrument Co., Moline, IL) (1 L vessel). The freeze-dried wheat bran samples were added to the Updegraff reagent (acetic acid, nitric acid, water; 8:1:2 v/v) at a 15:1 solvent to sample ratio (0.5 g bran/7.5 g solvent) (Updegraff 1969). The samples were heated at 100 °C for 30 min (Updegraff 1969). After heating, the samples were cooled to room temperature and were centrifuged at 21,100 × g for 15 min and the supernatant was discarded. The pellets were washed with 40 mL water 3 times with centrifuging in between using the same settings at mentioned above. The supernatant

was discarded after washing. The pellets were freeze dried and then weighed to determine the yield of insoluble material. This experiment was repeated except the hydrothermally treated bran samples were treated with the Updegraff reagent at 25 °C, not 100 °C.

The undissolved bran fractions from the 140 °C + xylanase treatment and from the TS α-amylase + protease + xylanase treatment were treated with the Updegraff reagent at 100 °C (same concentrations and conditions as described above) and air dried before X-ray diffraction (XRD) analysis. These fractions were analyzed using XRD before and after Updegraff reagent treatment.

General Analysis. Protein content was determined by nitrogen combustion (N% × 5.70). Ash content was determined using AACCI method 08-03.01. The moisture contents of the samples were determined by oven drying for 1 h at 130 °C (AACCI method 44-15.02). Starch content was determined using the Total Starch Assay Procedure (Megazyme, Wicklow, Ireland) following AACC method 76-13.01. Mixed-linkage β-glucan content was determined using the β-Glucan Content of Barley and Oats-Rapid Enzymatic Procedure AACC method 32-23.01. Klason lignin was determined as described in Merali et al. (2013). Fat analysis was performed using a CEM Smart System 5 with Smart Trac Rapid Fat Analysis. Protein, Ash, lignin, and fat analysis were performed using the insoluble bran fraction.

Ferulic Acid Determination. Ferulic acid was hydrolyzed and extracted from untreated wheat bran and the soluble fraction from the TS α-amylase + protease + xylanase bran treatment using the method described in Swennen et al. (2006). The quantification of the extracted ferulic acid was determined using a reversed-phase HPLC with a diode array detector (DAD). The reversed-phase HPLC method was performed with a SHIMADZU (Kyoto, Japan) system equipped with a DAD. The mobile phase A was 0.1% TFA in HPLC grade water and mobile

phase B was 0.1% TFA in HPLC grade acetonitrile. The Kinetex F5 column (150 mm x 4.6 mm) with a pentafluorophenyl with TMS endcapping stationary phase, 100 Å pore size, and 5 µm particle size was purchased from Phenomenex (Torrance, CA, USA). The DAD detector was set to scan signals from 220 nm to 800 nm. The total pump speed was kept at 0.8 mL/min. A 10 uL sample was injected each time and the HPLC gradient was programmed as follows: 10% mobile phase B was used from sample injection to 10 min; the percentage of mobile phase B increased linearly from 10% to 20% between 10 min to 17 min; 20% mobile phase B was used from 17 min to 22 min; finally the column was equilibrated with 10% mobile phase B between 22 min and 27 min. Resolved peaks were identified according to their retention times and UV spectrums from DAD. The analysis was performed at room temperature. Quantification of trans-ferulic acid was conducted using total area under the peak with external standard curves.

Total Sugars Analysis. Sulfuric acid (2.0 mL, 12 M) was added to either 20 mg of the spray dried solubles or untreated bran and subsequently placed in a 35 °C water bath for 30 min and then diluted to a 2 M sulfuric acid concentration by adding 10 mL of deionized water. The test tubes were then placed in an oven set at 100 °C for 2 h. After cooling to 25 °C, the samples were diluted 100× with deionized water. Samples were filtered through a 0.45 µm filter (Thermo Scientific 30mm nylon syringe filter) before injection into the High-Performance Anion-Exchange Chromatograph (HPAEC). Total sugars were analyzed using a HPAEC (Dionex ICS-3000, Dionex Corp., Sunnyvate, CA, USA) equipped with a pulsed amperometric detector, a guard column, a CarboPacTM PA1 analytical column, and an AS-DV autosampler. Eluent A was 150 mM NaOH and eluent D was 15 mM NaOH. The gradient program was as followed for a 45 min run: 100% of eluent D at 0 min, 100% eluent A at 15 min, and 100% eluent D at 30 min. The separations were carried out at 25 °C with a flow rate of 1 mL/min. The column was then

equilibrated with eluent D for 15 min. Arabinose, galactose, glucose, and xylose (Sigma-Aldrich Inc., St. Louis, MO, USA) were used as standards. Arabinose and xylose were injected at a concentration of 0.0526 mg/mL and glucose and galactose were injected at a concentration of 0.0631 mg/mL. Data analysis was performed using Chromeleon 6.8 (Thermo Fisher Scientific, Waltham, MA).

Gel Permeation Chromatography (GPC). The spray dried supernatant was dissolved in the mobile phase overnight at a concentration of 1 mg/mL. After that, they were filtered through a 30 mm nylon 0.45 µm syringe filter (Thermo Fisher Scientific, Waltham, MA) before injection. The molecular weight distribution was determined by a GPC (Agilent, Santa Clara, CA) using a triple detection system. A Viscotek 270 dual detector (light scattering plus viscometer) (Malvern PANalytical, Almelo, The Netherlands) and Viscotek VE3580 refractive index detector (Malvern PANalytical, Almelo, The Netherlands) on an Agilent Technologies 1100 series liquid chromatograph (Agilent, Santa Clara, CA) equipped with an autosampler and diode array detector (DAD). The DAD was set at 280 nm. The light scattering detector, which consisted of a right angle light scattering (RALS) and low angle light scattering (LALS) detector, was calibrated using a PEO standard (18,783 weight average molecular weight) (Malvern PANalytical, Almelo, The Netherlands). The mobile phase was water in 100 mmol sodium nitrate and 0.03% sodium azide. The flow rate was 1 mL/min with a run time of 50 min and injection volume of 100 µL. Samples passed through a pre-column and two SEC columns (Suprema pre-column, 10 µm, 8 × 50 mm; Suprema 3000 Å, 10 µm, 8 × 300 mm; Suprema 100 Å, 100 µm, 8 × 300 mm) (Phenomenex, Torrence, CA). Data analysis was performed using OmniSEC 4.7 (Malvern PANalytical, Almelo, The Netherlands).

Brookfield Viscometer. Wheat bran solubles were analyzed using a Brookfield viscometer (DV-II+ Pro, Brookfield Ametek, Middleboro, MA). Viscosity measurements of aqueous solutions of wheat bran solubles (10% w/w solution, 1.5 g in 13.5 g water) were prepared. The viscometer was used to determine viscosity at 100 rpm. The measurements were taken at 25 °C using spindle SC4-27. The results are the average of two replicates.

X-ray Diffraction (XRD) analysis. Wheat bran was analyzed using a multi-purpose X-ray diffractometer (PANalytical Empyrean, The Netherlands). It was operated at 40 kV and 20 mA with a 2θ range of 2-35, 0.006° step size, 40 seconds/step, 255 active channels, 10 mm mask, and 0.02 rad soller slit on a diffracted beam side. The anti-scatter slit size was 1/8 degree and the aperture size was 1/16 degree for 27 mm front loaded samples. X-rays were produced using a copper X-ray tube. A large nickel beta filter was used to remove beta scattering. A PIXcel 3D-Medpix3 1x1 PASS detector was used. Samples were analyzed at ~12% moisture.

Solid-state ^{13}C CP/MAS NMR analysis. High-resolution solid-state ^{13}C cross-polarization magic-angle spinning nuclear magnetic resonance (^{13}C CP/MAS NMR) analysis of bran was carried out at Bo = 9.4 T on a Bruker AVANCE III 400 WB spectrometer as previously described (Wei et al. 2010). The samples were analyzed at ~25% moisture after conditioning in a saturated NaCl solution environment for 1 week before analysis. A 7 mm probe was used for analysis. The corresponding ^{13}C resonance frequency was 100.6 MHz. Samples were packed in a 7 mm ZrO_2 rotor and spun at the magic angle (54.7°) at a spin rate of 6 kHz. ^{13}C CP/MAS NMR spectra were recorded with a contact time of 1.2 ms and a recycle delay of 2 s. The chemical shifts were referenced to tetramethylsilane (TMS) at 0 ppm. Typically, 8000 to 12000 transients were accumulated for the ^{13}C spectra.

Small angle X-ray scattering analysis. Small-angle X-ray scattering (SAXS) measurement of bran was performed using a Bruker NanoStar SAXS instrument equipped with a Vantec 2000 detector and pin-hole collimation for point focus geometry as previously described (Cai et al. 2014). The samples were analyzed at ~25% moisture after conditioning in a saturated NaCl solution environment for 1 week before analysis. The X-ray source was a rotating copper anode (0.1 nm filament) operating at 50 kV and 30 W, fitted with cross coupled Göbel mirrors, resulting in Cu Kα radiation wavelength of 1.5418 Å. The scanning region of the diffraction angle (2θ) was from 0.1° to 3.2°. The optics and sample chamber were under vacuum to minimize air scattering. The power-law exponent values were calculated by determining the slope of the region in which experimental data for all the different samples followed a linear trend in the log I versus log q plot.

Light Microscopy. Treated bran samples were dissected using a scalpel into the outer pericarp, intermediate layer (nucellar layer, testa, and inner pericarp from inner to outer layers), and the aleurone. The dissected bran layers were observed in water using an optical microscope with a digital camera (model BX51, Olympus Co., Tokyo, Japan).

Statistical Analysis. Each sample was measured in replicate (n = 2) and means and standard deviations were reported. Means were compared using one-way ANOVA to test for significance followed by the Tukey HSD test for significance between means at a $P < 0.05$ (Origin 8.5, Northampton, MA).

RESULTS AND DISCUSSION

Untreated Wheat Bran. Wheat bran from the Hal Ross flour mill was ~1000 µm (**Table 4.1**) which represented wheat bran from a commercial flour mill. The wheat bran was comprised of 24.4% arabinoxylan (AX) with an arabinose/xylose (A/X) ratio of 0.63 (**Table 4.2**). This bran sample was hydrothermally and enzymatically treated in the subsequent experiments.

Hydrothermally Treated UB. Untreated wheat bran was hydrothermally treated to examine the effects of temperature and mixing time on wheat bran solubility and AX extraction. The solubles yield significantly increased with temperature (**Table 4.3**). The percentage of AX in the soluble fraction and the percentage of UB AX solubilized (AX yield) generally increased with mixing time and temperature while the A/X ratio decreased (**Table 4.3**). The solubles and AX yield significantly increased by 4.6% and 3.8% respectively from the 25 °C, 3 h treatment to the 95 °C, 3 h treatment. There was a larger significant increase in the solubles (8.1%) and AX (11.4%) yield between the 95 °C, 3 h treatment and 140 °C, 40 min treatment (**Table 4.3**). The high A/X ratio of the hydrothermal treatments (especially 25 °C treatment) may have been due to the release of individual arabinose and xylose monomers and not AX polymers. The bran cooked at 95 °C and 140 °C did not result in the extraction of significant amounts of AX because only 5.6% and 17.0% of the UB AX was solubilized (**Table 4.3**). Most of the solubilized glucose was from starch and not from cellulose or mixed-linkage β-glucan (**Table 4.3**).

The molecular weight determined using GPC of the soluble fraction from hydrothermal treatments appeared to increase in order from smallest to largest 25 °C < 70 °C < 95 °C < 140 °C (**Figure 4.2**). This trend in molecular weight was reflected in the viscosity (cP) of the solubles

(**Table 4.3**) which shared the same trend. The molecular weight of the solubles were mostly between 600 and 14,000 (**Figure 4.2**). The peak at 21 min (the lowest molecular weight peak) corresponded to a molecular weight of 558 which reflected approximately a 3-unit carbohydrate chain (**Figure 4.2**).

Xylanase Treated UB; Hydrothermally Treated UB Followed by Xylanase; and UB Treated with α-amylase, Protease, and Xylanase. Hydrothermally treated UB and xylanase treated UB were examine for their effects individually and collectively on wheat bran solubility and AX extractability. Compared to hydrothermal treatment (95 °C, 3 h and 140 °C, 40 min), the addition of xylanase hydrolysis (95 °C + xylanase and 140 °C + xylanase) to these hydrothermal treatments increased the solubles yield by 14.9% and 20.0% respectively and the AX yield by 41.5% and 43.3% respectively (**Table 4.3 and 4.4**). Compared to xylanase treatment, the addition of a cooking step (95 °C and 140 °C) prior to xylanase hydrolysis significantly increased the solubles yield by 11.9% and 25.1% respectively and the AX yield by 36% and 49.2% respectively (**Table 4.4**). Xylanase hydrolysis and hydrothermal treatment alone did not result in significant solubilization of wheat bran AX (**Table 4.3 and 4.4**). It was observed upon dissecting the aleurone layer from the bran for microscopy analysis that after cooking that it could be removed more easily than if uncooked. Cooking could alter the physical structure of the aleurone layer increasing the effectiveness of xylanase action on wheat bran AX. Hydrothermal treatment could also remove (Maes et al. 2004) and/or inhibit (Van Craeyveld et al. 2010) endogenous xylanase inhibitors increasing the effectiveness of xylanase hydrolysis. In addition, a cooking step may have resulted in a decrease in mixture viscosity which allowed xylanase to access the substrate more easily.

TS α-amylase + xylanase treated UB compared to ITS α-amylase + xylanase significantly increased the solubles yield (8.1%) and AX yield (27.1%) (**Table 4.4**). This could be due to the cooking step in the TS α-amylase + xylanase treatment. TS α-amylase has a higher optimum temperature than ITS α-amylase (90 °C vs. 70 °C) and TS α-amylase + xylanase resulted in a significantly higher solubles yield (2.9%) but statistically similar AX yields compared to 95 °C + xylanase (**Table 4.4**). The addition of α-amylase resulted in more starch hydrolysis and thus a greater overall solubles yield but could have depressed xylanase activity decreasing AX hydrolysis.

TS α-amylase + protease + xylanase treated UB resulted in a significantly higher AX yield (7.3%) compared to TS α-amylase + xylanase (**Table 4.4**). Protein hydrolysis could have increased access to water insoluble AX or co-solubilized AX during the hydrolysis. The percentage of lignin and fat in the soluble fraction was low (**Table 4.2**). Most of the lignin and fat present in UB remained in the insoluble fraction. The lack of fat in the soluble fraction could help increase its shelf life. The TS α-amylase + protease + xylanase treatment outlined in **Figure 4.1** is the recommended bran treatment to most economically produce bran solubles. This procedure solubilized the most UB and UB AX with the exception of the 140 °C + xylanase treatment, which would be difficult to scale up due to the high cooking temperature.

The reduction in the A/X ratio by xylanase hydrolysis resulted in a corresponding decrease in the solubles viscosity and molecular weight. Starch and protein hydrolysis also contributed to reductions in the soluble fraction viscosity and molecular weight. The A/X ratios of the 95 °C + xylanase (0.25); 140 °C + xylanase (0.27); TS α-amylase + xylanase (0.28); and TS α-amylase + protease + xylanase (0.23) treatment solubles were much lower compared to the xylanase treatment (0.50) indicating the preference of the xylanase for hydrolyzing AX in lowly

substituted regions such as the aleurone and nucellar layer (**Table 4.4**). Xylanase decreased the A/X ratios of the 95 °C, 3 h (0.72) and 140 °C, 40 min (0.58) hydrothermal treatment solubles (Table III) to 0.25 and 0.27 respectively (**Table 4.4**). The reduction in A/X ratio was also reflected in the decrease in the viscosity and molecular weight of the solubles. The viscosity of the 95 °C, 3 h (174 cP) and 140 °C, 40 min (201 cP) hydrothermal treatment solubles (**Table 4.3**) was reduced to 23 cP and 25 cP respectively after xylanase hydrolysis (**Table 4.4**). This coincided with a reduction in the amount of high molecular weight material when comparing the molecular weight distributions of both of these hydrothermal treatments before (**Figure 4.2**) and after (**Figure 4.3**) xylanase hydrolysis. The hydrolysis of starch and protein by both hydrothermal and enzymatic treatments prior to xylanase hydrolysis increased the amount of low molecular weight materials (**Figure 4.3**), which contributed to the decrease in viscosity and molecular weight of the soluble fraction (**Table 4.4 and Figure 4.3**). The hydrothermal (95 °C and 140 °C) treatment prior to xylanase treatment increased the amount of low molecular weight sugars and the RI signal intensity compared to the xylanase treatment alone (**Figure 4.3**). The peak at 21 min corresponded to a molecular weight of 610 which corresponds to approximately a 3-unit carbohydrate chain (**Figure 4.3**).

Compared to the AX product produced by Swennen et al. (2006) which comprised 17% of the original wheat bran AX, the TS α-amylase + xylanase; TS α-amylase + protease + xylanase; 95 °C + xylanase; and 140 °C + xylanase treatments produced a product of bran solubles that contained a higher percentage UB AX (**Table 4.4**). In this study, the solubles produced prior to xylanase treatment were retained, which decreased the percentage of AX (23-27%) (**Table 4.4**) in the solubles fraction compared to the purified AX product produced by Swennen et al. (2006) which was 72% AX. Comparing between the four treatments previously

mentioned, the TS α-amylase + xylanase treatment solubles contained the highest concentration of glucose which was comprised of starch and non-starch (cellulose and mixed-linkage β-glucan) glucose (**Table 4.4**). The hydrothermal treatments followed by xylanase hydrolysis resulted in a slightly higher AX concentration compared to treatments using α-amylase and protease (**Table 4.4).** As expected, the TS α-amylase + protease + xylanase treatment solubilized the most protein **(Table 4.4**). The retention of all the bran solubles from enzymatic and hydrothermal treatments could make the solubilization process more economically feasible. The retained protein and glucose polymers (starch, mixed linkage β-glucan, and cellulose) could provide functional benefits in addition to the AX in baking.

Effect of UB Particle Size on Solubles Yield and Protein Content after Protease Treatment. The UB had a particle size ~1000 μm and a portion was milled to a particle size ~200 μm for GB (**Table 4.1**) while maintaining a similar chemical composition (**Table 4.2**). The GB was ball milled for 48 h to produce BMB. As the particle size decreased, the amount of solubles produced from protease treatment increased (**Table 4.5**). Increasing access to the bran cell walls increased bran solubility, but not dramatically as solubility only increased by 2.7% for GB and 7.2% for BMB compared to UB. Protein was likely still trapped within the cell walls by physical interactions and covalent linkages.

Updegraff Reagent Treatment of Insoluble Fractions. The Updegraff reagent can hydrolyze biological plant material leaving the crystalline cellulose intact at 100 °C. Hydrothermal treatment at 140 °C most likely did not structurally alter or destroy the bran crystalline cellulose structure (**Table 4.6**). If it did, the Updegraff reagent treatment at 100 °C would have likely hydrolyzed more of the 140 °C hydrothermally treated bran resulting in a lower insolubles yield compared to the 25 °C treatment (**Table 4.6**). Instead, the insolubles yield

was the same for both hydrothermal treatments after treatment with the Updegraff reagent (**Table 4.6**). Differential solubility existed when the hydrothermally treated bran (25 °C and 140 °C) was treated with the Updegraff reagent at 25 °C (**Table 4.6**). The 140 °C treatment may have altered the physical structure of the aleurone layer. This could have contributed to the dissolution of the aleurone layer when treated with xylanase after hydrothermal treatment.

Physical Structure of Insolubles Analyzed using Light Microscopy, XRD, Solid-state ^{13}C CP/MAS NMR, and SAXS. The 95 °C + xylanase, 140 °C + xylanase, TS α-amylase + xylanase, and TS α-amylase + protease + xylanase bran treatments resulted in the complete disorganization and detachment of the aleurone layer while all other treatments resulted in the aleurone layer remaining intact. A cooking step (95 °C or 140 °C) followed by xylanase treatment was required for the loss of aleurone cell wall structure. The loss of the aleurone layer corresponded to an A/X ratio of 0.23-0.28 for the soluble fraction (**Table 4.4**). Compared to the control (UB) (**Figure 4.4A, B, and C**), the outer pericarp and intermediate layer physical structure were not affected by 140 °C treatment with (**Figure 4D and E**) and without (**Figure 4.4G and H**) xylanase hydrolysis and TS α-amylase + protease + xylanase treatment (**Figure 4.4I and J**). The cell wall structure appeared unchanged. Compared to the control aleurone layer (**Figure 4.4C**), the 140 °C treatment aleurone cellular contents were partially solubilized (**Figure 4.4F**). The cell wall structure did not appear to be affected though.

X-ray diffraction of the control (UB) and insoluble fractions from TS α-amylase + protease + xylanase and 140 °C + xylanase bran treatments showed amorphous curves which probably indicated that too much non-crystalline material was present in the samples for the crystalline structure to be detected (**Figure 4.5A**). After Updegraff treatment at 100 °C, XRD analysis of the insolubles showed that the material possessed cellulose crystallinity (**Figure**

4.5B). Chemical composition of the insoluble fraction confirmed that it was mostly comprised of glucose likely from cellulose (**Table 4.2**). This confirmed that the 140 °C treatment did not destroy bran crystallinity. The only known source of crystallinity in biomass cell walls is cellulose (Xu et al. 2013). It could be assumed that the portion of the wheat bran physical structure unaffected was the pericarp layer, which contains a majority of the bran cellulose (Antoine et al. 2003).

Solid-state ^{13}C CP/MAS NMR was used to analyze UB, the insoluble fraction from UB hydrothermally treated at 140 °C for 40 min, the insoluble fraction from UB hydrothermally treated at 140 °C for 40 min followed by xylanase treatment, and the insoluble fraction from UB treated with thermostable α-amylase + protease + xylanase (**Figure 4.6**). The carbonyl carbon chemical shift at 174 ppm, from ester and amide carbons, was unchanged between treatments compared to UB. This indicates that significant amounts of carbonyl carbons associated with protein, lipids, and cutin remained in the insoluble fraction. The C-1 cellulose resonance at 105 ppm became more defined and intense for the insoluble fraction from UB hydrothermally treated at 140 °C for 40 min followed by xylanase and the insoluble fraction from UB treated with thermostable α-amylase + protease + xylanase (**Figure 4.6C, D**). The concentration of cellulose in these samples was associated with the loss of the aleurone layer structure (**Figure 4.4**) and hydrolysis of arabinoxylan, starch, and mixed-linkage β-glucan (**Table 4.4**). Cellulose likely remained in the insoluble bran fraction after hydrothermal and enzymatic treatments. The chemical shift from 28 to 32 ppm associated with bulk methylene in cutin and lipids remained unchanged between treatments compared to UB (**Figure 4.6**). Most of these chemical components likely remained in the insoluble fraction. The composition of the soluble fractions

(**Table 4.2 and 4.4**) confirm that most of the protein, cellulose, and lipid remained in the insoluble fraction.

SAXS data (**Figure 4.7**) show the SAXS intensities as a function of q (magnitude of the scattering wave vector) for UB, the insoluble fraction from UB hydrothermally treated at 140 °C for 40 min, the insoluble fraction from UB hydrothermally treated at 140 °C for 40 min followed by xylanase treatment, and the insoluble fraction from UB treated with thermostable α-amylase + protease + xylanase plotted double logarithmically. The SAXS intensity measured within the q range used for this analysis corresponding to the estimated length scale of 125 Å to 5 Å would be expected to result from cellulose microfibrils (Martinez-Sanz et al. 2015) and other chemical components such as adjacent arabinoxylan, mixed-linkage β-glucan, starch, and protein. The power-law exponent values in the $0.008 < q < 0.221$ $Å^{-1}$ q range of UB (2.1), the insoluble fraction from UB hydrothermally treated at 140 °C for 40 min (2.2), and the insoluble fraction from UB hydrothermally treated at 140 °C for 40 min followed by xylanase (2.1) were smaller than the insoluble fraction from UB treated with thermostable α-amylase + protease + xylanase (3.4) (**Figure 4.7**). This indicated that a more densely compacted structure was measured for the insoluble fraction from UB treated with thermostable α-amylase + protease + xylanase compared to the other treatments (Martinez-Sanz et al. 2015). The power-law exponent value for the insoluble fraction from UB treated with thermostable α-amylase + protease + xylanase was measured in the $0.008 < q < 0.061$ $Å^{-1}$ q range corresponding to the estimated length scale of 125 Å to 16 Å. The structures measured for this treatment appeared to be larger and more compact compared to the other samples.

CONCLUSION

Unlike previous research, the starch and protein were kept and not removed before xylanase treatment. This could make the process more economical because more material was recovered. Physical properties such as molecular weight and viscosity were determined in addition to composition to evaluate the solubilized material. Wheat bran hydrolyzed with thermostable α-amylase at 95°C for 2h at pH=6.7, protease at 70°C for 3h at pH=6.3, and xylanase at 50°C for 24h at pH=5.5 was the recommended treatment for the production of solubles because of high bran and AX solubilization without 140°C treatment. The combined solubles had a viscosity of 23 cP (10% w/w solids) and a molecular weight between ~600 and 20,000. The percentage of AX solubilized from untreated wheat bran was 50% and the percentage of AX in the solubles was 23%. This procedure solubilized the most untreated bran compared to other enzymatic and hydrothermal treatments, except the 140 °C hydrothermal treatment followed by xylanase, which would be difficult to scale up due to the high treatment temperature. The retained protein and glucose polymers (starch, mixed-linkage β-glucan, and cellulose) could provide functional benefits in addition to the arabinoxylan.

The hydrothermal treatment of untreated wheat bran at 95 °C and 140 °C followed by xylanase increased the solubles yield and arabinoxylan yield compared to hydrothermal and xylanase hydrolysis alone. Hydrothermal treatment (> 95 °C) combined with xylanase treatment resulted in the loss and complete disorganization the aleurone layer. Treatments lacking either a hydrothermal treatment (> 95 °C) or xylanase treatment resulted in the aleurone layer remaining intact. Hydrothermal treatment may have altered the physical structure of the aleurone layer

aiding in the complete loss of its cell wall structure when treated with xylanase. For each treatment (enzymatic and hydrothermal), the outer pericarp and intermediate layer physical structure were not affected. X-ray diffraction and chemical composition analysis of both insoluble fractions from thermostable α-amylase, protease, and xylanase treated bran and 140 °C treatment followed by xylanase confirmed that they did not destroy wheat bran crystallinity.

LITERATURE CITED

Antoine, S. Peyron, F. Mabille, C. Lapierre, B. Bouchet, J. Abecassis, and X. Rouau, Individual contribution of grain outer layers and their cell wall structure to the mechanical properties of wheat bran. 2003. J. Agric. Food Chem. 51:2026-2033.

Arte, E., Katina, K., Holopainen-Mantila, U., Nordlund, E. 2016. Effect of hydrolyzing enzymes on wheat bran cell wall integrity and protein solubility. Cereal Chem. 93:162-171.

Amrein, T.M., Gränicher, P., Arrigoni, E., Amadò, R. 2003. In vitro digestibility and colonic fermentability of aleurone isolated from wheat bran. Lebensm.-Wiss. U.-Technol. 36:441-460.

Balandrán-Quintanta, R.R., Mercado-Ruiz, J.N., Mendoza-Wilson, A.M. 2015. Wheat bran proteins: A review of their uses and potential. Food Reviews International. 31:279-293.

Beaugrand, J., Crônier, D., Thiebeau, P., Schreiber, L., Debeire, P., and Chabbert, B. 2004a. Structure, chemical composition, and xylanase degradation of external layers isolated from developing wheat grain. J. Agric. Food Chem. 52:7108-7117.

Beaugrand, J., Reis, D., Guillon, F., Debeire, P., and Chabbert, B. 2004b. Xylanase-mediated hydrolysis of wheat bran: Evidence for subcellular heterogeneity of cell walls. Int. J. of Plant Sci. 165:553-563.

Benamrouche, S., Crônier, D., Debeire, P., and Chabbert, B. 2002. A chemical and histological study on the effect of (1-4)-β-endo-xylanase treatment on wheat bran. J. Cereal Sci. 36:253-260.

Brouns, F., Hemery, Y., Price, R., and Anson, N.M. 2012. Wheat aleurone: separation, composition, health aspects, and potential food use. Critical Reviews in Food Science and Nutrition. 52:553-568.

Cai, J., Yang, Y., Man, J., Huang, J., Wang, Z., Zhang, C., Gu, M., Liu Q., and Wei, C. 2014. Structural and functional properties of alkali-treated high-amylose rice starch. Food Chem. 145:245-253.

Gauthier, A., Derenne, S., Dupont, L., Guillon, E., Largeau, C., Dumonceau, J., and Aplincour, M. 2002. Characterization and comparison of two lingo-cellulosic substrates by ^{13}C CP/MAS NMR, XPS, conventional pyrolysis and thermochemolysis. Anal. Bioanal. Chem. 373:830-838.

Ha, M.-A., Jardine W.G., and Jarvis, M.C. 1997. Solid-state ^{13}C NMR of cell walls in wheat bran, J. Agric. Food Chem. 45:117-119.

Immerzeel, P., Falck, P., Galbe, M., Adlercreutz, P., Karlsson, E.N., Stålbrand, H. 2014. Extraction of water-soluble xylan from wheat bran and utilization of enzymatically produced xylooligosaccharides by Lactobacillus, Bifidobacterium and Weissella spp. LWT – Food Science and Technology. 56:321-327.

Jacquemin, L., Mogni, A., Zeitoun, R., Guinot, C., Sablayrolles, C., Saulnier, L., Pontalier, P.-Y. 2015. Performance evaluation of a semi-industrial production process of arabinoxylans from wheat bran. Process Biochemistry. 50:605-613.

Locci, E., Laconi, S., Pompei, R., Scano, P., Lai A., and Marincola, F.C. 2008. Wheat bran biodegradation by Pleurotus ostreatus: A solid-state carbon-13 NMR study. Bioresour. Technol. 99:4279-4284.

Maes, C., and Delcour, J.A. 2002. Structural characterization of water extractable and water unextractable arabinoxylans in wheat bran. J. of Cereal Sci. 35:315-326.

Maes, C., Vangeneugden, B., and Delcour, J.A. 2004. Relative activity of two endoxylananases towards water-unextractable arabinoxylans in wheat bran. J. Cereal Sci. 39:181-186.

Martínez-Sanz, M., Lopez-Sanchez, P., Gidley, M.J. and Gilbert, E.P. 2015. Evidence of differential interaction mechanism of plant cell wall matrix polysaccharides in hierarchically-structured bacterial cellulose. Cellulose. 22:1541-1563.

Merali, Z., Ho, J.D., Collins, S.R.A., Gall, G.L., Elliston, A., Käsper, A., and Waldron, K.W. 2013. Characterization of cell wall components of wheat straw following hydrothermal pretreatment and fractionation. Bioresource Technology. 131:226-234.

Murata, Y., Kubo, S., Togawa, E., Ramle, S.F.B.M., Sulaiman, Hashim, O., Ibrahim, W.A., Kosugi, A., Hirooka, A. and Abe, H. 2015. Detection of vascular bundles using cell wall birefringence on exposure to polarized light. Ind. Crops Prod. 65:190-197.

Pareyt, B., Goovaerts, M., Broekaert, W.F., and Delcour, J.A. 2011. Arabinoxylan oligosaccharides (AXOS) as a potential sucrose replacer in sugar-snap cookies. 2011. LWT-Food Science and Technology. 44:725-728.

Prückler, M., Siebenhandl-Ehn, S., Apprich, S., Höltinger, S., Haas, C., Schmid, E., and Kneifel, W. 2014. Wheat bran-based biorefinery 1: composition of wheat bran and strategies of functionalization. LWT – Food Science and Technology. 56:211-221.

Reisinger, M., Tirpanalan, O., Pruckler, M., Huber, F., Kneifel, W., and Novalin, S. 2013. Wheat bran biorefinery-A detailed investigation on hydrothermal and enzymatic treatment. Bioresource Tech. 144:179-185.

Rosa-Sibakov, N., Poutanen, K., and Micard, V. 2015. How does wheat grain, bran and aleurone structure, impact their nutritional and technological properties? Trends in Food Science and Technology. 41:118-134.

Rose, D.J. and Inglett, G.E. 2010. Two-stage hydrothermal processing of wheat (Triticum aestivum) bran for the production of feruloylated arabinoxylooligosaccharides. J. Agric. Food Chem. 58:6427-6432.

Updegraff, D.M. 1969. Semimicro determination of cellulose in biological materials. Analytical Biochemistry. 32:420-424.

Santala, O., Lehtinen, P., Nordlund, E., Suortti, T., and Poutanen, K. 2011. Impact of water content on the solubilization of arabinoxylan during xylanase treatment of wheat bran. J. Cereal Sci. 54:187-194.

Santala, O.K., Nordlund, E.A., and Poutanen, K.S. 2013. Treatments with xylanase at high (90%) and low (40%) water content have different impacts on physicochemical properties of wheat bran. Food Bioprocess Technol. 6:3102-3112.

Swennen, K., Courtin, C.M., Lindemans, G., and Delcour, J.A. 2006. Largescale production and characterization of wheat bran arabinoxylooligosaccharides. J. Sci. Food Agric. 86:1722-1731.

Updegraff, D.M. 1969. Semimicro determination of cellulose in biological materials. Analytical Biochemistry. 32:420-424.

Van Craeyveld, V., Dornez, E., Holopainen, U., Selinheimo, E., Poutanen, K., Delcour, J.A., and Courtin, C.M. 2010. Wheat bran AX properties and choice of xylanase affect production of wheat bran-derived arabinoxylan-oligosaccharides. Cereal Chem. 87:283-291.

Van den Borne, J.J.G.C., Kabel, M.A., Briens, M., and van der Poel, A.F.B. 2012. Effects of pretreatment of wheat bran on the quality of protein-rich residue for animal feeding and on monosaccharide release for ethanol production. Bioresource Technology. 124:446-454.

Wei, C., Xu, B., Qin, F., Yu, H., Chen, C., Meng, X., Zhu, L., Wang, Y., Gu, M., and Liu, Q. 2010. C-type starch from high-amylose rice resistant starch granules modified by

antisense RNA inhibition of starch branching enzyme. J. Agric. Food Chem. 58:7883-7388.

Xu, F., Shi, Y.-C., and Wang, D. 2013. X-ray scattering of lignocellulosic biomass: A review. Carbohydr. Polym. 94:904-919.

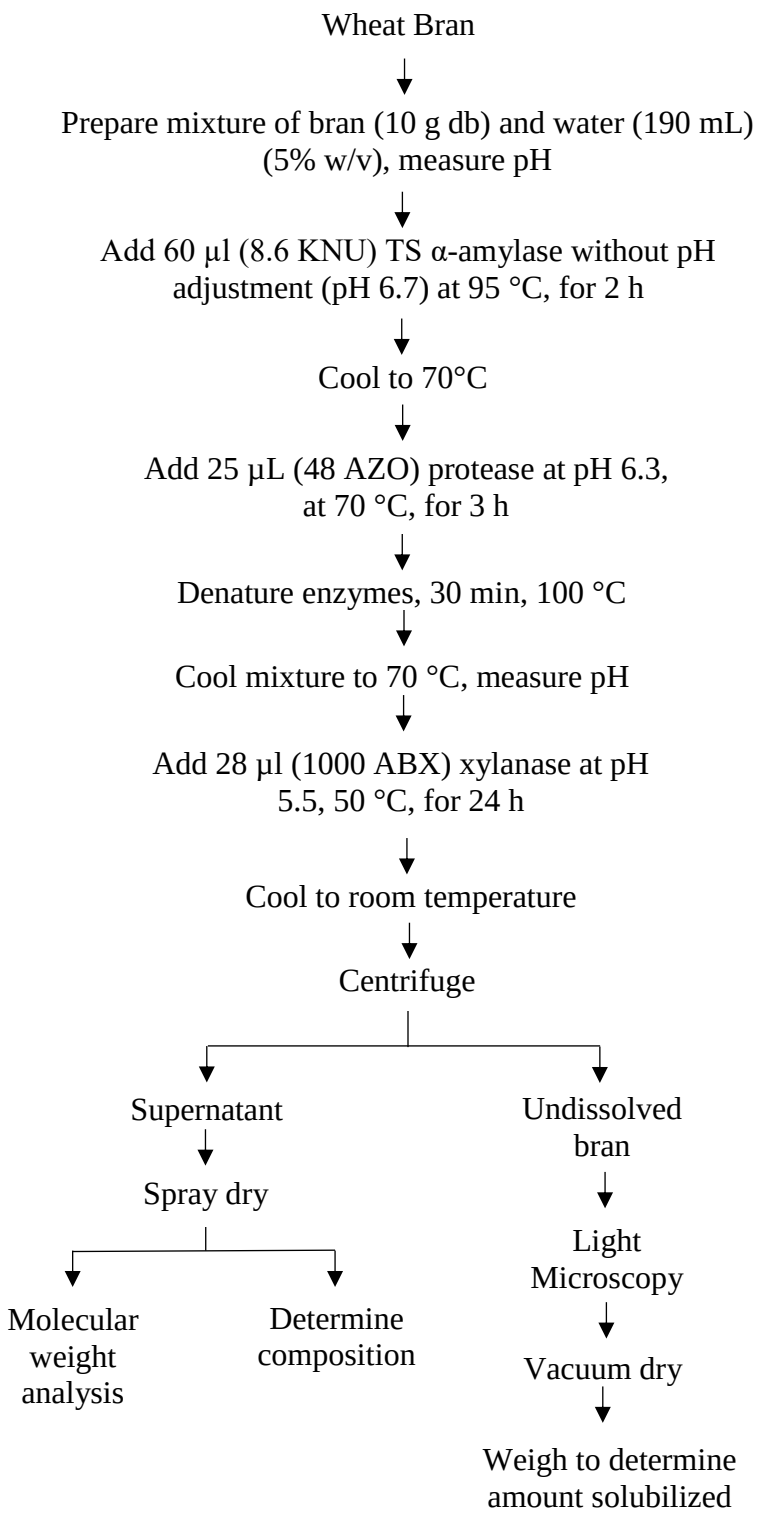

Figure 4.1 Procedure for determining the effect of thermostable α-amylase (TS α-amylase), protease, and xylanase treatment on soluble and insoluble bran components; n=2.

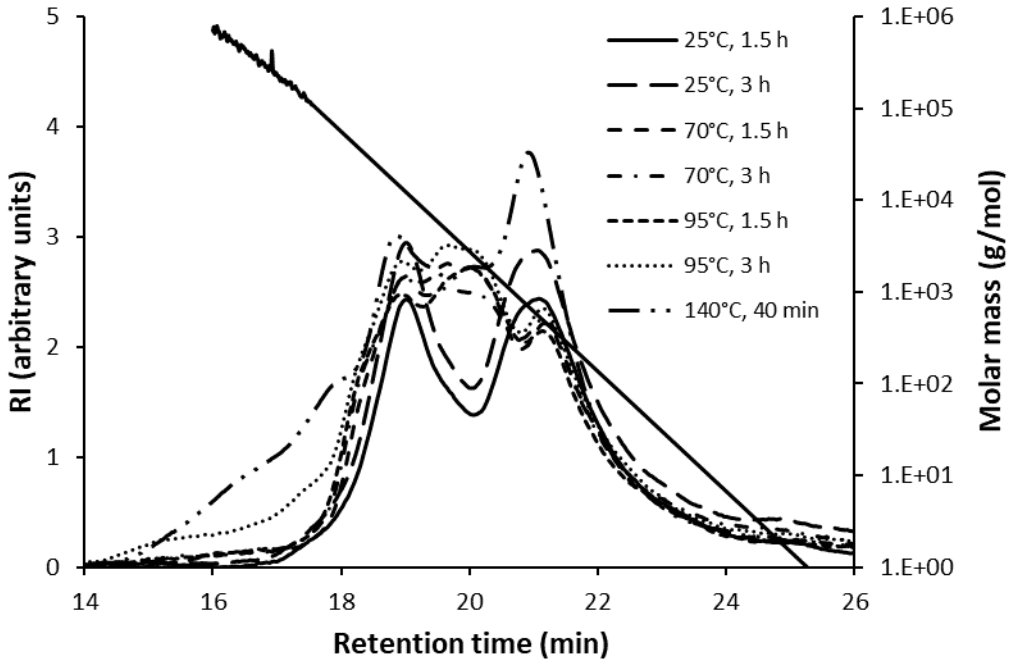

Figure 4.2 Molecular weight distribution of solubles from untreated wheat bran (UB) hydrothermally treated at various temperatures (25 °C, 70 °C, 95 °C, and 140 °C) and times (40 min, 1.5 h, and 3 h) (reference Figure 6.1).[1]

[1]Molecular weight distribution was calculated using triple detection (light scattering, refractive index, and viscometer) data from 95 °C, 3 h treatment solubles.

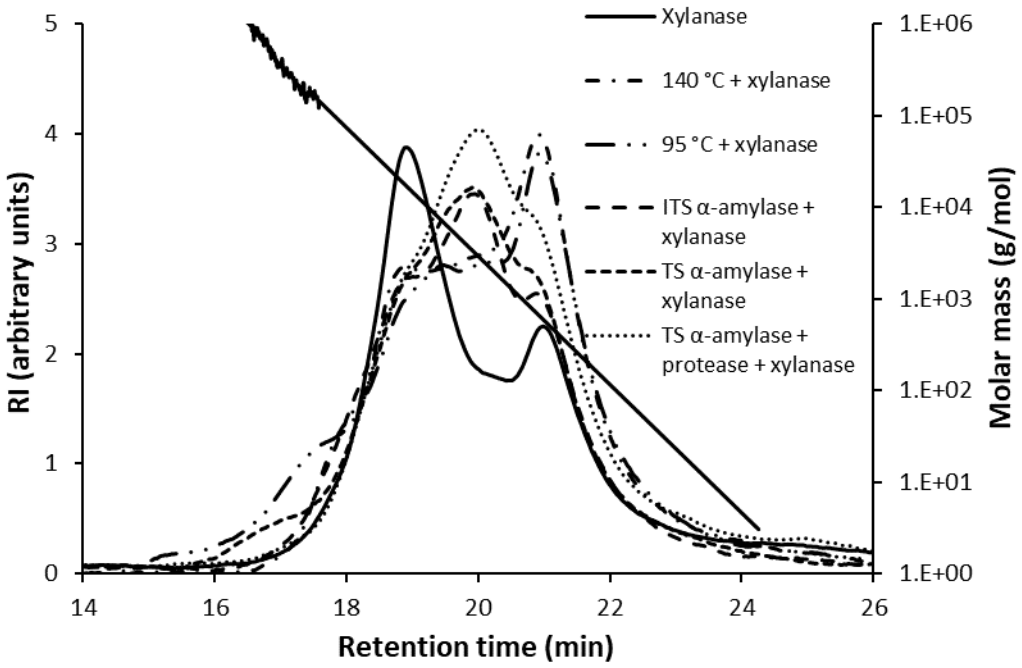

Figure 4.3 Molecular weight distribution of solubles from xylanase; 95 °C + xylanase; 140 °C + xylanase; intermediately thermostable α-amylase + xylanase (ITS α-amylase + xylanase); thermostable α-amylase + xylanase (TS α-amylase + xylanase); and TS α-amylase + protease + xylanase treated bran (Reference Figures 4.1, 6.2, 6.3, and 6.4).[1]

[1]Molecular weight distribution was calculated using triple detection (light scattering, refractive index, and viscometer) data from 95 °C + xylanase treatment solubles.

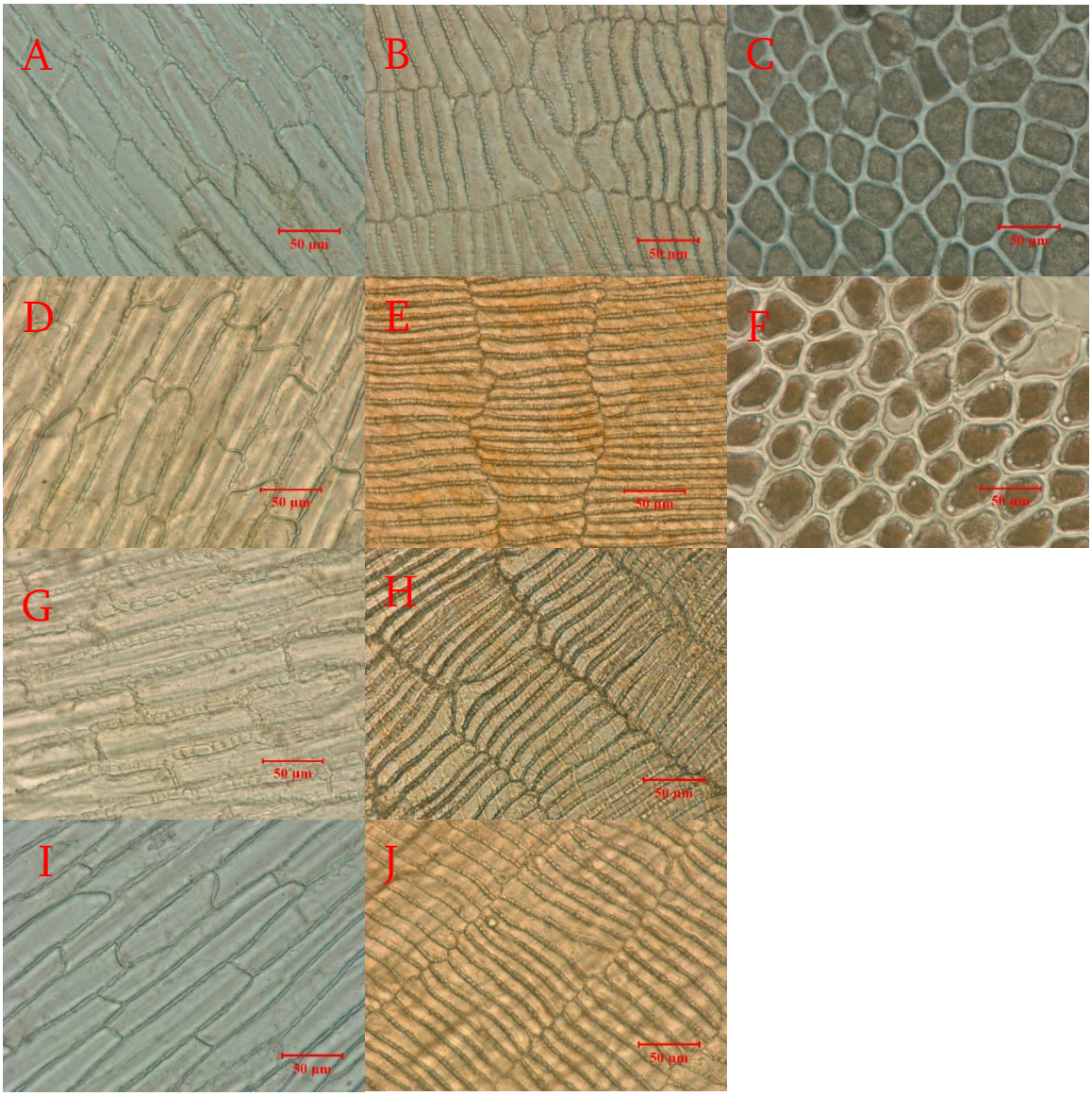

Figure 4.4 Outer pericarp (A, D, G, and I), intermediate layer (B, E, H, and J), and aleurone layer (C, F) imaged by light microscopy. Untreated wheat bran (UB) (A-C); insoluble fraction from UB hydrothermally treated at 140 °C for 40 min (D-F); insoluble fraction from UB hydrothermally treated at 140 °C for 40 min followed by xylanase treatment (G-H); insoluble fraction from UB treated with thermostable α-amylase + protease + xylanase (I-J).

Outer pericarp = epidermis + hypodermis.
Intermediate layer = cross cells + tube cells + testa+ nucellar layer.
Scale bar = 50µm.

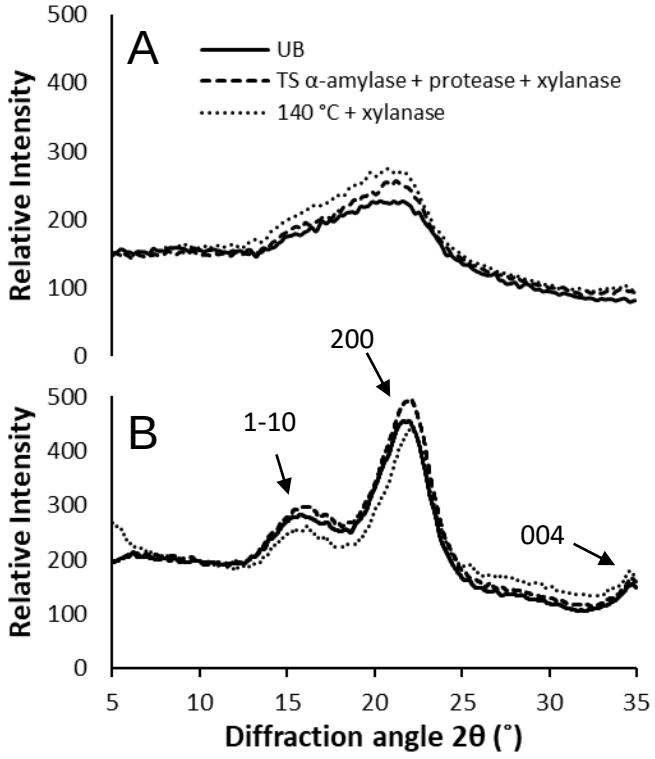

Figure 4.5 X-ray diffraction of untreated wheat bran (UB); insoluble fraction from UB treated with thermostable α-amylase + protease + xylanase; insoluble fraction from UB hydrothermally treated at 140 °C for 40 min followed by xylanase treatment (140 °C + xylanase) before (A) and after (B) Updegraff reagent treatment at 100 °C. The numbers marked in B, (1-10), (200), and (004) are planes of cellulose I crystals at 15.0°, 22.5°, and 35.0° respectively (Murata et al. 2015).

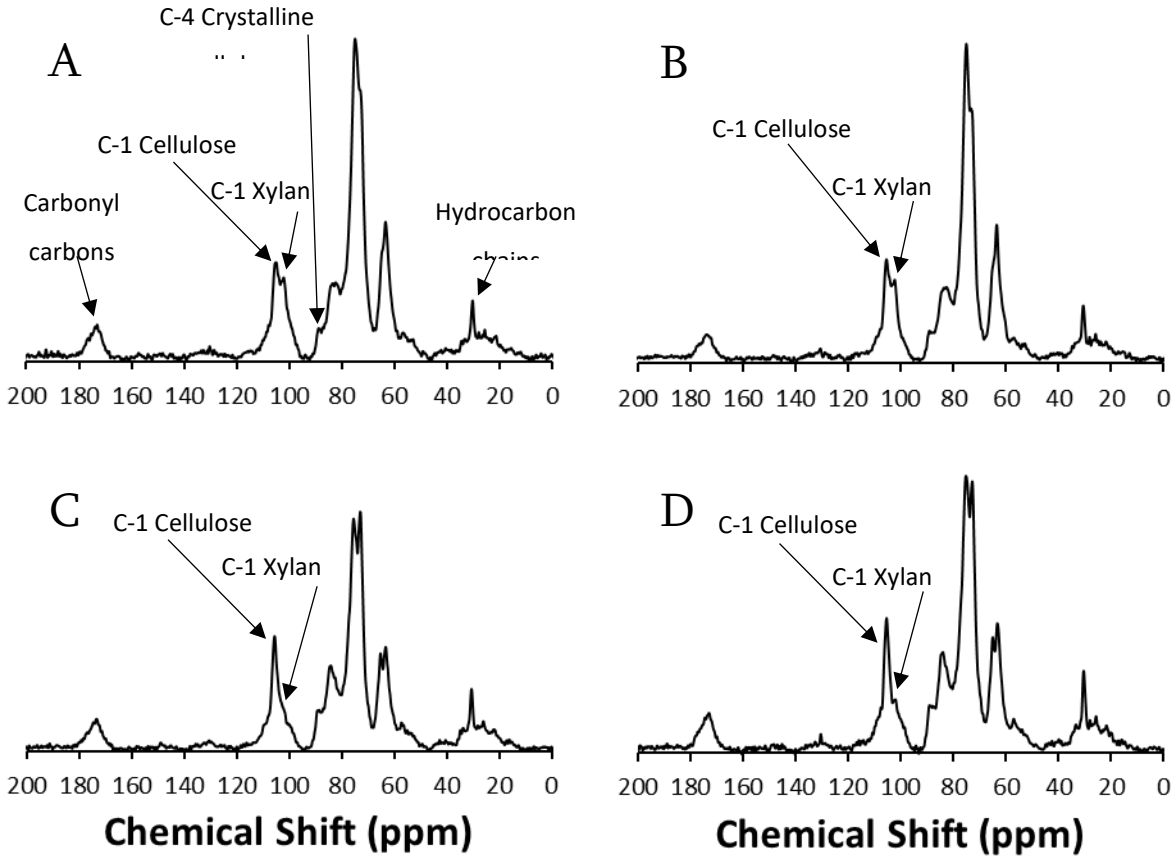

Figure 4.6 Solid-state ^{13}C CP/MAS NMR spectra of (A) untreated wheat bran (UB), (B) insoluble fraction from UB hydrothermally treated at 140 °C for 40 min, (C) insoluble fraction from UB hydrothermally treated at 140 °C for 40 min followed by xylanase treatment, (D) insoluble fraction from UB treated with thermostable α-amylase + protease + xylanase. Resonances identified using references (Ha et al. 1997; Locci et al. 2008; Gauthier et al. 2002).

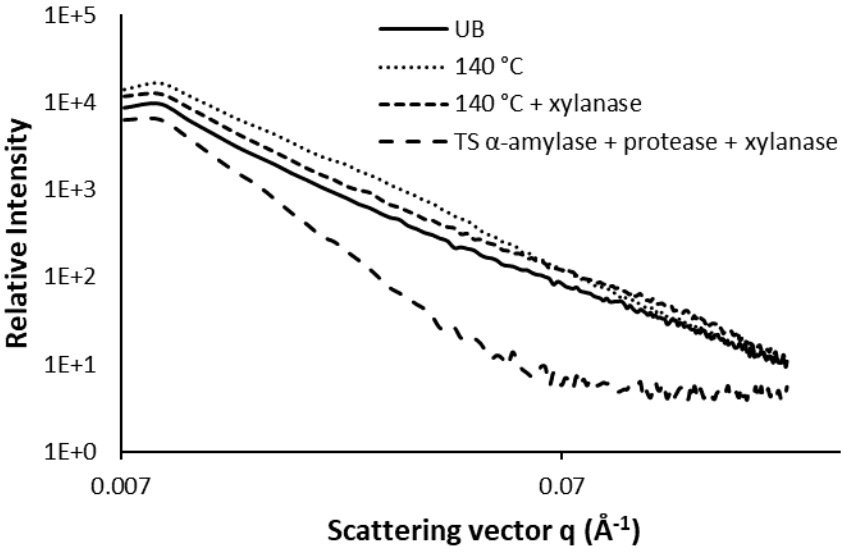

Figure 4.7 Small-angle X-ray scattering of untreated wheat bran (UB); insoluble fraction from UB hydrothermally treated at 140 °C for 40 min; insoluble fraction from UB hydrothermally treated at 140 °C for 40 min followed by xylanase treatment; and insoluble fraction from UB treated with thermostable α-amylase + protease + xylanase.

Table 4.1 Particle Size Distribution of Untreated Wheat Bran (UB) and Ground Wheat Bran (GB) as Determined by a Modified AACC 66-20.01 Ro-tap Sieve Shaker Method[1]

Particle size distribution of UB		Particle size distribution of GB	
Micron opening	Average (%) held over	Micron opening	Average (%) held over
2000	4.6±0.1	350	0.1±0.0
1400	23.1±0.4	210	38.2±0.4
1000	38.4±0.4	180	24.7±0.9
600	28.5±0.1	106	18.1±0.8
210	3.7±0.1	53	15.0±0.5
0	1.3±0.1	0	3.0±0.8

[1]Two pan cleaners were used per sieve; n = 3.

Table 4.2 Chemical Composition of Untreated Wheat Bran (UB); Soluble Fraction from Thermostable α-amylase + Protease + Xylanase UB Treatment; Insolubles from 100 °C Updegraff Treatment of UB, Insoluble Fraction from 140 °C + Xylanase UB Treatment, and Insoluble Fraction from Thermostable α-amylase + Protease + Xylanase UB Treatment

Composition (%)[1]	UB	TS α-amylase + protease + xylanase	UB Updegraff insolubles	140 °C + xylanase Updegraff insolubles	TS α-amylase + protease + xylanase Updegraff insolubles
Arabinoxylan[2]	24.4±0.2	23.2±0.6	2.7	2.8	2.5
Arabinose	10.7±0.2	4.9±0.1	0	0	0
Xylose	17.0±0.1	21.5±0.6	3.1±0.0	3.2±1.3	2.8±0.2
A/X Ratio[3]	0.63	0.23	0	0	0
Glucose (starch + β-glucan + cellulose)	26.2±0.5	32.2±0.3	76.2±0.6	91.7±0.1	91.6±2.1
Starch	11.6±0.3	21.7±0.3			
β-Glucan	2.5±0.1	4.8±0.1			
Cellulose[4]	12.6	5.7	76.2±0.6[5]	91.7±0.1[5]	91.6±2.1[5]
Ash	8.1±0.0	12.4±0.3			
Protein	15.0±0.0	17.6±0.0			
Lignin	9.3±0.3	2.0±0.5			
Fat	6.9±0.4	1.5±0.2			
Ferulic Acid	0.3±0.0	0.3±0.0			

[1]Expressed as weight percentage (dm) of UB, n = 2.
[2]AX = Arabinoxylan = 0.88 × (%arabinose + %xylose).
[3]A/X = arabinose/xylose ratio.
[4]Cellulose = glucose – starch – mixed-linkage β-glucan.
[5]The glucose % in the insoluble fraction after Updegraff reagent treatment was assumed to be comprised of cellulose (Updegraff 1969).

Table 4.3 Yield (%) and Composition (%) of Solubles from Hydrothermally Treated Bran at Various Temperatures (25 °C, 70 °C, 95 °C, and 140 °C) and Times (40 min, 1.5 h, and 3 h) (Reference Figure 6.1)

Treatment Temperature	25 °C		70 °C		95 °C		140 °C
and Time	1.5 h	3 h	1.5 h	3 h	1.5 h	3 h	40 min
Yield (%)							
Solubles[1]	22.2±0.2a	23.5±0.2a	25.5±0.3b	26.1±1.0b	27.7±0.2bc	28.1±0.3c	36.2±0.3d
AX[2]	1.8±0.2a	1.8±0.0a	3.0±0.1ab	3.5±0.1ab	4.8±0.6bc	5.6±0.9c	17.0±0.8d
Composition (%)[3]							
AX[4]	2.0±0.2	1.8±0.0	2.8±0.1	3.3±0.1	4.2±0.5	4.8±0.9	11.5±0.5
Arabinose	1.1±0.2	1.0±0.0	1.4±0.0	1.6±0.1	2.0±0.2	2.3±0.4	4.8±0.3
Xylose	1.2±0.1	1.1±0.1	1.8±0.1	2.2±0.0	2.8±0.4	3.2±0.6	8.2±0.3
A/X Ratio[5]	0.92	0.91	0.78	0.73	0.71	0.72	0.58
Starch	9.4±0.1	8.8±0.1	8.7±0.3	9.0±0.1	18.0±0.2	17.7±0.1	21.1±0.3
Mixed-Linkage Beta-Glucan		0.2±0.1		0.3±0.0		1.8±0.1	3.2±0.1
Cellulose[6]		0.0		0.2		0.0	0.0
Ash	24.0±0.2	21.4±0.3	20.0±0.1	19.9±0.2	18.7±0.1	18.0±0.1	19.3±0.1
Protein	18.2±0.0	18.4±0.1	17.2±0.1	17.8±0.2	17.0±0.2	16.0±0.2	21.5±0.1
Physical Properties							
Viscosity (cP)[7]	-	23±3	-	140±2	-	174±2	201±0.5

AX = Arabinoxylan.

Numbers in the same row followed by a letter in common are not significantly different at $p < 0.05$; n = 2.

[1]Expressed as weight percentage (dm) of UB; [(10 g UB – insoluble bran g)/10] × 100 = solubles yield (%); n = 2.

[2]Expressed as a weight percentage (dm) of UB AX.

[3]Expressed as weight percentage (dm) of solubles.

[4]AX = 0.88 × (%arabinose + %xylose).

[5]A/X = arabinose/xylose ratio.

[6] Cellulose = glucose – starch – mixed-linkage β-glucan.

[7]Viscosity was measured at 10% solids content using a Brookfield viscometer.

Table 4.4 Yield (%) and Composition (%) of Solubles from Xylanase; 95 °C + Xylanase; 140 °C + Xylanase; Intermediately Thermostable α-amylase + Xylanase (ITS α-amylase + xylanase); Thermostable α-amylase + Xylanase (TS α-amylase + xylanase); and TS α-amylase + Protease + Xylanase Treated Bran (Reference Figures 4.1, 6.2, 6.3, and 6.4)

Treatment	Xylanase	95 °C+ xylanase	140 °C + xylanase	ITS α-amylase + xylanase	TS α-amylase + xylanase	TS α-amylase + protease + xylanase
Yield (%)						
Solubles[1]	31.1±0.2a	43.0±0.3b	56.2±0.5c	37.8±1.1d	45.9±0.5e	52.5±0.6f
AX[2]	11.1±1.0a	47.1±1.2be	60.3±0.9c	15.6±0.4d	42.7±1.4b	50.0±1.3e
Composition (%)[3]						
AX[4]	8.7±0.8	26.7±0.7	26.2±0.4	10.1±0.3	22.7±0.8	23.2±0.6
Arabinose	3.3±0.5	6.0±0.0	6.3±0.4	3.9±0.3	5.6±0.2	4.9±0.1
Xylose	6.6±0.4	24.3±0.7	23.4±0.9	7.6±0.0	20.2±0.7	21.5±0.6
A/X Ratio[5]	0.50	0.25	0.27	0.51	0.28	0.23
Starch	4.1±0.3	18.2±0.2	18.4±0.4	21.5±0.1	24.1±0.0	21.7±0.3
Mixed-Linkage Beta-Glucan	0.7±0.0	5.8±0.2	3.0±0.5	3.5±0.2	5.4±0.3	4.8±0.1
Cellulose[6]	1.5	2.9	6.4	4.4	5.5	5.7
Ash	24.4±0.0	16.2±0.1	12.6±0.1	19.9±0.1	15.6±0.2	12.4±0.3
Protein	16.7±1.0	11.5±0.1	14.8±0.9	14.8±0.3	18.6±0.1	17.6±0.0
Physical Properties						
Viscosity (cP)[7]	58±1	23±4	25±3	28±3	26±3	23±3

AX = Arabinoxylan.

Numbers in the same row followed by a letter in common are not significantly different at $p < 0.05$; n = 2.

[1]Expressed as weight percentage (dm) of UB; [(10 g UB – insoluble bran g)/10] × 100 = solubles yield (%); n = 2.

[2]Expressed as a weight percentage (dm) of UB AX.

[3]Expressed as weight percentage (dm) of solubles.

[4]AX = 0.88 × (%arabinose + %xylose).

[5]A/X = arabinose/xylose ratio.

[6] Cellulose = glucose – starch – mixed-linkage β-glucan.

[7]Viscosity was measured at 10% solids content using a Brookfield viscometer.

Table 4.5 Yield (%) of Solubles and Protein (%) of Insoluble Fraction of Untreated Wheat Bran (UB), Ground Wheat Bran (GB), and Ball Milled Wheat Bran (BMB) after Protease Treatment

Bran sample	Solubles yield (%)[1]	Protein (%) of insoluble fraction[2]
UB	33.8±0.4	12.2±0.2
GB	36.5±0.8	8.2±0.1
BMB	41.0±0.2	9.5±0.2

[1]Expressed as weight percentage (dm) of UB; [(10 g UB – insoluble bran g)/10] × 100 = solubles yield (%); n = 2.
[2]Expressed as weight percentage (dm) of insoluble bran; n = 2.

Table 4.6 Effect of Hydrothermally Treated Bran at 25 °C and 140 °C (40 min) on Updegraff Reagent Insolubles Yield (%) at 25 °C and 100 °C

Updegraff reagent insolubles yield (%)	25 °C	140 °C
25 °C	66.4±0.3a	55.6±0.2b
100 °C	16.9±0.1a	17.0±0.0a

Expressed as weight percentage (dm) of UB; n = 2.
Numbers in the same row followed by a letter in common are not significantly different at $p < 0.05$.

Chapter 5 - Conclusions and future work

The use of solid-state ^{13}C CP/MAS NMR, X-ray diffraction (XRD), and small angle X-ray scattering (SAXS) to analyze the physical structure of a hard red winter wheat bran (variety Everest) and its dissected layers was reported for the first time. The ^{13}C CP/MAS NMR and XRD confirmed the presence of crystalline cellulose in untreated wheat bran, enzymatically treated bran, and its dissected layers. Most of the crystalline cellulose was present in the outer pericarp, which had a crystallinity index of 16.0%. A much lower proportion was in the intermediate layer. The aleurone layer was found to be completely amorphous. The cell walls of the outer pericarp, intermediate layer, and aleurone layer exhibited birefringence due to the orientation of cell wall components. This birefringence was independent of the presence of crystalline cellulose because even the aleurone cell walls exhibited birefringence. Arabinoxylan was found to be concentrated in the outer pericarp and intermediate layer. The protein and carboxyl carbon resonances were most intense for the aleurone layer indicating that protein was most concentrated there.

A NaOH/urea solvent was used to solubilize wheat bran and attempted to destroy its cell wall structure. This procedure recovered more wheat bran AX for characterization than any previous study using alkaline dissolution. X-ray diffraction of the material insoluble in NaOH/urea showed that the remaining cellulose was crystalline. Along with crosslinks, the crystalline cellulose may have provided the Everest wheat bran cell walls with structure to prevent the complete solubilization of the arabinoxylan and protein. Physical interactions and covalent crosslinks help wheat bran cell walls resist complete solubilization. Scanning electron microscopy and bright field microscopy helped confirm that the insoluble fraction was the

pericarp layer of the wheat bran. These images also showed that the cell walls were still intact after NaOH/urea treatment. The ^{13}C CP/MAS NMR and XRD data from Chapter 2 confirmed that most of the crystalline cellulose was in the outer pericarp in confirmation of the microscopy data in Chapter 3. In addition, enzymatic treatment of the high molecular weight material insoluble in 80% ethanol provided evidence of carbohydrate-protein conjugation.

Wheat bran physical structure was also studied after hydrothermal and enzymatic treatment. Hydrothermal treatment may have altered the physical structure of the aleurone layer aiding in its complete dissolution upon endoxylanase hydrolysis. Hydrothermal treatment (> 95 °C) combined with endoxylanase hydrolysis resulted in the complete loss and disorganization of the aleurone layer. Treatments lacking a hydrothermal treatment resulted in the aleurone layer remaining intact. For each treatment (enzymatic and hydrothermal), the outer pericarp and intermediate layer physical structure were not affected. This was confirmed using bright field microscopy and XRD.

Wheat bran was enzymatically and hydrothermally treated to solubilize the bran fraction. Unlike previous research, in this study, the starch and protein were kept and not removed before endoxylanase treatment. The retained protein and glucose polymers (starch, β-glucan, cellulose) could provide functional benefits in addition to the arabinoxylan and could make the process more economical. The combined solubles of the wheat bran hydrolyzed with thermostable α-amylase, protease, and xylanase was the recommended treatment. It had a viscosity of 23 cP (10% w/w solids) and a molecular weight between ~600 and 20,000. The percentage of untreated wheat bran AX that was solubilized was 50% and the percentage of AX in the solubles was 23%. Alkali treatment proved to be the most effective solvent at dissolving wheat bran. Although,

alkali, hydrothermal, and enzymatic treatments failed to destroy the crystalline cellulose structure and fully solubilize wheat bran.

Future work could include the addition of several more hard red winter varieties and classes of wheat. The solid-state ^{13}C CP/MAS NMR, XRD, and SAXS characterization of bran could change between varieties and wheat class. A determination of what kind of physical or chemical treatment is required to destroy cellulose crystallinity and how it effects overall bran solubilization and susceptibility to enzymatic hydrolysis should be investigated. The analysis of wheat bran dissected layers using a SAXS that can probe cell wall structures 1000 Å and larger could provide insight into how various treatments (physical, chemical, and enzymatic) impact a wider variety of cell wall structures such as bundles of cellulose microfibrils.

The addition of more wheat varieties, classes, and bran samples from several commercial flour mills to the Chapter 4 study would be necessary before the enzymatic and hydrothermal treatment of wheat bran could to be promoted to the industry. The percentage of arabinoxylan, protein, cellulose, and adhering endosperm in wheat bran could be different which would affect the amount of bran solubilized. The ability to control these variables would be necessary for the production of a consistent product that achieved product specifications and target yields. A business plan would have to be completed to determine the potential profitability of producing wheat bran solubles through hydrothermal and enzymatic processing.

Chapter 6 - List of appendix material

Appendix A. Crystallinity index calculation

The calculations for total area and the area of the crystal regions of the X-ray diffractograms were performed using the Igor software package (Igor Pro, Wavemetrics, Lake Oswego, OR). The total area term in equation (1) below refers to the area under the diffractogram curve. The Area (crystal) term corresponds to the area under the crystalline peaks at 15.0 and 22.5 degrees 2θ. The referenced used is listed below.

The calculations for total area and the area of the crystal regions of the X-ray diffractograms were performed using the Igor software package (Igor Pro, Wavemetrics, Lake Oswego, OR). The total area term in equation (1) below refers to the area under the diffractogram curve. The Area (crystal) term corresponds to the area under the crystalline peaks at 15.0 and 22.5 degrees 2θ. The referenced used is listed below.

$$\text{Crystallinity Index: } = \frac{\sum Area\ (crystal)}{Area\ (total)} \times 100 \qquad (1)$$

Martínez-Sanz, P. Lopez-Sanchez, M.J. Gidley and E.P. Gilbert, Evidence of differential interaction mechanism of plant cell wall matrix polysaccharides in hierarchically-structured bacterial cellulose, *Cellulose*, 2015, **22**, 1541-1563.

Appendix B. Hydrothermal and enzymatic treatment of wheat bran methodology

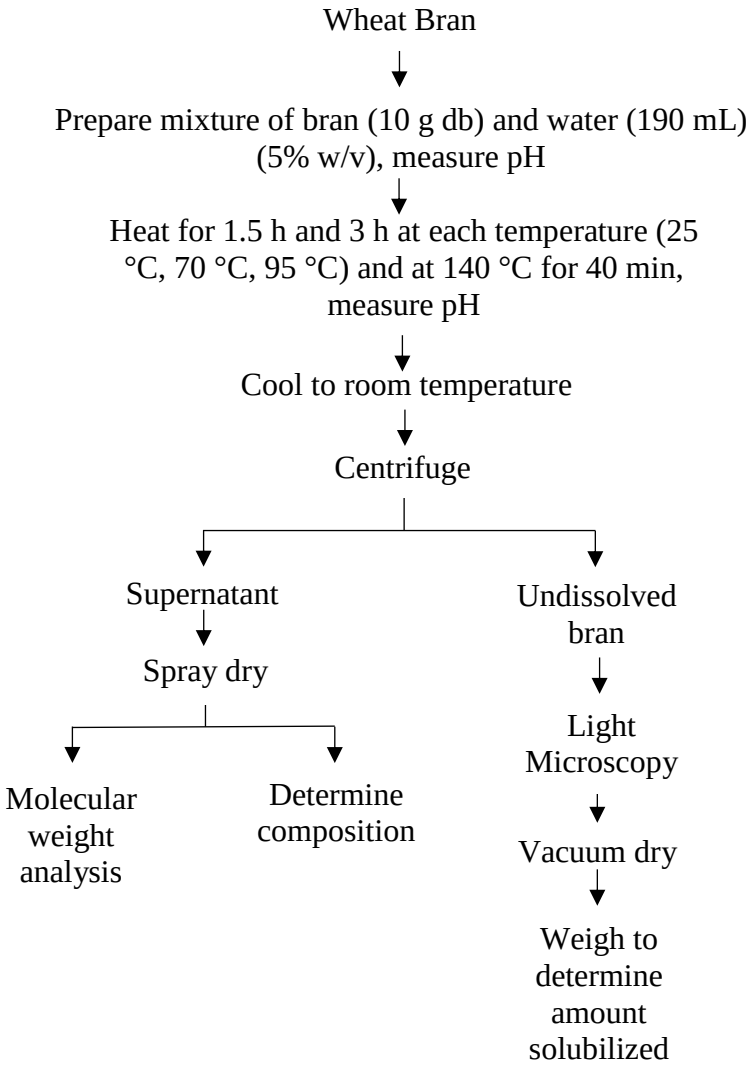

Figure 6.1 Procedure for the effect of hydrothermal treatment on soluble and insoluble bran components; n=2.

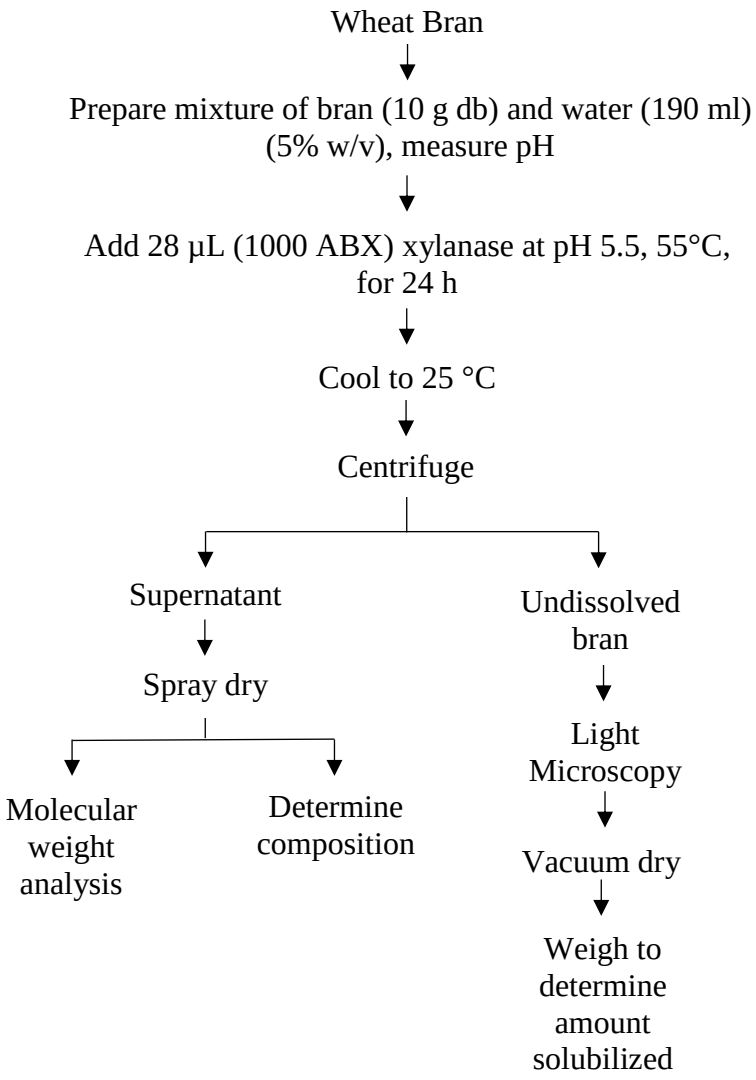

Figure 6.2 Procedure for determining the effect of xylanase treatment on soluble and insoluble bran components; n=2.

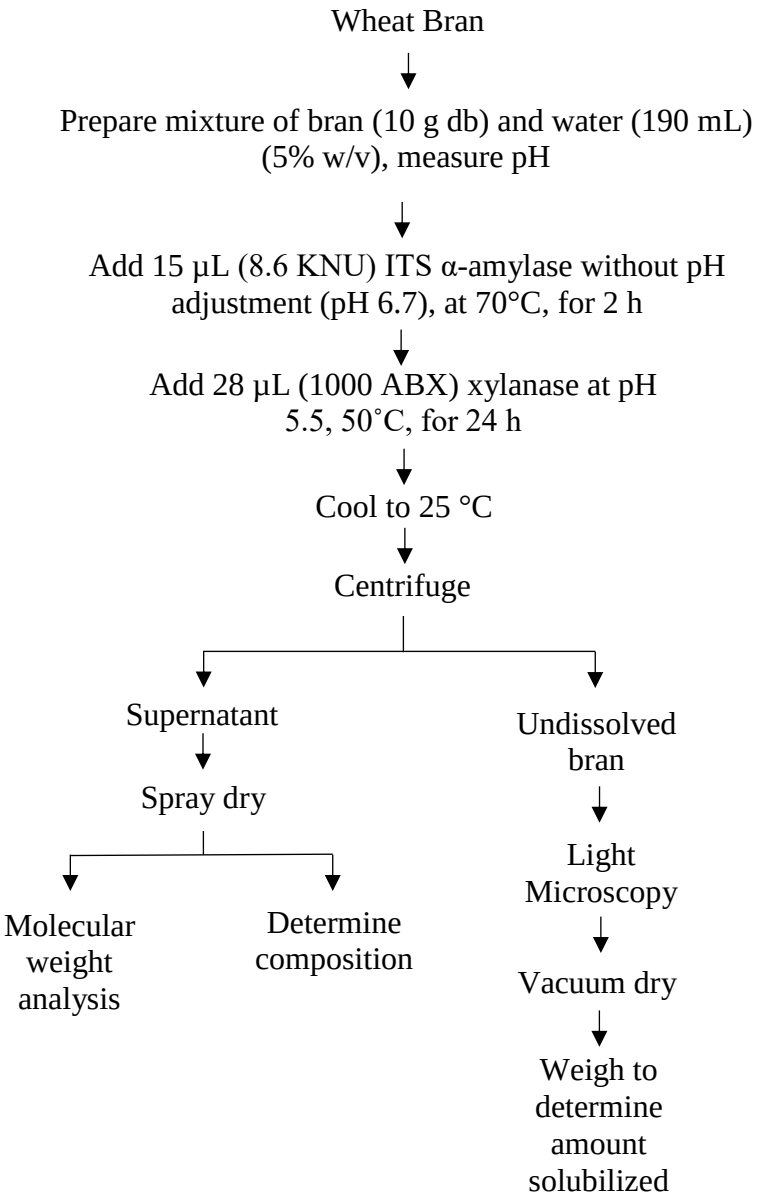

Figure 6.3 Procedure for determining the effect of intermediately thermostable α-amylase (ITS α-amylase) and xylanase treatment on soluble and insoluble bran components; n=2.

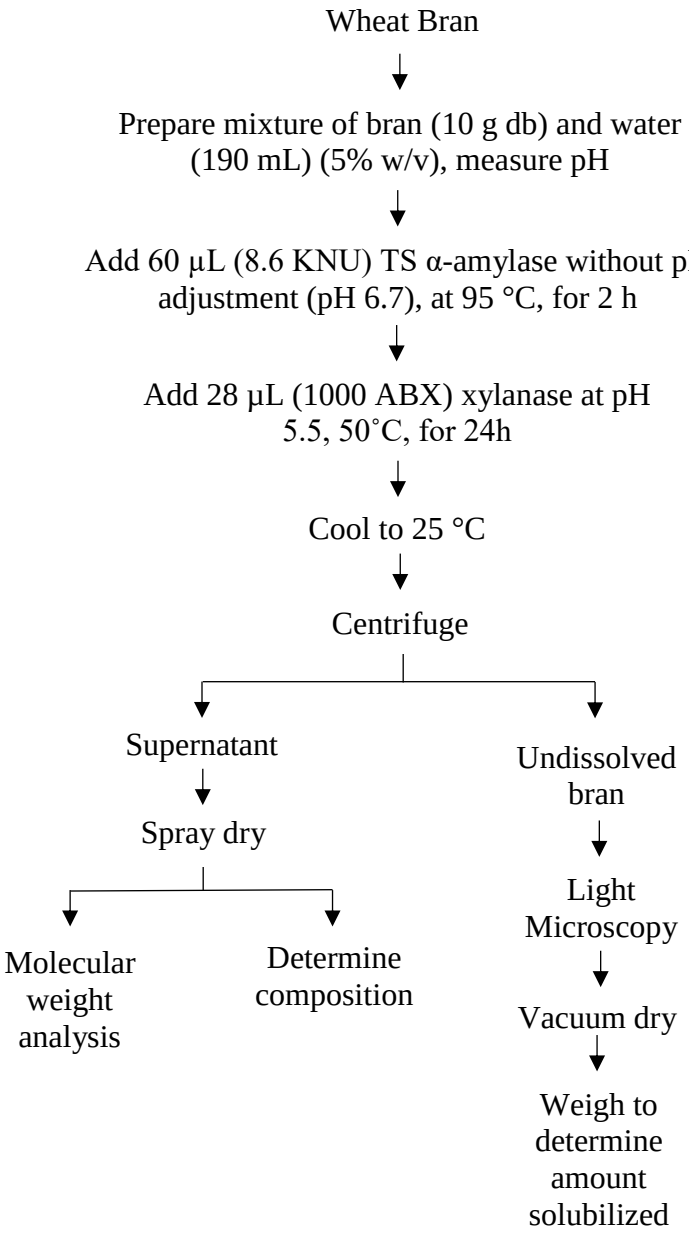

Figure 6.4 Procedure for determining the effect of thermostable α-amylase (TS α-amylase) and xylanase treatment on soluble and insoluble bran components; n=2.

Appendix C. Wheat bran layer dissection

Everest wheat kernels were soaked in 50% ethanol for 16 h

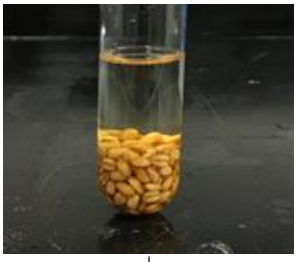

The germ and crease were removed using a scalpel

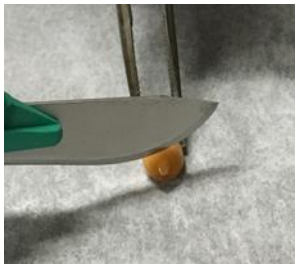

The endosperm was scraped away using a scalpel

After the endosperm was scraped
away, the outer pericarp was removed

↓

Next, the aleurone was scraped away under the
magnification of a dissection microscope

↓

The intermediate layer was left

↓

The dissected layers were imaged with a bright
field microscope. It is critical to image the
layers before they air dry to prevent air cells
from being trapped in the cell walls.

↓

Air dried and stored in desiccator
before analysis

Outer pericarp

Intermediate layer

Aleurone

Appendix D. NaOH/urea wheat bran dissolution method

Cool NaOH/urea solvent to -12.6 °C resulting in slight ice formation

Add 2 g destarched deproteinized bran to make 0.5% (w/w) mixture

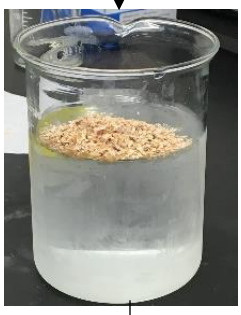

Homogenize for 10 min at 750 rpm

Stir for 12 h at 25 °C